THE INFLUENCE OF HEAVY VEHICLE DYNAMICS ON RIGID PAVEMENT RESPONSE

by

EDWARD ABBO

B.S.E., Princeton University
(1985)

Submitted to the Department of Mechanical Engineering in Partial Fulfillment of the Requirements for the Degree of

MASTER OF SCIENCE IN MECHANICAL ENGINEERING

at the

MASSACHUSETTS INSTITUTE OF TECHNOLOGY

February 1987

Signature of Author _____

Department of Mechanical Engineering
February 1987

Certified by _____

Professor J.K. Hedrick
Thesis Supervisor

Accepted by _____

Chairman, Department of Mechanical Engineering

THE INFLUENCE OF HEAVY TRUCK DYNAMICS ON RIGID PAVEMENT RESPONSE

by

Edward Abbo

Submitted to the Department of Mechanical Engineering
on January 16, 1987 in partial fulfillment of the
requirements for the Degree of Master of Science in
Mechanical Engineering

ABSTRACT

The purpose of this paper is to develop a methodology to analyze rigid pavement response to moving, dynamic vehicle loads which may be used to predict pavement performance. Current models of vehicle-pavement interaction employ simplified models of vehicle loading, such as a static load. However, instantaneous dynamic vehicle loads may be considerably higher than static loads, and thus dynamic loading can have a considerable impact on rigid pavement performance.

The paper investigates the influence of heavy truck vehicle dynamics on rigid pavements. In order to predict the forces at the road-tire interface, full non-linear models were used to describe the behaviour of articulated vehicles traversing rigid pavements. Non-linear leaf-spring suspension and tire models were used.

Following a review of rigid pavement models, we selected and modified PMARP (Purdue Method for Analysis of Rigid Pavements), to couple with our vehicle model. Part of the modifications made to PMARP included addition of temperature gradient and moisture gradient effects and performance submodels. The pavement failure and performance models include fatigue cracking, pumping, load transfer decay, joint faulting, slab roughness, and present serviceability index.

The model loads a series of slabs with the dynamic tire forces of all the axles of the vehicle as it traverses the slabs. The tire force profiles are generated from the vehicle model for each seasonal value of pavement joint-fault magnitude, slab roughness and warping. Since the pavement experiences the effect of dynamic loading of all the axles of the vehicle, we express our damage results in terms of vehicle equivalency factors.

The final part of the study discusses the effects of varying vehicle parameters on road damage. The parameters examined include suspension type, friction parameters, tire pressure, axle spacing and suspension spring constants.

Thesis Supervisor: J.K. Hedrick

Title: Professor of Mechanical Engineering

Table of Contents

ACKNOWLEDGEMENTS

First and foremost, I would like to thank my thesis advisor, Professor J. Karl Hedrick for sharing his knowledge and time with me. It has been a privilege and a pleasure to work with him. I would like to thank Dr. Mike Markow and Brain Brademeyer for thier time and suggestions with regard to the rigid pavement modelling.

I would also like to thank members of the VDL for their sense of humour during the long hours spent there in the past year and a half.

1

Introduction

1.1 Introduction

One of the main concerns of highway engineers is the effect of traffic loading on pavement performance. On designing a pavement system estimates of traffic volume and composition is a major factor influencing the course of the design. Of equal importance is the environment to which the pavement will be subjected. Typically pavements will endure several million loadings over their twenty to thirty years of service. The pavement must therefore, be designed to withstand the loading applied economically and safely while providing an adequate level of service to the user.

From an economic point of view, the cost of maintaining the highway systems in the United States is over half the cost of maintaining the total infrastructure. Over the next twenty years the cost of maintaining the highways is estimated at 1.6 trillion dollars [1]. An understanding of the contribution of traffic loading and the effect of vehicle dynamic loading on pavement performance is therefore critical to restraining maintenance costs.

The analysis of pavement response to traffic loading is not trivial. The pavement response depends on the interaction of many factors. These factors include environmental effects, design of the pavement structure, age related effects, subgrade types and level of maintenance performed. The extensive pavement research performed over the past thirty years has focused almost entirely on the pavement response and has neglected "back-effects" associated with the vehicle and pavement systems. It has been recognized that vehicles impose loads on pavements which deteriorate the latter. But the pavement deterioration in turn acts as additional

excitation to the vehicle which produces larger dynamic loadings. This accelerated deterioration effect has not been well modelled previously. A possible reason being that the vehicle dynamics are not well understood by highway engineers. Evidence supporting this is the simplistic loading models applied to existing pavement models, such as a static load.

To model this accelerated pavement deterioration we shall treat the pavement and the vehicle as complete interacting systems. We thus impose a moving dynamic loading on the pavement and reflect the deteriorated pavement surface condition to the vehicle model, which in turn generates a larger dynamic loading. The research is thus a combination of two parts. The first will use computer dynamic models of tractor semi-trailers to determine the dynamic loads exerted on the pavement for each stage of the pavement deterioration. The second part will load a modified finite element rigid pavement model with the predicted vehicle loading and thereby predict the primary and secondary responses over the pavement life.

There are several advantages to the modelling and simulation approach. Primarily it eliminates the need to build expensive test tracks with measuring devices such as weigh-in-motion pads or strain gauges in the pavement layers. Secondly, subsequent to model validation it will provide a powerful tool for both vehicle and pavement design engineers. For vehicle suspension engineers the design process will involve optimizing suspension design with respect to both vehicle ride quality and also pavement performance. For highway engineers it will provide a better understanding of the critical loading areas and will provide a relatively inexpensive means of testing new designs. In summary this analysis will increase the awareness of highway engineers of the effects of vehicle dynamic effects and the vehicle design engineer of pavememt design techniques.

Early theoretical formulations of rigid pavement behaviour date back to 1926 when Westergaard [2], calculated the response to a point loading of a linearly elastic plate supported by an elastic subgrade. The Winkler subgrade model provides a supporting force proportional to the deflection at the particular point of the subgrade. The Westergaard solution is however, inadequate when dealing with

discontinuities in the pavement structure such as the slab joints. Rigid pavement analysis employing finite element formulation have been developed to overcome the problem of discontinuities and provide an adequate static response analysis to an applied loading.

A significant contribution to understanding the effect of heavy vehicle dynamic loads on pavements was made by Sweatman [3]. Sweatman indicated that for flexible pavements, the tyre force can be considered as a gaussian random variable, and that the road damage is a function of the static load and the standard deviation of the dynamic load. Sweatman defined the Road Stress Factor,Φ,

$$\begin{aligned} \Phi &= \left(\frac{1}{K}\right) E[F^4] \\ &= \left(\frac{1}{K}\right) E[F]^4(1 + 6.DLC^2 + 3.DLC^4) \end{aligned} \tag{1.1}$$

where, K is the Axle Equivalence Factor, F is the Tire Force, and the DLC is the Dynamic Load Coefficient (the coefficient of variation of the tire force). More recently O'Connell [4] developed a modified Road Stress Factor for rutting and cracking, thereby emphasizing the different mechanisms involved in each of the pavement damage modes. The tyre force generated by traversing a rigid pavement however, cannot be described as a gaussian random variable and therefore the Road Stress Factor detailed above cannot be applied as a measure of damage.

1.2 Report Outline

This report documents the approach used to model moving dynamic loads on rigid pavements and the contribution of dynamic loading to rigid pavement performance.

Chapter 2 describes the tractor semi-trailer models used. The suspension types modelled include the single axle leaf-spring, the walking-beam and four-leaf short-rocker tandem suspensions. The adaptive footprint tyre model is also described and used to give accurate tyre force predictions especially when dealing with sharp irregularities in the road profile as would occur at the joints of rigid pavements.

Chapter 3 descibes the tractor semi-trailer dynamic response to rigid pavements and presents the results of extensive simulations to determine vehicle and pavement parameters to which the dynamic loading is sensitive. An aggregate loading is defined to determine the positions along the slab that experience the largest loading due to the passage of all the axles of a tractor semi-trailer.

Chapter 4 describes the finite element approach to modelling rigid pavements. A review of existing rigid pavement models is detailed and the basis by which a rigid pavement model is selected is described. The modifications needed included adapting the model to account for moving dynamic loads, addition of performance models, and thermal gradient effects.

Finally chapters 5 and 6 present the parametric studies performed using the coupled vehicle/pavement models. Conclusions on the effect of various vehicle and pavement parameters on pavement performance are developed. The results are also compared to the case of modelling the vehicle loading as a static load.

2

Vehicle Modelling

2.1 Introduction

Since we are required to predict pavement primary response (i.e. deflections, stresses, etc) to vehicle loading, we need tire force histories as outputs of our vehicle models. This means that our simulations are to be performed in the time domain. The more economical alternative of performing a frequency domain analysis by applying linearization techniques, thus would not be suitable for our particular study.

The vehicle models used were those developed by Gibson [5]. They are the half-vehicle models (or bicycle models) illustrated in figure 2.1. The vehicle degrees of freedom modeled include tractor semi-tralier pitch and heave motions and the suspension specific degrees of freedom. We therefore neglect roll dynamics associated with the vehicle. Gillespie [6] showed that roll dynamics only become important for low vehicle speeds (under 20 mph) at which vehicle dynamics do not produce a significant effect on pavement deterioration. Roll dynamics however, may be significant when considering rigid pavement faults that are not perpendicular to the direction of travel of the vehicle. This results in a step input to the left wheel path being delayed from that to the right wheel path.

The vehicle nonlinearities modelled include:

- Leaf-spring suspension;
- tire;

- Wheel hop.

It has been shown that the nonlinear leaf-spring model predicts larger response fluctuations then the linear models. Furthermore, Boghani [8] showed that the point contact tire model used in most dynamic simulations is inadequate when used to model tire forces due to sharp irregularities in the pavement.

2.2 Suspension Models

The majority of the suspension systems available use the leaf-spring element as the compliant element. Other truck suspension types include the air-bag and torsion-bar suspension.

The suspensions used for this study include:

- Single leaf-spring;
- Four-leaf short-rocker tandem;
- Walking-Beam tandem.

The equations of motion for the suspensions listed above are illustrated in figure 2.2. The model used for the leaf-spring element is described in section 2.5.

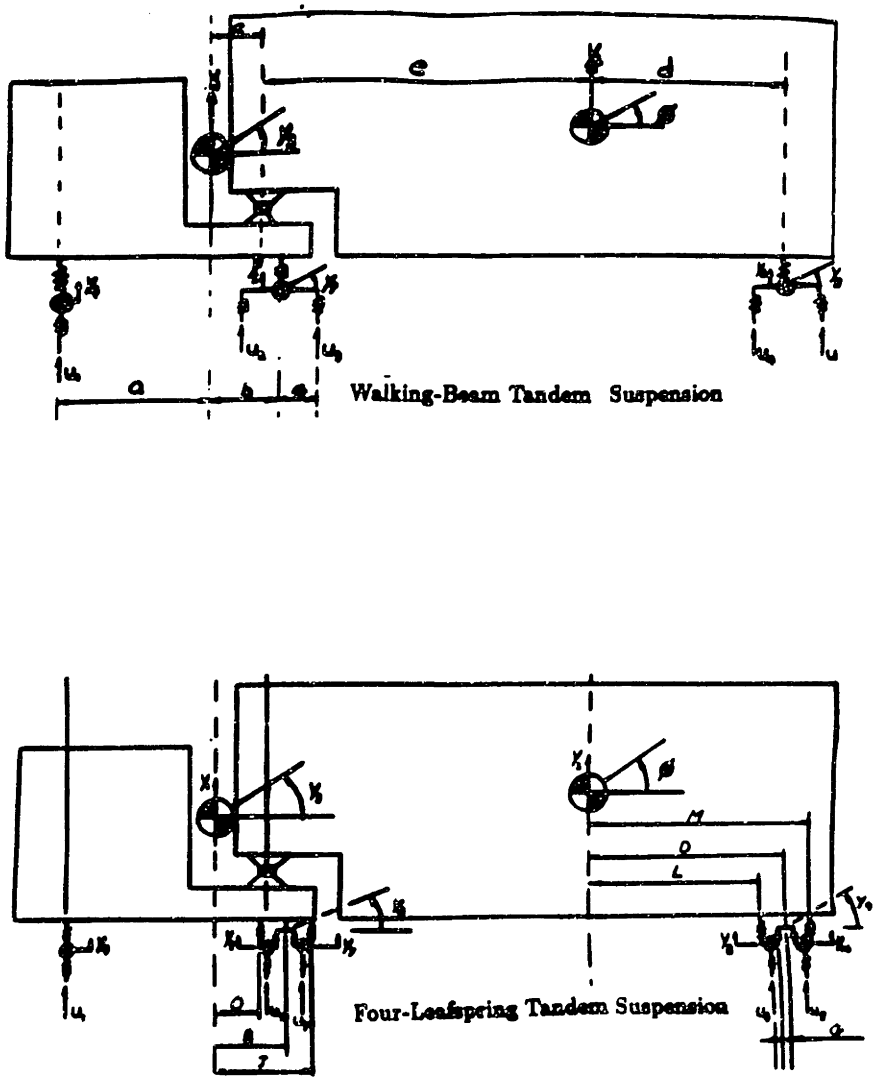

Figure 2.1 Schematic of Vehicle Models used in Dynamic Simulations
(a) Walking-Beam Tandem Suspension
(b) Four-leaf Short-Rocker Tandem Suspension

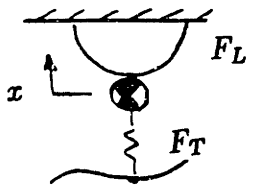

$$F_T - F_L - M_u g = M_u \ddot{x}$$

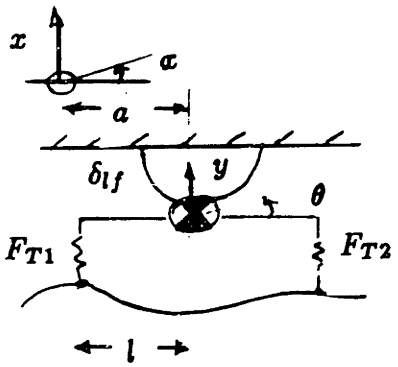

$$F_{T1} + F_{T2} - F_L - M_u g = M_u \ddot{y}$$

$$(F_{T2} - F_{T1})\, l - \tau_o\, sgn(\dot{\theta}) = I\ddot{\theta}$$

$$\delta_{lf} = y - x - a \sin\alpha$$

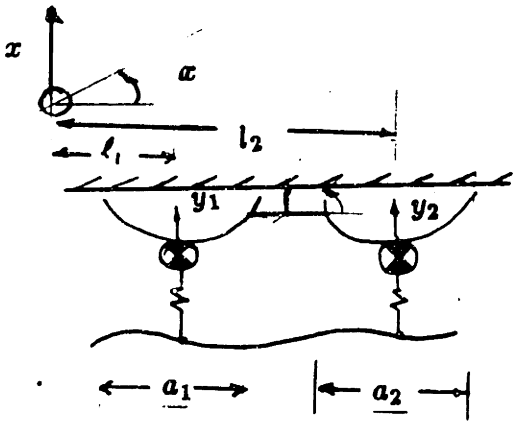

$$F_{T2} - F_{l_2}(\delta_2) - M_2 g = M_2 \ddot{y}_2$$

$$F_{T1} - F_{l_1}(\delta_1) - M_1 g = M_1 \ddot{y}_1$$

$$\frac{l}{2}(F_{l_1} - F_{l_2}) - \tau_o\, sgn(\dot{\theta}) = I_{sr}\ddot{\theta}$$

$$\delta_1 = y_1 - x - l_1 \sin\alpha + \frac{a_1 l}{2} \sin\theta$$

$$\delta_2 = y_2 - x - l_2 \sin\alpha + \frac{a_2 l}{2} \sin\theta$$

Figure 2.2 Suspension Models
(a) Single Leaf-Spring
(b) Walking-Beam Tandem
(c) Four-Leaf Short Rocker Tandem

2.3 Vehicle Excitation

2.3.1 Introduction

The road surface provides a displacement input to each of the wheels of the vehicle. The vehicle when traversing a road surface responds to each of these excitations according to the governing equations of motion. It is important to note that even newly constructed road surfaces are irregular, however carefully they are prepared. Considerable work has been done on modelling the road profile, and it has been established that a stationary gaussian stochastic process provides a satisfactory model [7].

If a road profile is denoted by $y(x)$ and the profile is a realization of a stationary gaussian random process then the profile can be fully described by the spatial autocorrelation function:

$$\phi_{yy}(s) = E\left[y(x)\, y(x+\delta)\right] \tag{2.1}$$

The autocorrelation function is also related to the auto-spectral density (or Power Spectral Density (PSD)) by the fourier transform:

$$S_{yy}(n) = \int_{-\infty}^{\infty} \phi_{yy}(\delta)\, \exp(-i\, 2\pi\, \delta n)\, d\delta \tag{2.2}$$

where n is the wavenumber, the reciprocal of wavelength.

2.3.2 Road Roughness

A more detailed analysis of the road roughness model is described by O'Connell [4], but a brief description is included below for completeness.

The road PSD is flat for frequencies below 0.01 cycles/ft (Ω_0) above which it rolls off at the rate of -40 dB/decade:

$$S_y(\Omega) = \begin{cases} \frac{A}{(\Omega+\Omega_0)^2}, & \text{if } 0 \le \Omega \le \Omega_c; \\ 0, & \text{elsewhere.} \end{cases} \tag{2.3}$$

where,

A is the Road Roughness parameter,

Ω_0 is the Road Break-frequency

Ω_c is the Cut-Off frequency above which there is negligible road input.

The road roughness is described by the variance of its spectral slope (slope variance SV). Thus, the spectral density of the slope $S_s(\Omega)$ is given by:

$$S_y(\Omega) = S_y(\Omega).\Omega^2 = \frac{A\Omega^2}{(\Omega + \Omega_0)^2} \tag{2.4}$$

and if we assume a zero mean slope, $E[\dot{y}] = 0$ then:

$$\begin{aligned} SV &= Var[\dot{y}] = E[\dot{y}^2] - E[\dot{y}]^2 \\ &= E[\dot{y}^2] = \int_0^\infty S_s(\Omega) d\Omega \approx A\Omega_c \end{aligned} \tag{2.5}$$

for Ω_0 less than Ω_c. In order to obtain a time domain representation of the road inputs, gaussian white noise was passed through a linear shaping filter. Roads for various slope variances were obtained by scaling the base road by the square root of the required slope variance. Figure 2.3 shows the PSD of the generated road profile.

2.3.3 Joint-Fault Model

To model the faults that occur at regular distances along rigid pavements we linearly superposed a periodic saw-tooth wave on the rough road representation of the previous section. The resulting road profile over a slab length is therefore:

$$y(x) = y_r(x) + y_{jf}(x) \tag{2.6}$$

where $y_r(x)$ is the profile due to the slab roughness and

$$y_{jf}(x) = \begin{cases} (\frac{h}{L})\, x, & 0 \le x \le L; \\ 0, & \text{x = L.} \end{cases} \tag{2.7}$$

where:

h = joint fault magnitude;

L = joint spacing.

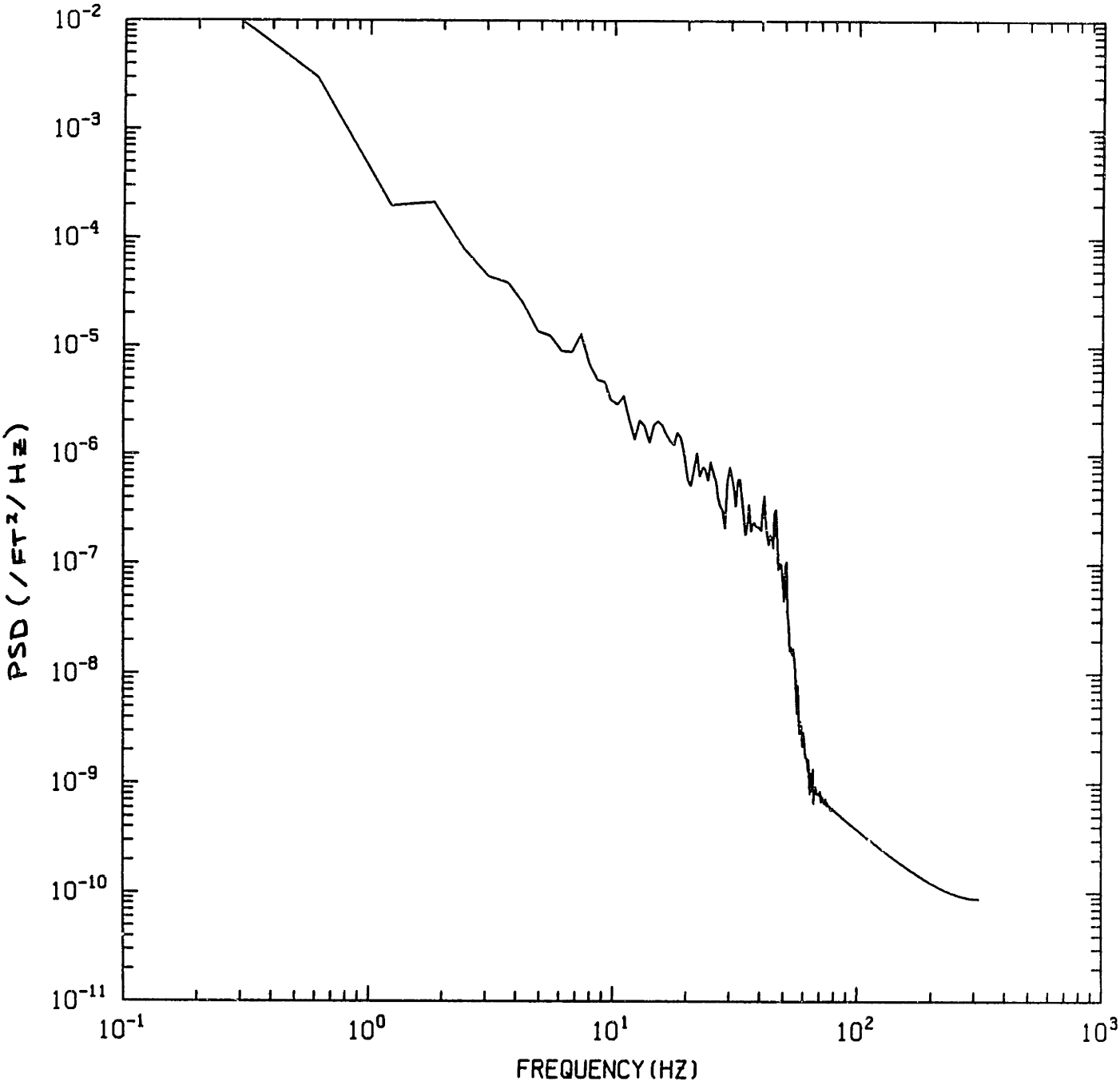

Figure 2.3 Power Spectral Density of Typical Flexible Pavement

2.3.4 Slab-Warping Model

Thermal and moisture gradient across the slab thickness result in significant bending moments along the edges of the slab. The warping is modelled as a periodic hemispherical wave added to the above road model:

$$(x - \frac{L}{2})^2 + (y_w(x) - (\frac{L}{2} - \delta))^2 = R^2 \tag{2.8}$$

$$R^2 = (\frac{L}{2})^2 + (R - \delta) \tag{2.9}$$

where:

δ = mid-slab deflection due to warping;

R = radius of curvature of slab;

L = slab joint spacing;

y_w = vertical displacement due to warping.

The final road profile is thus generated by summing the three components over the slab length:

$$y(x) = y_r(x) + y_{jf}(x) + y_w(x) \tag{2.10}$$

2.4 Tire Model

2.4.1 Introduction

In an investigation where the primary concern is the vertical forces transmitted by a vehicle onto the pavement, it is critical to understand and model the interface between the two systems well. In our model the only inputs to the vehicle are generated by road disturbances which pass through the tire to determine the vehicle dynamic response. This in turn determines the dynamic loading imposed on the pavement.

A literature search revealed basicaly four tire models that are being used currently in dynamic vehicle simulations [8]:

- Point Contact Model;
- Rigid Tread Band Model;
- Fixed Footprint Model;
- Adaptive Footprint Model.

Since we are dealing primarily with rigid pavements in this report we needed to consider more sophisticated models than the point contact model, which performs adequately on rough roads or flexible pavements ($SV \approx 50 \times 10^{-6} in^2$).

In reality however, the tire is composed of an inflation pressure and a carcass force component. For non-planar footprint conditions the inflation pressure and carcass force components generally share the applied force unequally, each having its own non-linear constitutive equation. When modelling the tire as an equivalent stiffness we essentially combine the compliant elements. Models exist that analyze the tire carcass as a thin damped elastic shell. They are however, inappropriate for dynamic vehicle simulations when dealing with a multi-axled vehicle, from an economical perspective. Furthermore, they have only been developed for a plane footprint loading.

The tire models we considered all need inputs such as local terrain profile, spindle height and generate transmitted forces only. We assume a non-yielding ground. This assumption is a valid one for highway pavements. It is worth noting that in the case of a tire crossing a fault where there has been slab support removal due to pumping, there will be significant ground yielding. We also neglect shear stresses in the footprint which are only important when considering braking and turning of a vehicle.

2.4.2 Point Contact Tire Model

The tire is assumed to be in contact with the terrain at a single point. The carcass and inflation pressure are modelled as a single spring in parallel with a damper which models carcass energy dissipation due to stretching. The tire mass is lumped together with the axle mass at the center of the wheel. The point contact model does not model sharp irregularities in the terrain realistically. The PSD over a rough road indicates that it contains a larger high frequency content. This is due to its inability to envelope irregularities in the terrain leading to wheel hop.

2.4.3 Rigid Tread Band Tire Model

This model differs from the point contact model in that it can contact the terrain in more than one point by modelling the tire geometry as a rigid tire. The spring/damper combination then experience a filtered version of the terrain that removes sharp irregularities. This model results in less wheel hop thereby reducing the spectral content at higher frequencies.

2.4.4 Fixed Footprint Tire Model

Interaction with the terrain for this model is at a fixed contact length independent of the tyrte deflection. A set of spring/ damper pairs are evenly distributed along the contact length to model the carcass and inflation pressure.

(d) Adaptive Footprint.

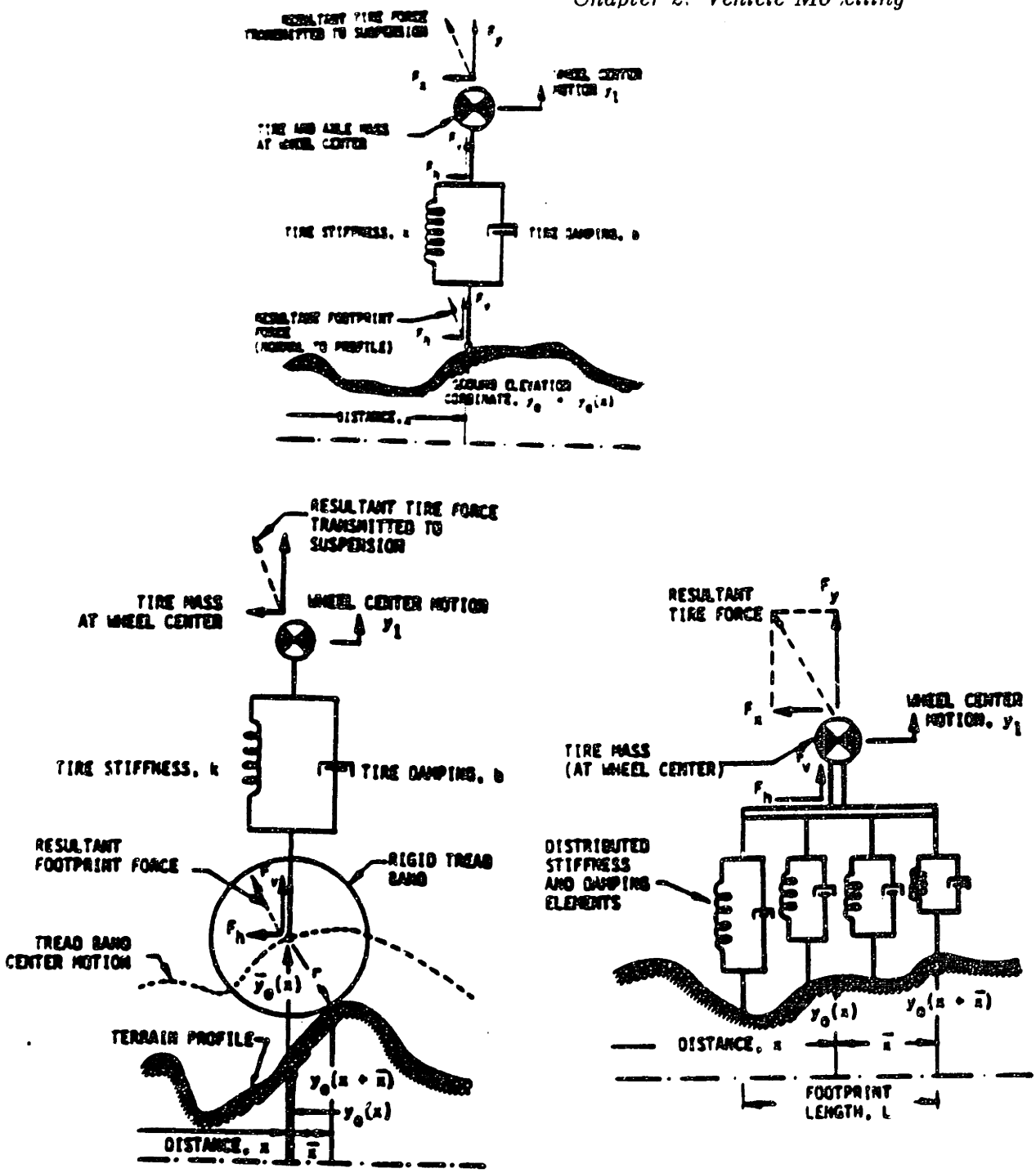

Figure 2.4 Tyre Models

(a) Point Contact
(b) Rigid Tread Band
(c) Fixed Footprint

The fixed footprint model thus envelopes small irregularities in the road just as the rigid tread band model but the difference being that the filtering is governed by the footprint length in the former case and by the tread band radius in the latter.

2.4.5 Adaptive Footprint Tire Model

The adaptive footprint model consists of a flexible tread band linked to the wheel centre by angularly distributed stiffness and damping which simulate carcass and tread stiffness. The difference between the fixed footprint model this model being that the footprint lenght and orientation relative to the wheel centre changes depending on tire deflection and terrain profile.

For our particular application we chose the adaptive footprint tire model for its ability to reduce the amount of wheel hop by filtering short wavelength irregularities thus attenating the high frequency excitation to axle of the vehicle.

Since the spacing of the points in the road profile are dependent on the vehicle velocity and simulation time step:

$$\Delta x = v\,\Delta t \tag{2.11}$$

Δx = road input spacing;

v = vehicle velocity;

Δt = simulation time step;

It becomes necessary to interpolate between road input points when we have many springs distributed along the contact length of the tire. The procedure for setting-up the adaptive tire model is outlined below:

(1) Obtain experimentally the vertical rolling force versus tire deflection characteristic of the tire to be modelled and determine the non-linear stiffness of the tire.

(2) Using the simulation model impose a series of center spring deflections in the loading range of the tire (say up to 6 kips) assuming a flat road surface.

For each center spring deflection determine the sum of the vertical deflections of all the springs in the model.

(3) Also based on the experimental deflection versus tire force data determine the vertical rolling tire force due to the center spring deflection of the model.

(4) For each value of center spring deflection δ_c we can thus obtain the sum of the deflections of all the springs

$$\delta_T = \sum_{i=1}^{N} \delta_i \tag{2.12}$$

of the model and the corresponding experimental vertical tire force, F. So

$$F = F(\delta_c) = F'(\delta_T) \tag{2.13}$$

(5) For subsequent tire loading and road inputs we determine the contact length and obtain the sum of vertical deflections of all the springs (δ_T), and use the table set-up in part (4) to obtain the vertical tire force.

The whole process of determining the contact length and then summing the deflections of the springs is to be done at each time step and is very time consuming especially when running a vehicle model with 5-axles.

2.4.6 Tire Model Validation

Two validation tests were performed. The first is a static test where the loaded tire (800 lbf 14" Goodyear P185/75-R14 at 28 psi) is rolled over two different blocks (dimensions: 1" high by 6" long and 2" by 6") and the vertical tire force generated is compared to those obtained by Jane [9]. We found the that we obtained a good match by using 50 springs in our adaptive tire model. Figure 2.5 illustrate the vertical tire force variation as the tire traverses the block.

The second test is a dynamic test based on running a tractor semi-trailer equipped with a four-leaf tandem suspension over a test track. The axle accelrations were recorded as the truck passed over a series of rumble strips. The rumble

strip consisted of ten $\frac{3}{4}$ inch high 90° angle irons welded on top of $\frac{1}{8}$ inch thick by 4 inch wide iron strips. The angle iron strips were placed 13 feet apart on the pavement. Figures 2.6 illustrate the experimental and model axle accelerations obtained. For further details on the testing refer to Gibson [5].

2.5 Leaf-Spring Model

The leaf-spring element is a highly non-linear compliance element, due to the nature of the inter-leaf coulomb friction. The equation developed by Fancher [10], was the basis for describing the hysteresis (force vs. deflection) curve of the leaf-spring:

$$\frac{\partial F}{\partial \delta} = (F_{env} - F)/\beta \tag{14}$$

where:

F = leaf-spring force;

δ = spring deflection;

β = decay constant;

F_{env} = Force on the envelope at the given deflection. Upper boundary for increasing deflection and lower boundary for decreasing deflection.

A digital solution to this is given by Fancher as:

$$F_i = F_{env_i} + (F_{i-1} - F_{env_i}) \exp(-|\delta_i - \delta_{i-1}|/\beta) \tag{2.15}$$

where subscript 'i' indicates the current time-step and 'i-1' indicates the previous time-step. Equation (15) was modified by O'Connell [4], to reduce the steady-state error at the envelope:

$$F_i = F_{env_i} + (F_{i-1} - F_{env_{i-1}}) \exp(-|\delta_i - \delta_{i-1}|/\beta) \tag{2.16}$$

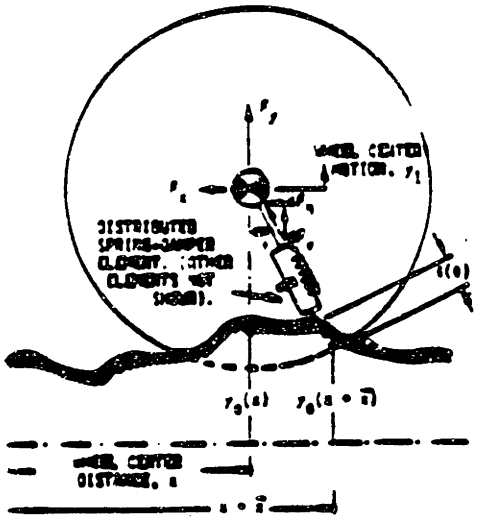

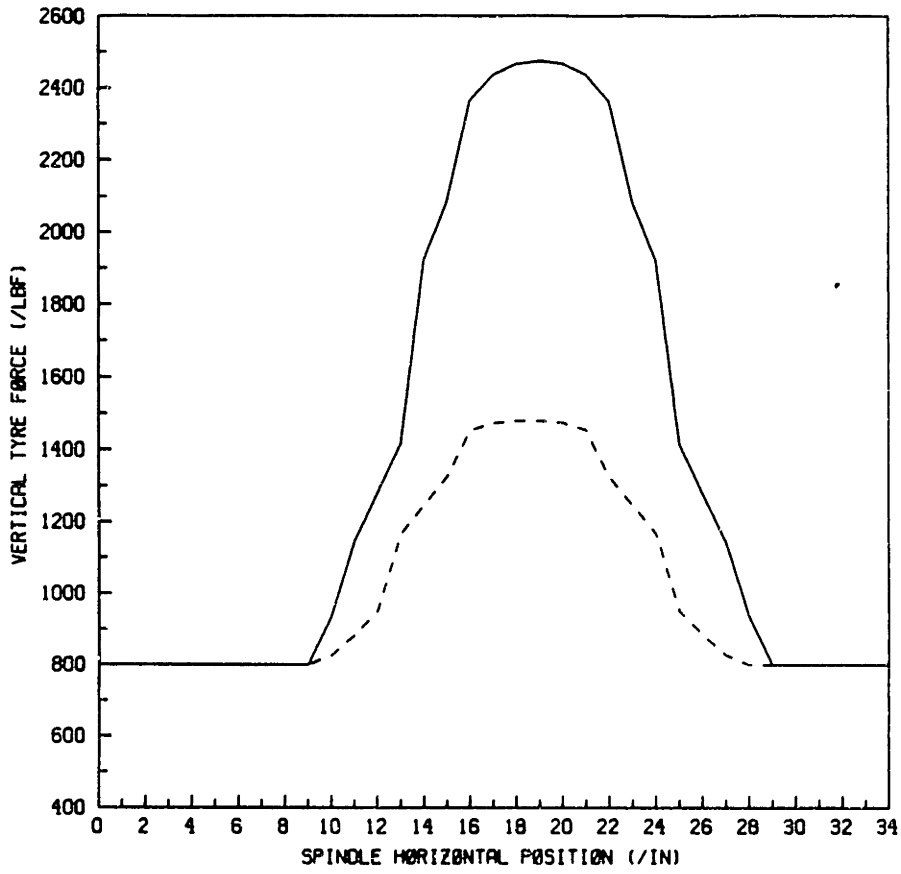

Figure 2.5 Adaptive Footprint Tyre Model Validation

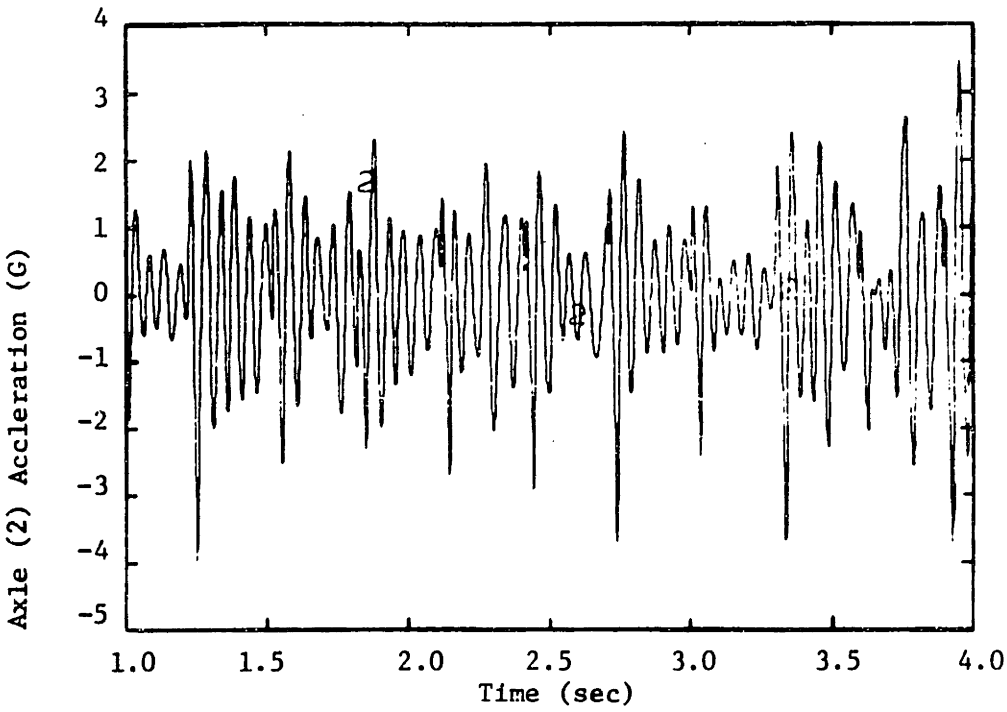

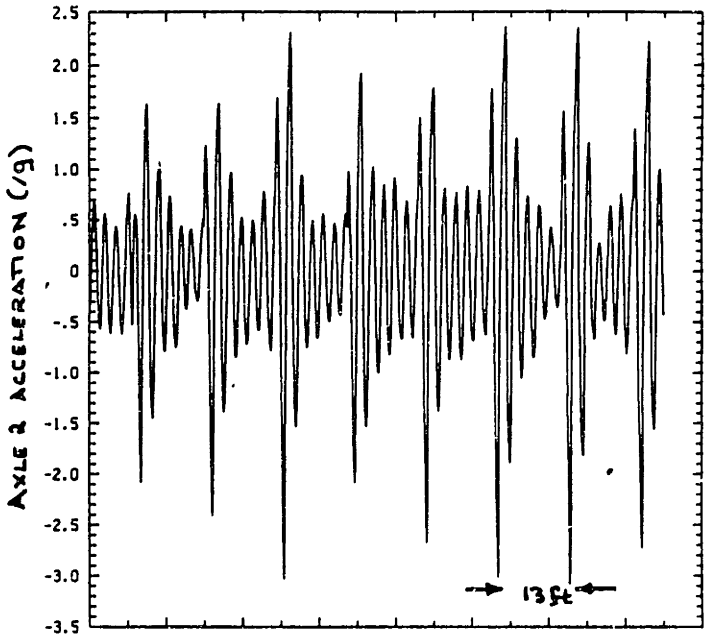

Figure 2.6 Rumble Strip Tyre Model Validation
(a) Experimental
(b) Adaptive Footprint Model

For our simulation purposes a linear envelope of the form:

$$F_{env_1} = k_1 \delta + P \tag{2.17}$$

$$F_{env_2} = k_2 \delta + P \tag{2.18}$$

where subscript '1' indicates upper envelope and '2' the lower envelope:

k_1, k_2 are the stiffnesses of the springs in loading and unloading;

P, Q are the intercepts of the envelope at $\delta = 0$ for the upper and lower envelopes respectively.

3

Vehicle Response to Rigid Pavements

3.1 Introduction

It has been a common misconception among highway engineers that the response or tire force exerted on the pavement due to an axle traversing a fault resembles a linear damped sinusoidal response as illustrated in figure 3.7. This is the response that we would expect to obtain if we modelled the tractor semi-trailer as a sprung and unsprung mass with linear damping and spring elements. In reality however the tractor semi-trailer consists of two interacting masses. The response will therefore be different if we input a step to the steer, drive or rear axles. Furthermore, the stiffness of the leaf-spring is larger when the spring deflection is increasing then when the deflection is decreasing ($\frac{k_1}{k_2} = 1.5$). The damping is also a function of deflection. When the spring is loaded there will be more energy dissipation associated with small oscillations than would occur at a lower loading.

Some typical tire force loading profiles are illustrated in figures 3.8. It is worth noting that the first peak magnitude (drive axle) following the joint is lower than the mean loading for faults less than about $\frac{1}{2}$ inch. The force is made up of two components. One due to the lumped weight at the axle and the second due to the effective body weight at the axle position. As the axle encounters the fault the leaf-spring extends in response to the reduced force at the road interface. This results in the wheel mode oscillation (approx. 10 Hz.). The body response to the fault is slower (approx 2 Hz.) and develops over the slab length. The tire force is thus the superposition of a high frequency component due to the wheel mode and a low frequency component due to the body mode. The reason the tire force response is

asymmetrical is because the leaf-spring stiffnesses k_1 and k_2 are not equal. In the case of the walking-beam tandem the leading axle response to the fault can be seen in the trailing axle tire force before the latter negotiates the fault. Notice also the that the response of the trailing axle to the fault is much more restrained than that of the leading axle (Figure 3.8).

A series of computer simulations were performed using the fully nonlinear vehicle models developed by Gibson [5]. The aim of these simulations is to determine sensitivity of the location of the peak loading and the magnitude of the loading to vehicle and pavement parameters. Based on the following results we propose guidelines for optimum vehicle and rigid pavement design.

The vehicle parameters selected were those considered by important by other researchers in the field [3,4,11] and include:

- Suspension type:
  - Single
  - Walking Beam Tandem
  - Four-leaf Tandem
- Average suspension stiffness,
- Leaf-spring Beta parameter,
- Tire pressure,
- Vehicle velocity,
- Axle spacing and
- Shock absorber damping.

Pavement parameters that are considered include:

- Road surface roughness,
- Joint faulting magnitude,
- Transverse joint spacing, and
- Slab Warping.

Figure 3.8 shows that the tire force profiles for the 6-DOF tractor semi-trailer are periodic. The random part of the signal (magnitude of the peaks and troughs vary and also higher frequency small magnitude distortions) is due to the different

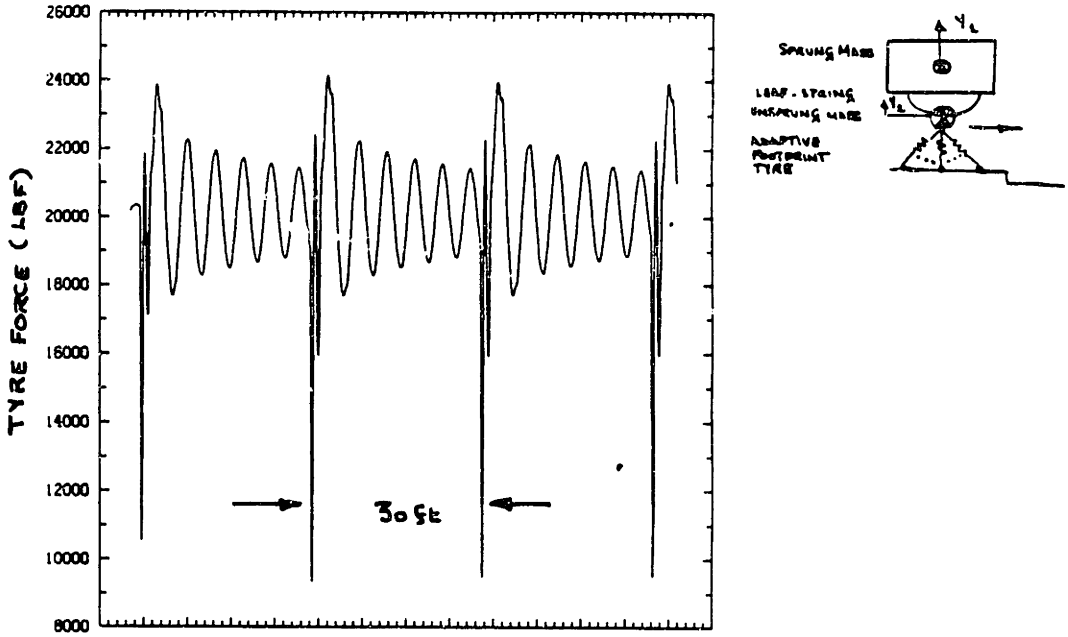

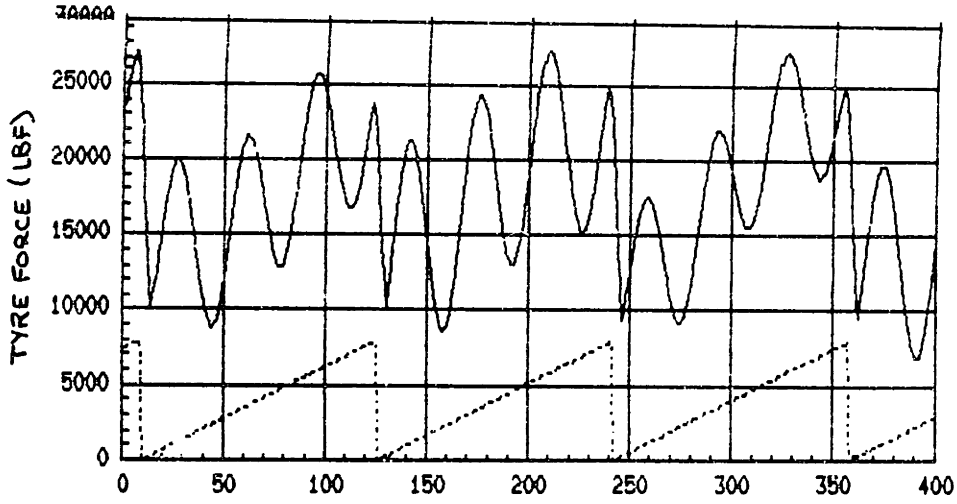

Figure 3.7 Tyre force response to joint fault
(a) 2 Degree of Freedom model
(b) Tractor Semi-Trailer with $k_1 = k_2$

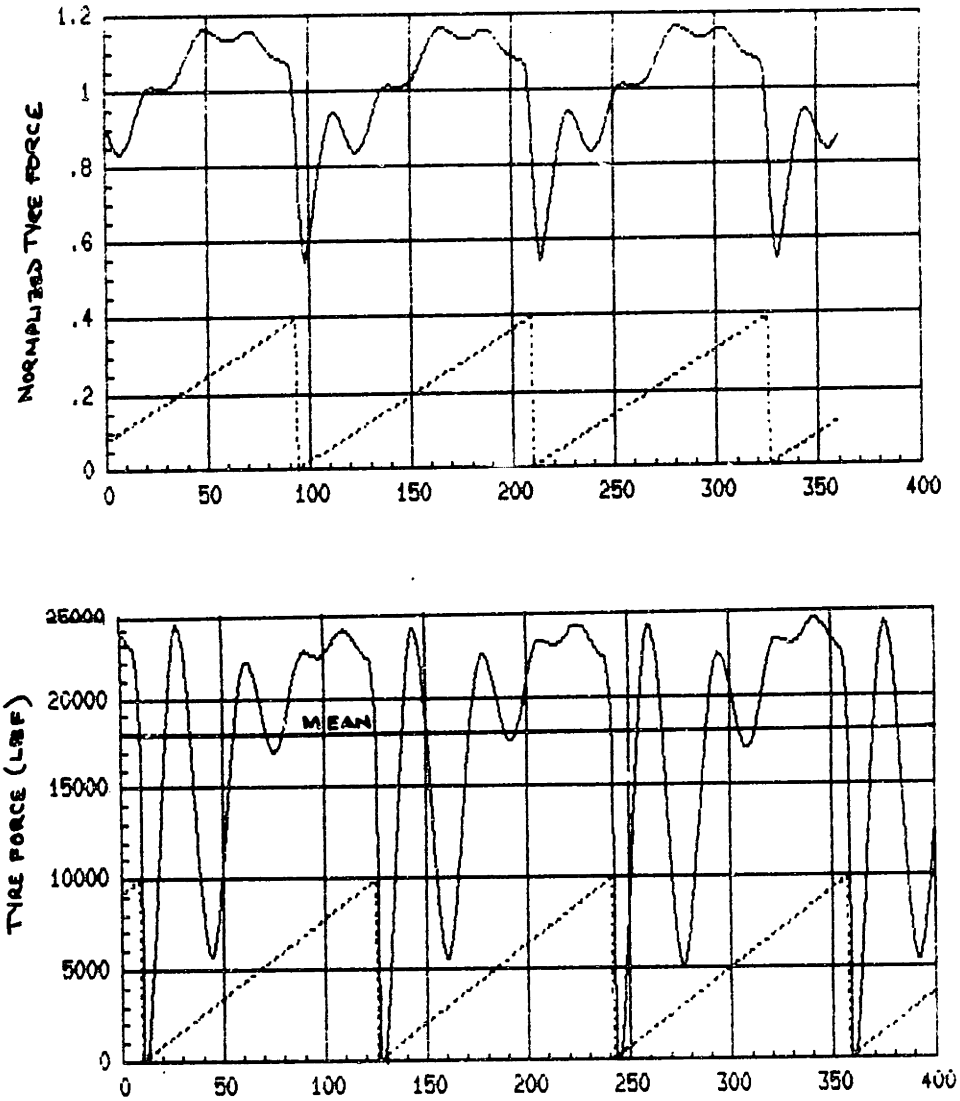

Figure 3.8 Tyre force response to fault (single : drive axle)
(a) 0.5 inch fault
(b) 1.0 inch fault

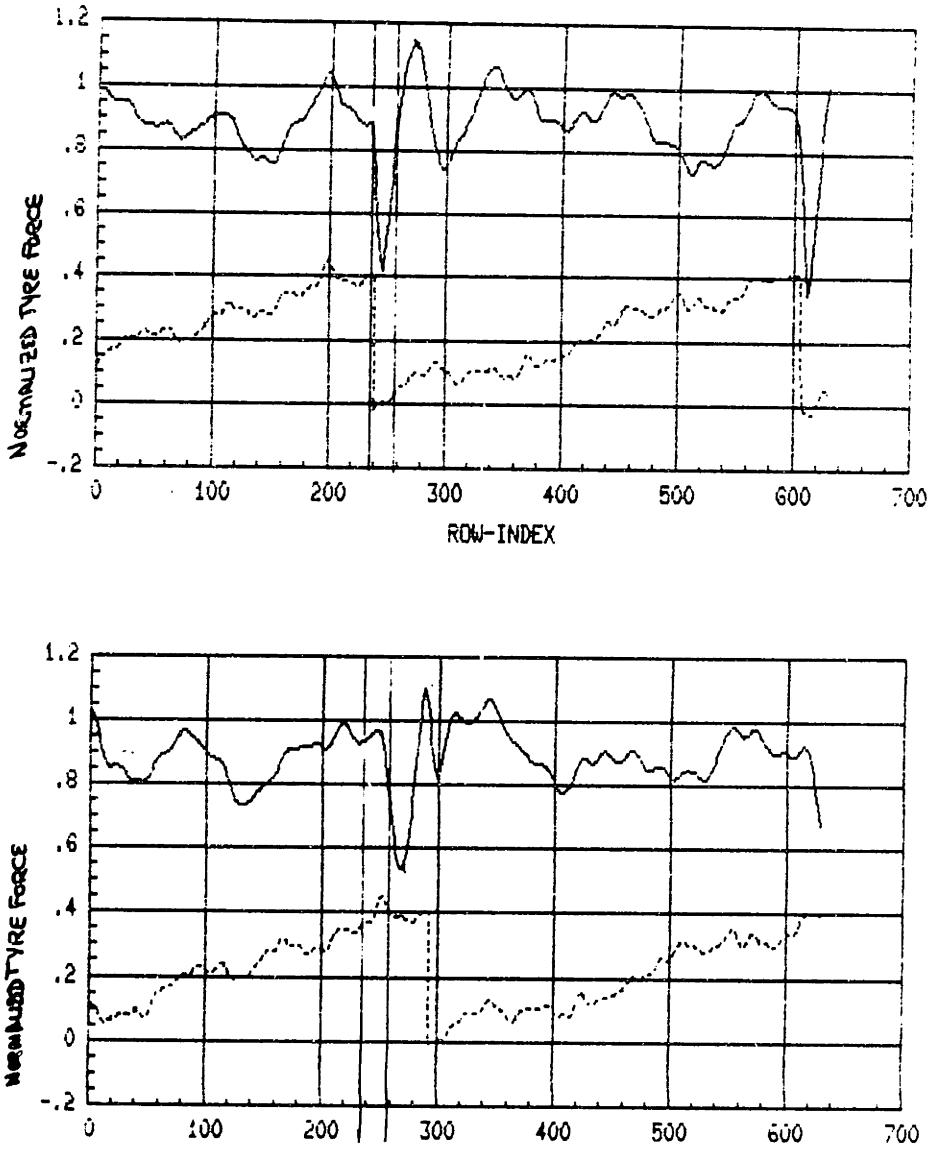

Figure 3.9 Walking-beam Tandem axle response to fault
(a) Lead axle
(b) Trailing tandem axle

vehicle initial conditions when the axle encounters the fault at the slab joint and also the road surface roughness (slope variance of $10 \times 10^{-6} in^2$).

Note that for faults of 1 in. or larger the signal becomes less random. That is the initial conditions of the vehicle at the fault become less important and the tire force profile is dominated by the occurence of the fault.

For our particular runs we can consider the tire force profile to be a stationary process if we neglect the start up and the end of the vehicle run. This means that we can apply normal FFT procedures [12,13], to determine the spectral content of the tire force profiles. However, for real field data where the joint faults will differ and the slab length will not be the same the response may not necessarily remain stationary. Non-stationary techniques of obtaining spectra such as time varying power spectra and time averaged power spectra also involve digital filtering of the signal and are outlined in Bendat & Piersol [14].

3.1.1 Aggregate Loading

In order to quantify the effects of dynamic wheel loads on pavements it is necessary to examine the accumulated damage due to all the axles of a vehicle passing over a particular point in the pavement. Deterioration of the pavement will be initiated at and propagate from locations at which high stresses occur.

This particular method divides the individual slabs into equally sized sections sufficiently small to enable resolution of the peak forces up to the highest frequencies of interest. The aggregate force at a particular point K is defined by

$$F_K = \sum_{j=1}^{N_a} P_{jk} \qquad k = 1,2,3\ldots,N_s \tag{3.1}$$

$N_a =$ Number of axles

$N_s =$ Total number of stations along slab length

The mean aggregate load was determined by averaging the aggregate load over several slabs (typically 20 slabs):

$$\hat{F}_K = \frac{1}{n}\sum_{i=1}^{n}\sum_{j=1}^{N_a} P_{ijk} \qquad k = 1,2,3,\ldots,N_a \tag{3.2}$$

where $n =$ number of slabs.

The mean aggreage load is then normalized by the vehicle static load.

It is important to note that the aggregate force at a point depends on each axle load that passes by. As a result, the maximum aggregate force will not necessarily occur at the same location as the maximum force generated by any axle.

3.2 Linearized Vehicle Model: Frequency Domain Analysis

It is instructive to consider an analysis of the linear model of the tractor semi-trailer (figure 3.10) using frequency domain techniques before attempting to comprehend the time response of the fully nonlinear model.

The mass, stiffness and damping matrices are constructed and the equations of motion may be written in the form below

$$M\ddot{y} + D\dot{y} + Ky = Fu \tag{3.3}$$

where,

y = system state vector;

u = input vector;

M = mass matrix;

D = damping matrix;

K = stiffness matrix;

F = input matrix.

For the linear model [15], the natural frequencies and their corresponding mode shapes are illustrated in figures 3.11 - 3.15 and Table 1.

The response of the linear system to a general input will be a combination of all the mode shapes. The weighting of each mode in the response will depend on the nature of the input itself. For example, it is intuitive that a step input to the steer axle will primarily excite the steer axle wheel mode and the tractor pitch mode. A step input to the drive axle on the other hand, primarily excites the wheel mode and tractor-trailer out phase pitch. The same input to the rear axle will excite the wheel mode and mode shapes 2 and 3. It is also important to note that the damping ratio associated with the wheel modes ($\varsigma = 0.2$) are much larger than those of the body modes ($\varsigma = 0.05$) because the former mode deflects the leaf-springs.

There will be differences between the frequencies calculated using the linear model and those obtained in the fully nonlinear model. Differences in the time response of the two systems are outlined below. Peak loading point along the slab for a vehicle travelling at 35 mph due to each mode is calculated in table [2].

In a comparison of spectral densities of tire force profiles generated by a linear and nonlinear model of a 4-axle vehicle model Cebon [11], notes the following distinctions:

(1) The leaf-spring on the linear model provides considerably more damping than the linearized equivalent for low frequencies (1-5 Hz).

(2) The tire forces generated by the trailer axles are dominated by the lightly damped trailer pitch mode. The linearized stiffnesses are too high which accounts for a decreased trailer pitch frequency for the nonlinear model.

(3) At higher freqeuncies, harmonics of the leaf-spring forces at the major peaks increase the tire forces for the nonlinear model.

Since the primary concern of our study is to determine pavement damage, it is essential therefore, to use a fully nonlinear vehicle model to provide a realistic representation of the pavement/vehicle interaction.

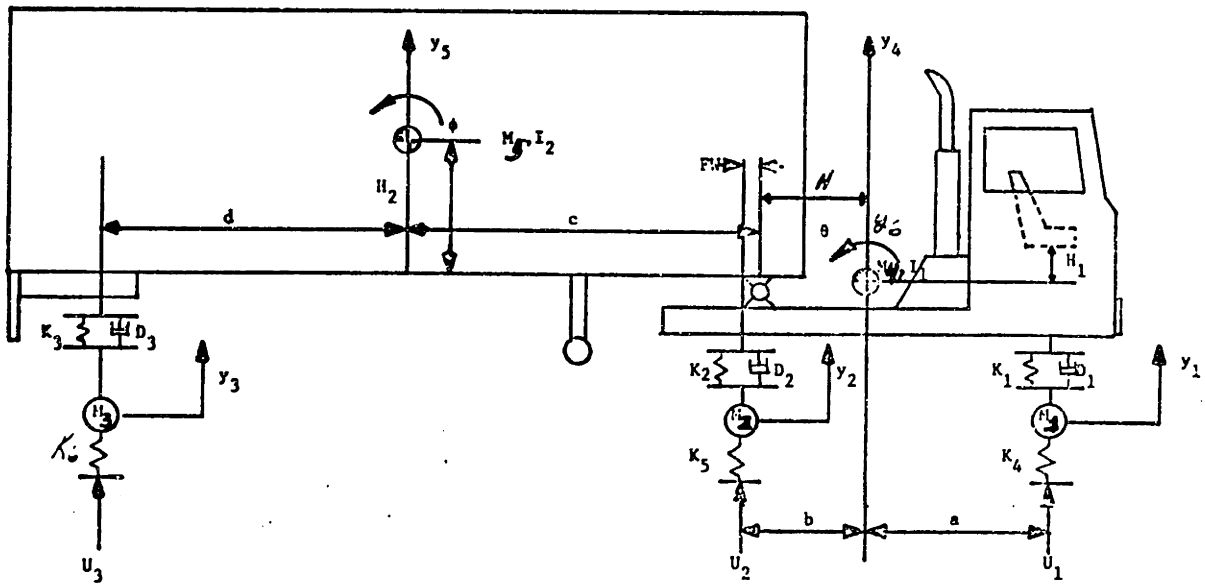

Figure 3.10 Linear Model of Tractor Semi-Trailer

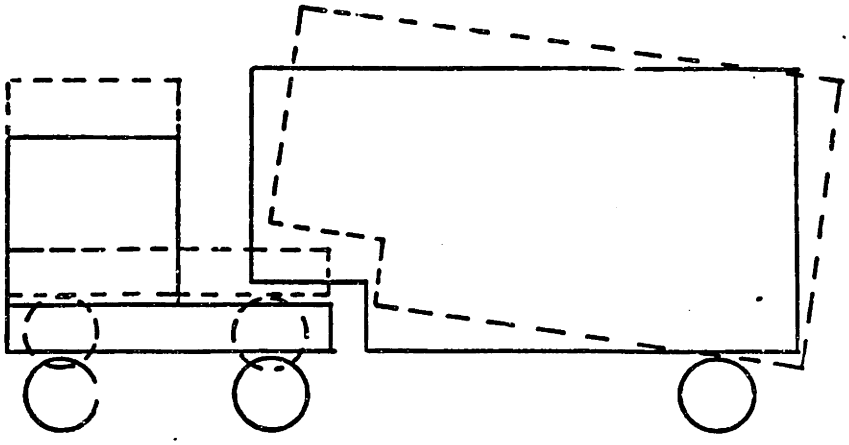

MODE SHAPE 1 WITH FORWARD FIFTH WHEEL POSITION (FW)
FW = 2.5 ft., Frequency = 1.6 Hz, Tractor Heave

Fifth Wheel Location (FW) ft	-.5	.5	1.5	2.5
First	1.8 Hz	1.8	1.7	1.6
Second	2.0	2.2	2.4	2.7
Third	3.5	3.6	3.7	3.9
Fourth	8.7	8.7	8.7	8.7
Fifth	11.3	11.3	11.4	11.4
Six	14.6	14.6	14.6	14.6

FREQUENCY

VARIATIONS IN RESONANT FREQUENCIES AS A FUNCTION OF FIFTH WHEEL POSITION

Figure 3.11

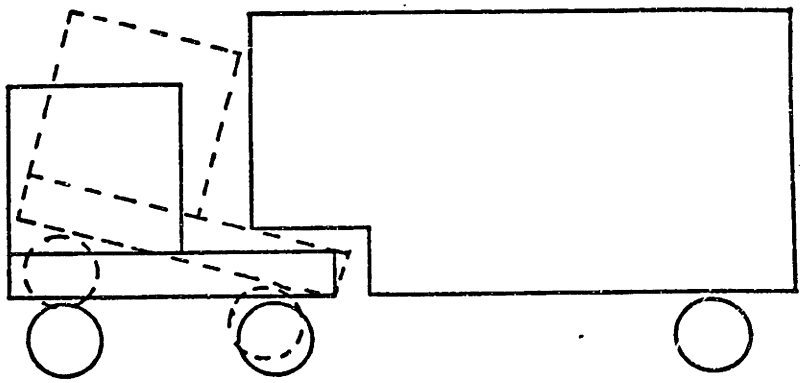

MODE SHAPE 1 WITH REARWARD FIFTH WHEEL POSITION (FW)
FW = .5 ft, Frequency = 1.8 Hz, Tractor Heave and Pitch

Figure 3.12

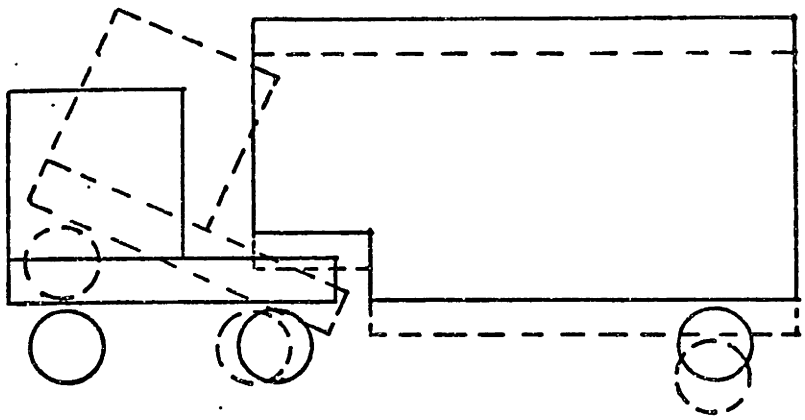

MODE SHAPE 2. TRACTOR PITCH
Frequency = 2.2 Hz When FW = .5 ft
Frequency = 2.7 Hz When FW = 2.5 ft

Figure 3.13

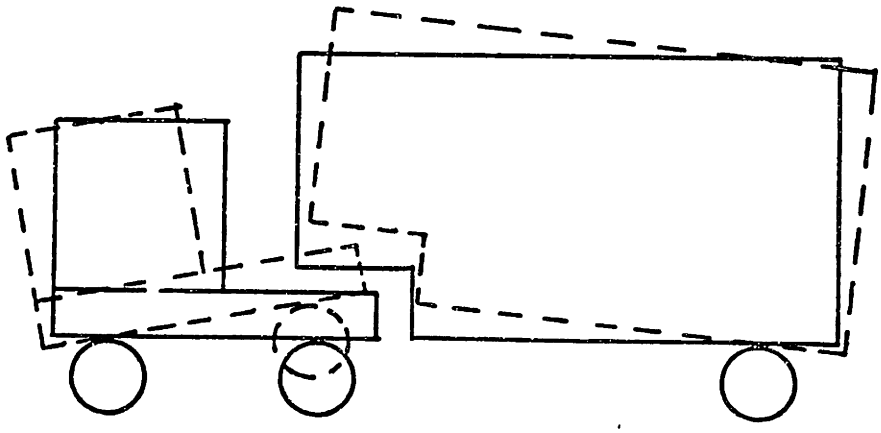

: MODE SHAPE 3. TRACTOR AND TRAILER PITCH OUT OF PHASE.
Frequency = 3.6 Hz When FW = .5 ft
Frequency = 3.9 Hz When FW = 2.5 ft

Figure 3.14

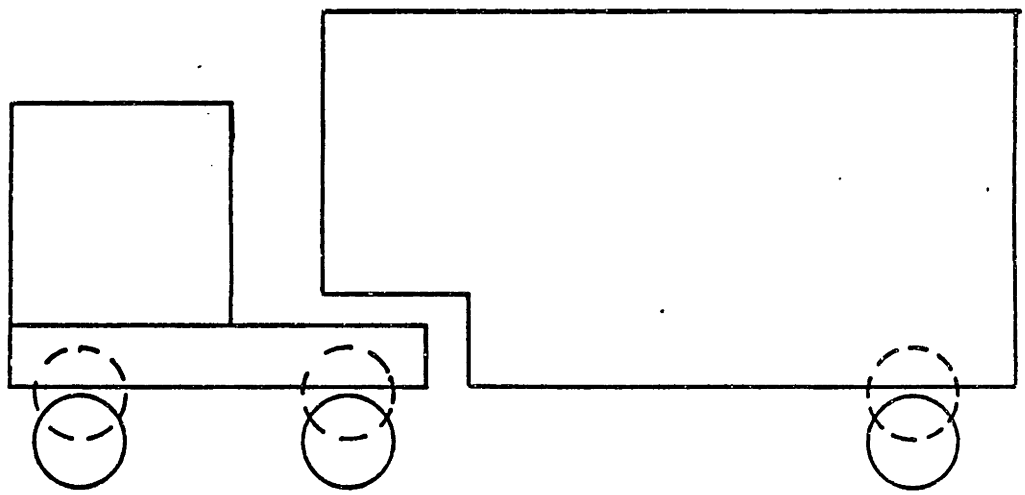

MODES 4, 5 and 6, AXLE RESONANCES. FRONT AXLE HEAVE FREQUENCY = 8.7 Hz DRIVING AXLE HEAVE FREQUENCY = 11.3 Hz. TRAILER AXLE HEAVE FREQUENCY = 14.6 Hz.

Figure 3.15

Mode	f (Hz)	λ (ft)	1st Peak	2nd Peak
1	1.8	28.5	21.4	49.9
2	2.8	13.5	10.1	23.6
3	4.8	10.7	8.0	18.7
4	10	5.13	3.9	9.0
5	15	3.42	2.6	6.0

Table 2 Peak loading Locations due to each Mode

3.3 Nonlinear Single Axle Vehicle Model

3.3.1 Introduction

The tire force profile of each of the axles is analyzed separately and the dominant frequencies identified. We then proceed to determine which axle is responsible for peak loading in different locations along the slab. Finally we aggregate the tire forces at discrete stations along the slab and determine regions of elevated loading and the effect of varying both vehicle and pavement parameters.

3.3.2 Steer Axle Response

The steer axle of a tractor semi-trailer is usually loaded between 6 - 10 kips. The interface with the road is thus a single tire. The stresses that result from the steer axle are much smaller than those produced by the drive and rear axles (18 kips load). The peak stresses produced by the steer axle nevertheless, do damage to the pavement and must be taken into account in a Miner's law accumulated damage type of criterion.

The steer axle response is dominated primarily by the tractor pitch mode (approx. 3 Hz) and a 10 - 15 Hz wheel mode. The wheel mode is damped not only by inherent leaf-spring damping but also by the shock absorber damping that is usually placed at the steer axle. The wheel mode typically produces a peak loading about 2 ft. away from the slab transverse edge. The magnitude of this peak may be significant relative to the other peaks if the axle is lightly loaded (5.5 kips in our baseline model). This mode however, is highly damped, and will not contribute significantly to further peaks. The magnitude of the peak due to the wheel mode is also highly dependent on the initial conditions of the axle on encountering the fault.

The lower frequency tractor pitch mode (3.8 Hz) results in dominant peaks at about 7 ft. and another about 20 ft. from the transverse joint (figure 3.16).

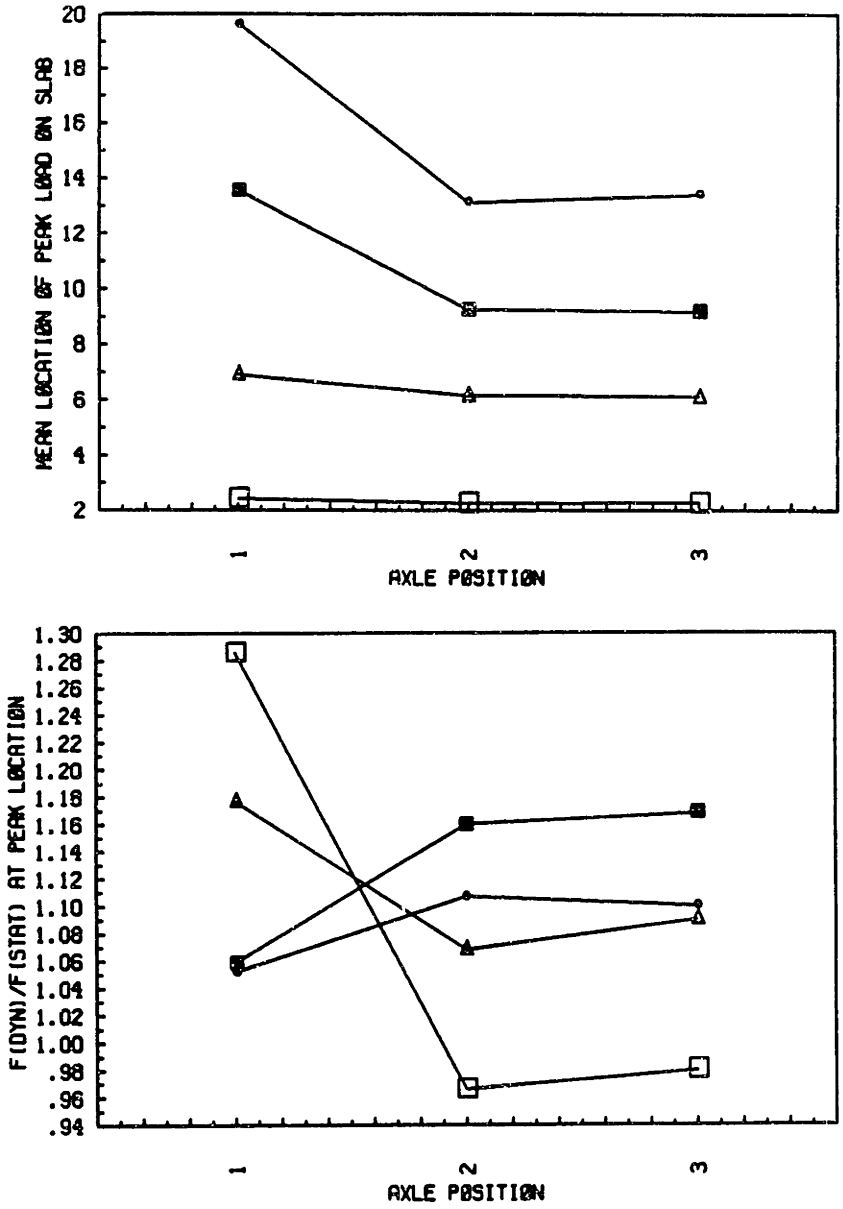

Figure 3.16 Single axle suspension
(a) Location of peak load
(b) Magnitude of peak load by axle

3.3.3 Drive and Rear Axle Responses

Since the drive and rear axles carry a much larger static loading, wheel hop is unlikely to occur for smaller joint faults (less than 0.5 in.). The first peak loading of the slab which is due to the wheel mode, is not significant (generally at or less than the axle static loading, figure 3.8). However, the wheel mode is important when superposed with the dominant body mode response leading to the most significant loading at 10 ft. from the slab transverse joint.

3.3.4 Effect of Average Suspension stiffness

While altering the drive axle suspension stiffness did not have a significant effect on the location of the mean peak loadings it did alter the mean peak force. By making the suspension stiffer, the wheel mode is not excited as much and an input to the tyre is transmitted to excite more of the body mode.

The aggregate force plots of figure 3.18 illustrate the above results, indicating that a 50 % reduction in average leaf-spring stiffness leads to a 4 % reduction in aggregate loading in the region close to the transverse joint, but produces a 4 % increase in aggregate loading over the 8 ft. - 12 ft. region of the slab and at the far edge of the slab.

3.3.5 Effect of Leaf-Spring Damping

Decreasing β is equivalent to increasing the coulomb friction level in the leaf-spring thereby increasing the damping for a large amplitude oscillations [4]. A reduction in coulomb friction level translates to more of the input exciting the wheel mode rather than the body mode. Note the similarity to varying the leaf-spring stiffness.

The aggregate force plot of figure 3.21 indicates the large increase in peak loading for higher values of β (10×10^{-3} ft). Increases in aggregate loading of 18 % to the first peak region occur for a 10 % decrease in β.

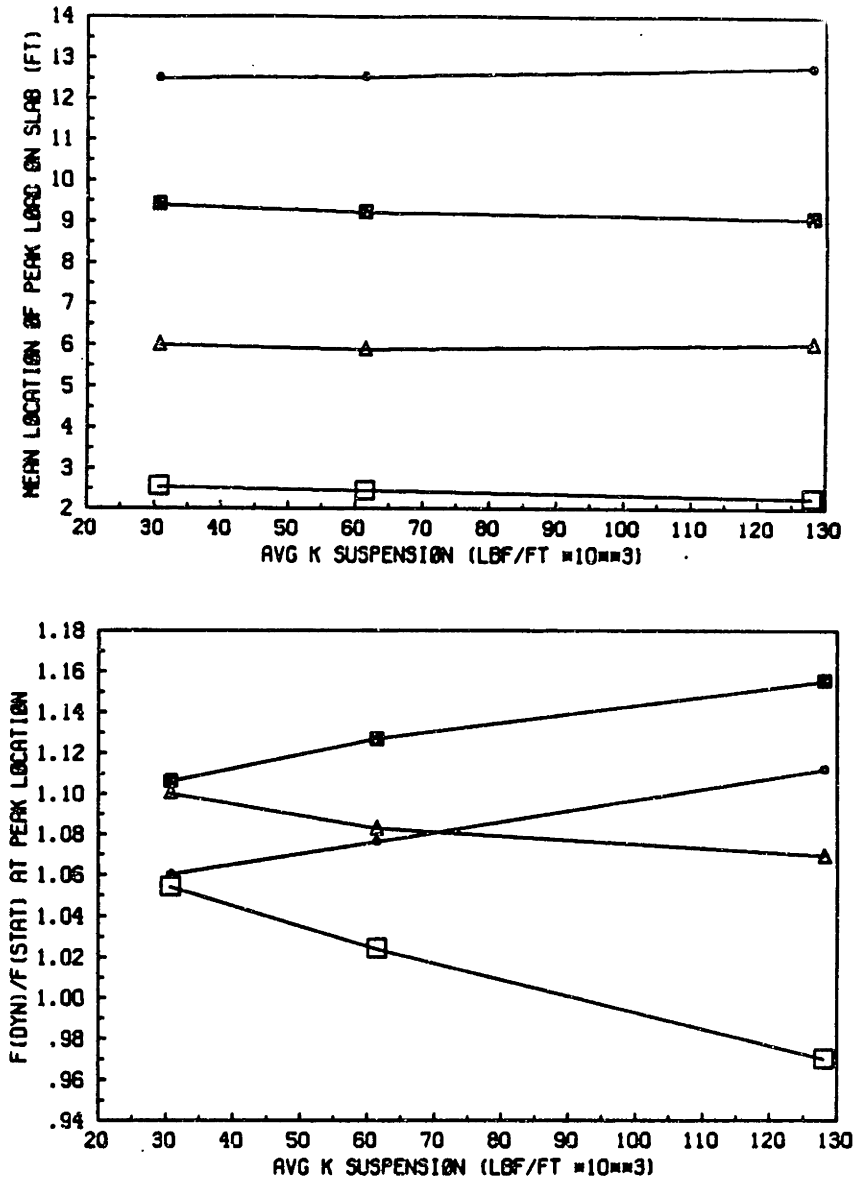

Figure 3.17 Effect of suspension stiffness on
(a) Location of peak load
(b) Magnitude of peak load

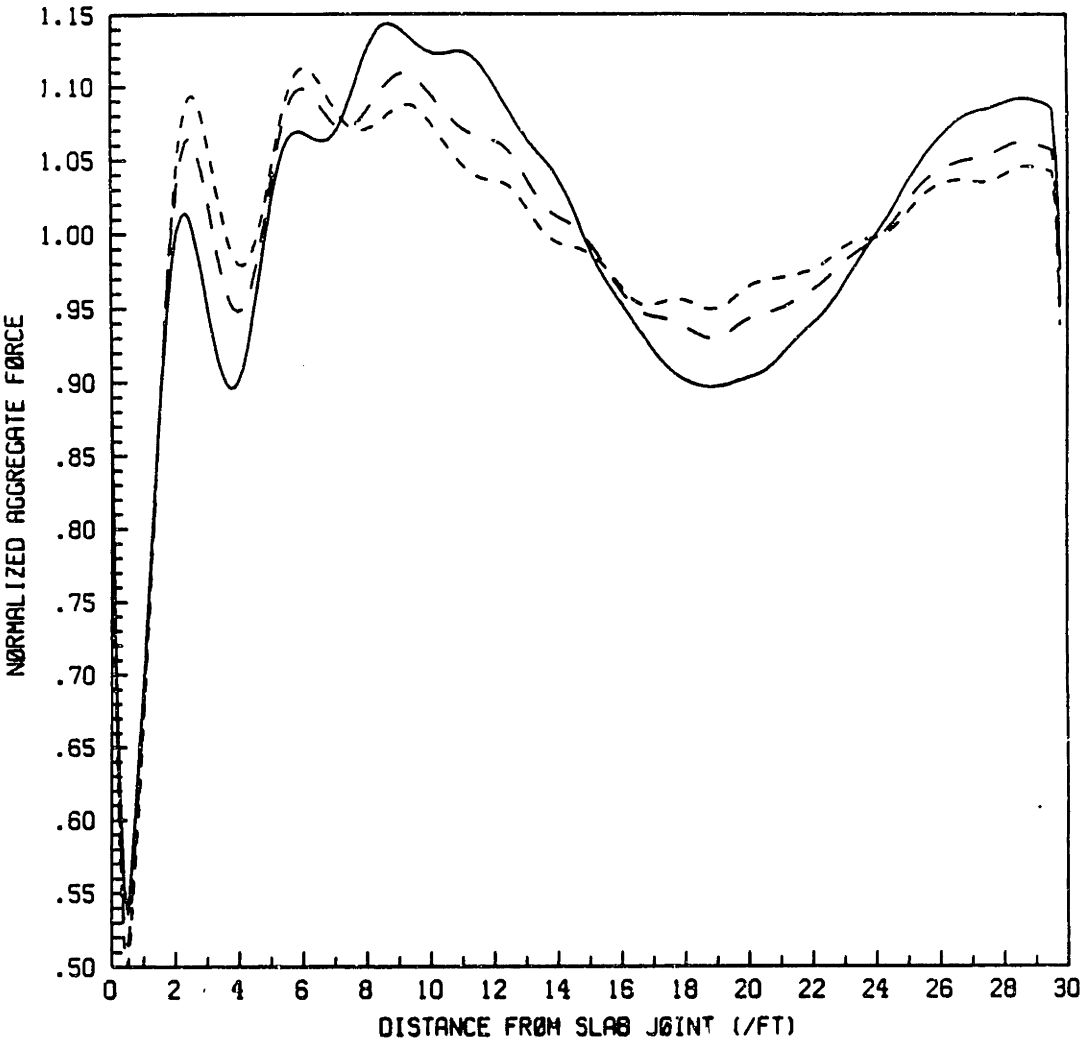

Figure 3.18 Effect of suspension stiffness on aggregate loading
(a) 128,000 lbf/ft (std)
(b) 61200 lbf/ft
(c) 30600 lbf/ft

Therefore, a β value of or less than 4×10^{-3} ft. is desirable. Note however that this conclusion is based on a joint fault height of $\frac{1}{2}$ inch and may differ as the joint fault becomes smaller. In the case of flexible pavements we determined that there was an optimum value of β close to 4×10^{-3} ft.

3.3.6 Effect of Joint Fault Magnitude

The magnitude of the joint fault did not affect the mean position of drive axle peak loads, however, there are smaller variances (in location) associated with larger fault magnitudes. The magnitude of the peaks increase with the increase in joint fault (31 % per inch as in figure 3.22).

The aggregate force plot of figure 3.24 indicates that there is a very small (3 %) difference in loading for joint faults less than 0.25 in., whereas there is up to 20 % increases for a change in fault from 0.25 in. to 0.75 in.

3.3.7 Effect of Slab Roughness

Roughness of the slab was varied by changing the slope variance between $1.7 \times 10^{-6} in^2$ and $22 \times 10^{-6} in^2$. A slope variance higher than 22×10^{-6} would imply that the pavement had ruttted. Rutting, however, is not a distress mechanism in rigid pavements [16].

The effect of slab roughness is to change the vehicle initial conditions at the joint fault and also to excite additional vehicle dynamics leading to larger variances in location and magnitudes. Changes in magnitudes of the peaks (4%) are insignificant over the range of roughnesses associated with rigid pavement surfaces.

3.3.8 Effect of Slab Length

Our baseline vehicle model has a steer to drive wheelbase of about 11.5 ft and a drive to rear wheelbase of 19.5 ft. Therefore, a 10 ft joint spacing will result in almost simultaneous inputs into each of the three axles exciting predominantly the vehicle bounce mode. For a joint spacing of 20 ft we have a small time delay

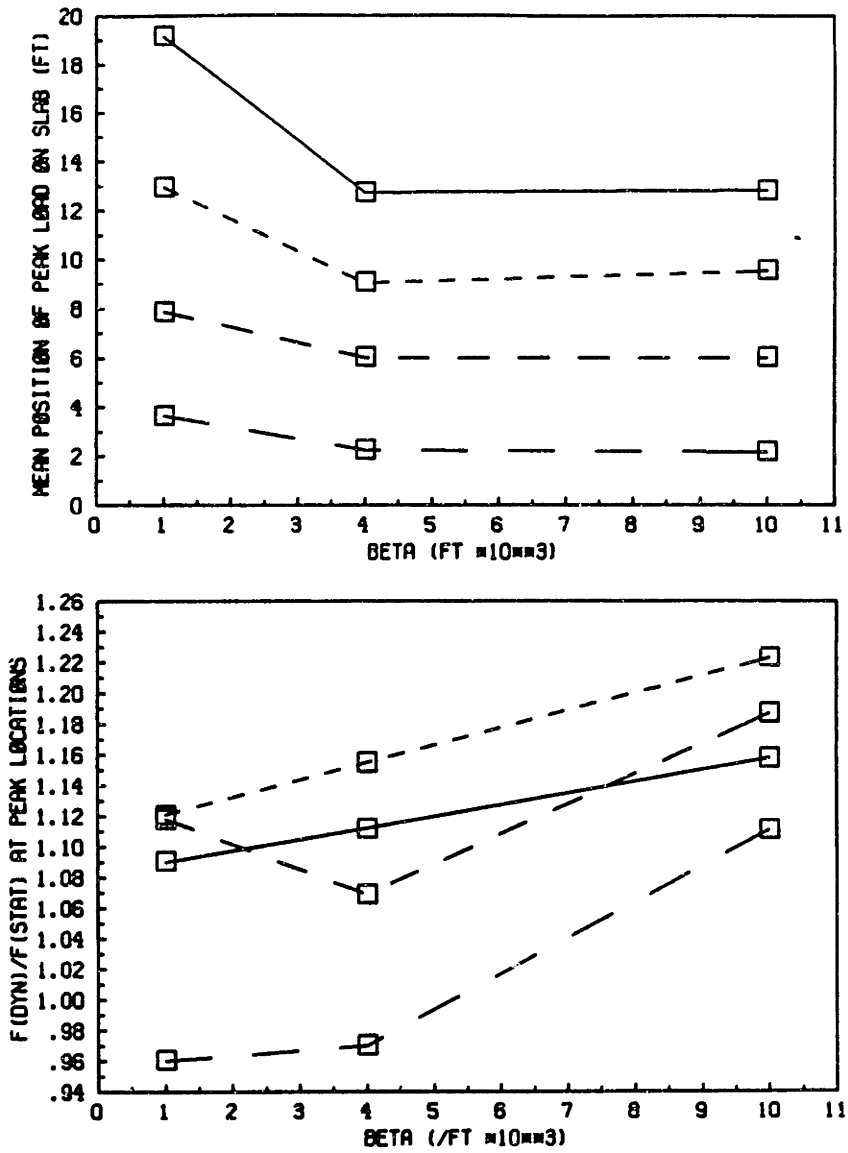

Figure 3.19 Effect of β parameter on
(a) location of peak force
(b) magnitude of peak force

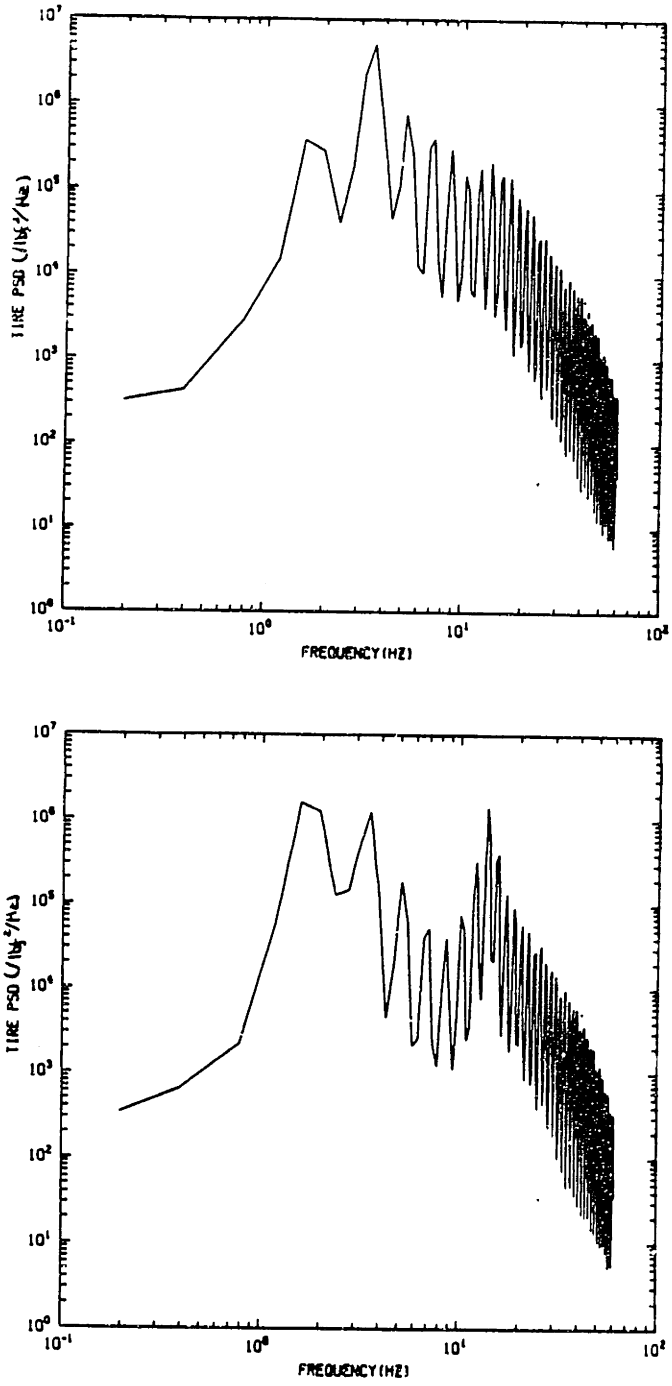

Figure 3.20 Effect of β parameter
(a) $\beta = 1 \times 10^{-3} ft$
(b) $\beta = 10 \times 10^{-3} ft$

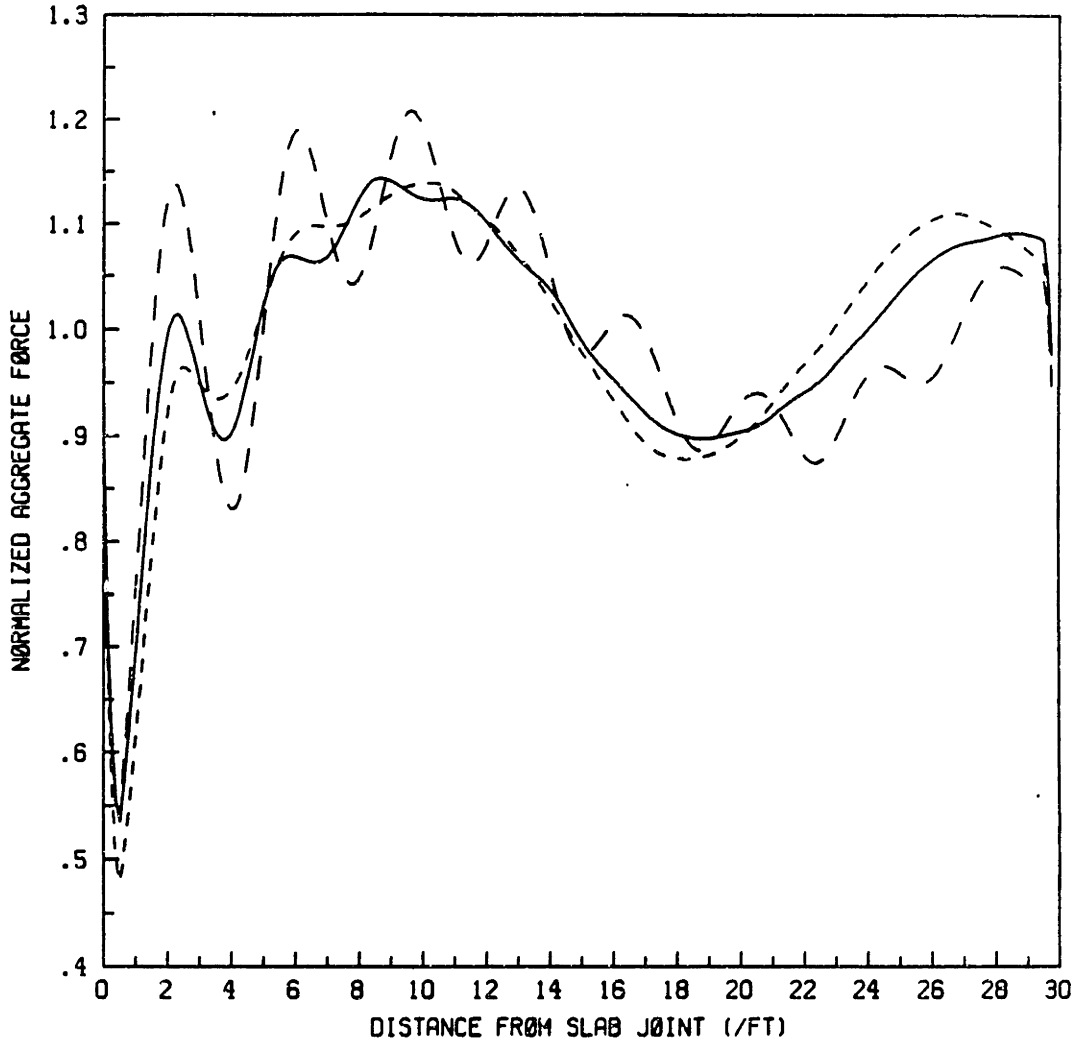

Figure 3.21 Effect of β parameter
- – – – – (a) $\beta = 1 \times 10^{-3} ft$
- ——— (b) $\beta = 4 \times 10^{-3} ft$
- — — — (b) $\beta = 10 \times 10^{-3} ft$

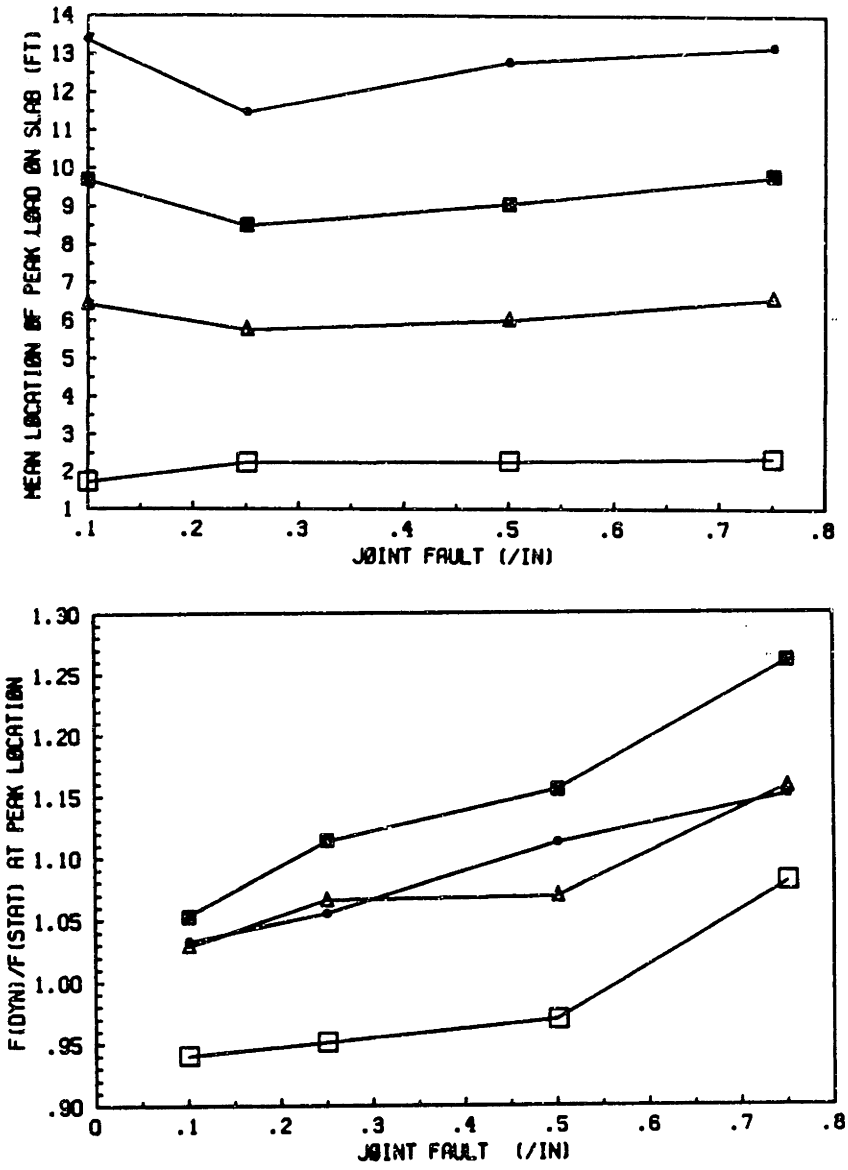

Figure 3.22 Effect of Joint Fault magnitude on
(a) location of peak force
(b) magnitude of peak force

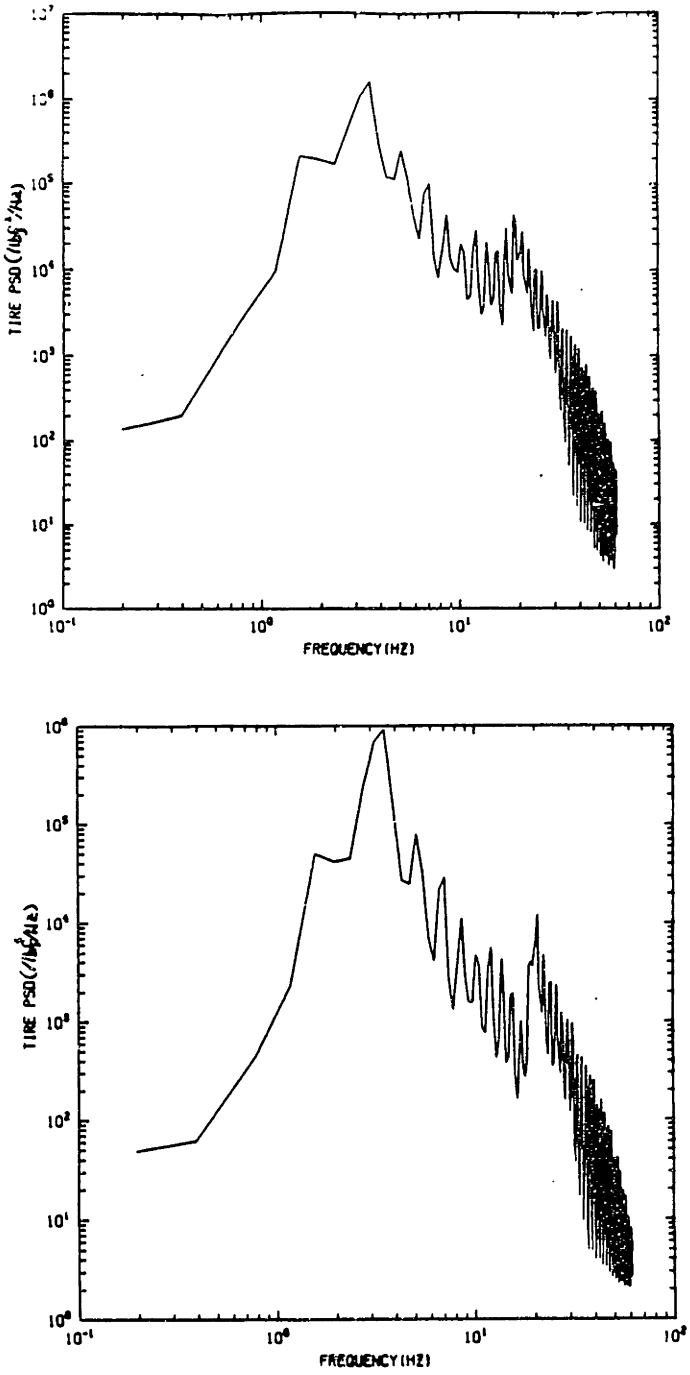

Figure 3.23 Effect of Joint Fault magnitude on PSD
(a) $\frac{1}{4}$ inch fault
(b) $\frac{1}{10}$ inch fault

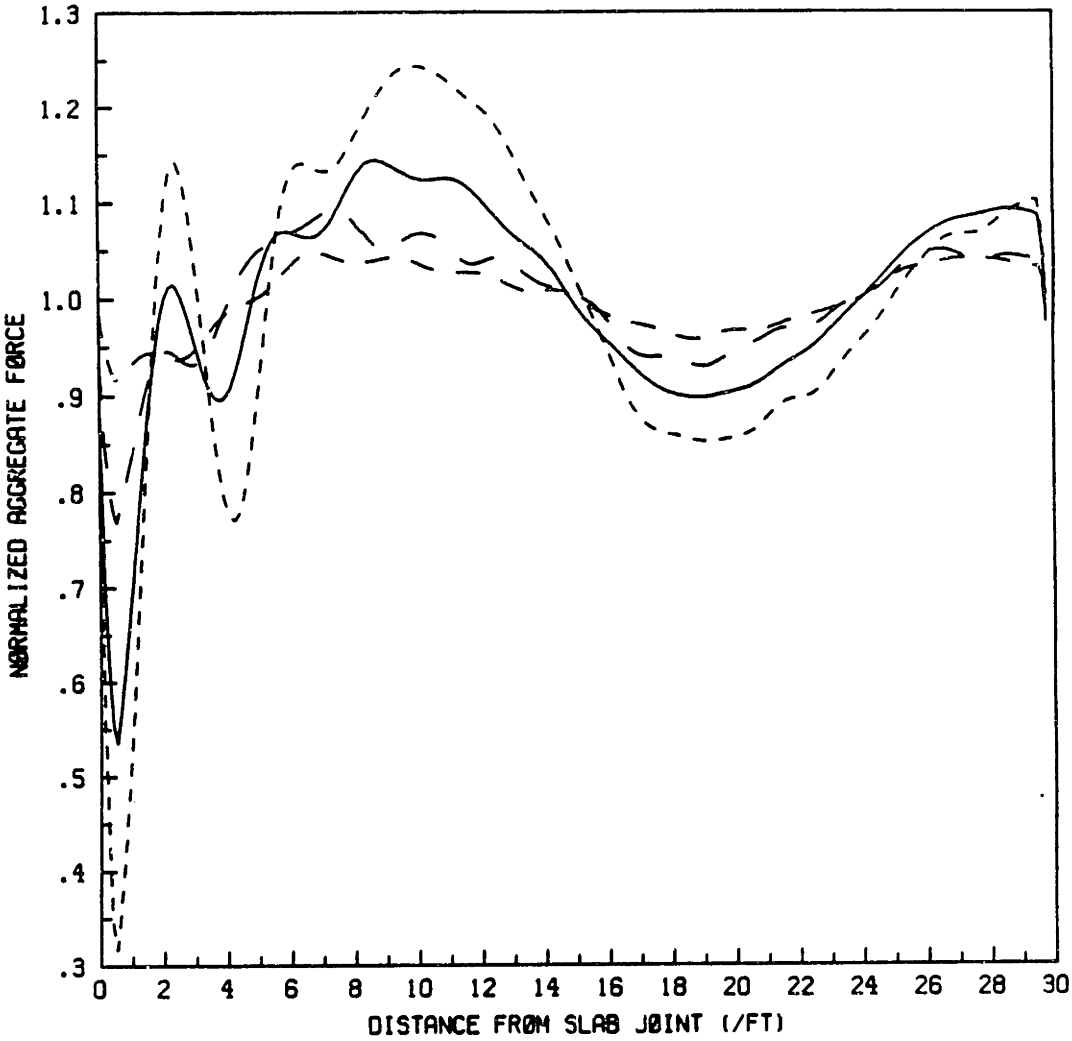

Figure 3.24 Effect of Joint Fault magnitude on Aggregate loading
- ------ (a) 0.75 inch fault
- ——— (b) 0.5 inch fault
- — — — (c) 0.25 inch fault
- — — (d) 0.1 inch fault

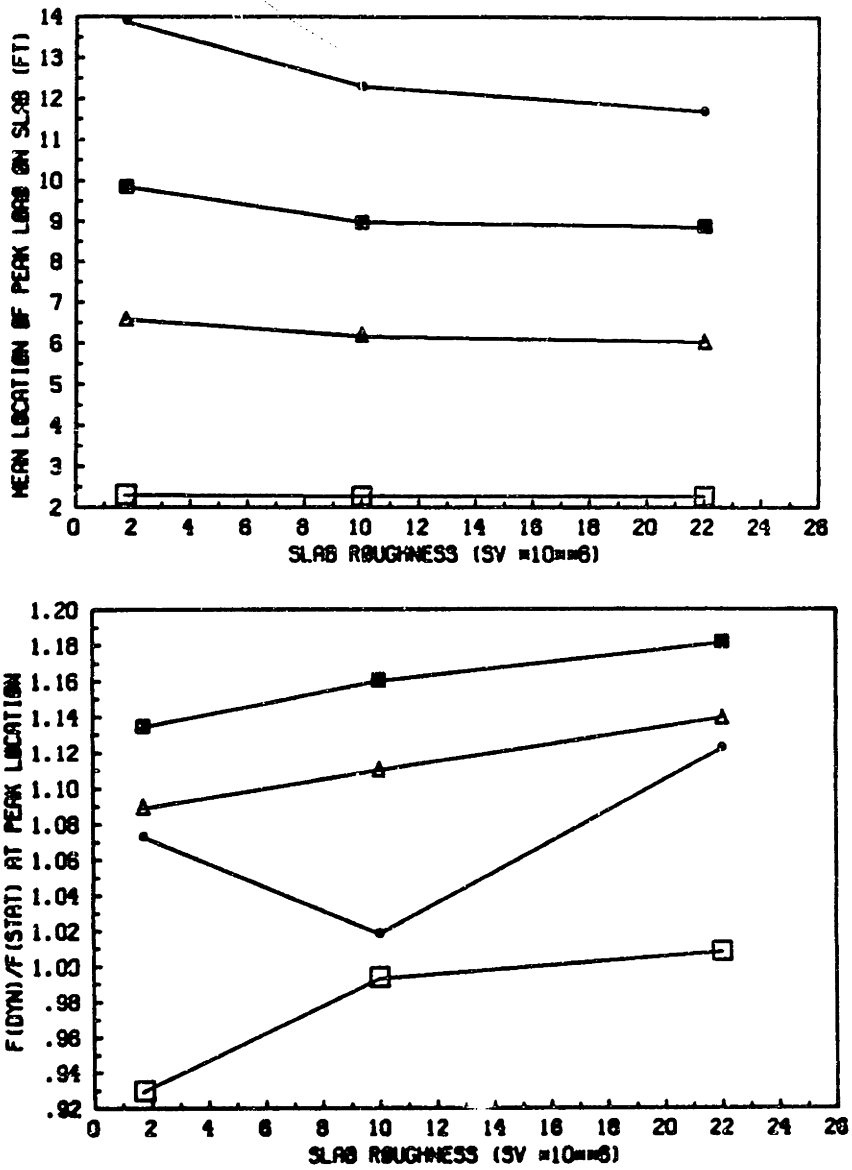

Figure 3.25 Effect of Slab roughness on
(a) location of peak force
(b) magnitude of peak force

between inputs to the drive and rear axles which excites trailer bounce and tractor pitch modes, which results in the largest pavement loads. The 30 ft and 45 ft joint spacing do not excite the out-of-phase tractor/trailer pitch as much (figure 3.26).

The aggregate force plots of figure 3.27 indicate that the joint spacing of 20 ft produce a 12 % increase in aggregate loading in the 10 ft region of the slab, in comparison to the 30 ft and 45 ft slab lengths but reduces the loading at the subsequent slab by up to 20 %.

3.3.9 Effect of Slab Warping

For our baseline vehicle velocity (35 mph) and slab length (30 ft) the warping of the slab corresponds to an input to the system at a frequency of 1.7 Hz ($f = \frac{v}{\lambda}$) which coincides with the tractor bounce and pitch mode natural frequency.

The peak loading regions for each indiviual axle shifts away from the slab joint for increased slab warping and the magnitude of the loading in the first and last third of the slab decreases, whereas the middle third section of the slab experiences increased loading up to 10% higher for each indiviual axle.

The aggregate loading figure 3.28 illustrates the shift in location of the peak loading due to exciting the lower frequency body mode. The increase in aggregate loading is up to 25% for a slab radius of curvature of 1350 ft. (equivalent to 1 in. deflection at the centre of a 30 ft long slab)

3.3.10 Effect of Vehicle Velocity

The location of the peaks increase with the increase of vehicle velocity (figure 3.29). This is expected since the peak location is proportional to the spatial wavelength ($\lambda = \frac{v}{f}$).

The largest peak which we attribute to the out-of-phase tractor/trailer however, has the largest magnitude for a vehicle velocity around 55 mph. At this velocity the input forcing frequency each axle experiences is given by

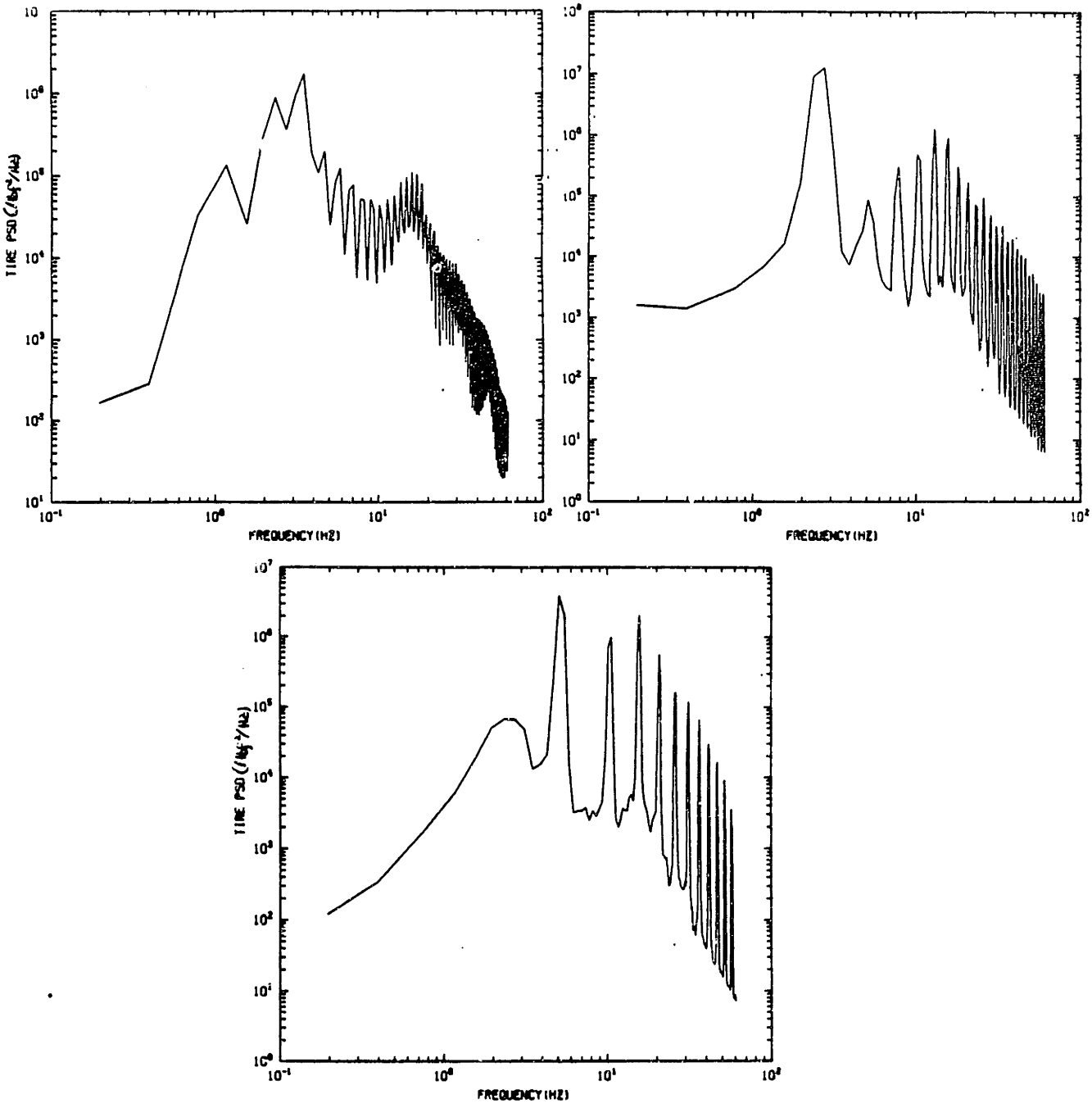

Figure 3.26 Effect of slab length on PSD
(a) 45 ft
(b) 20 ft
(c) 10 ft joint spacing

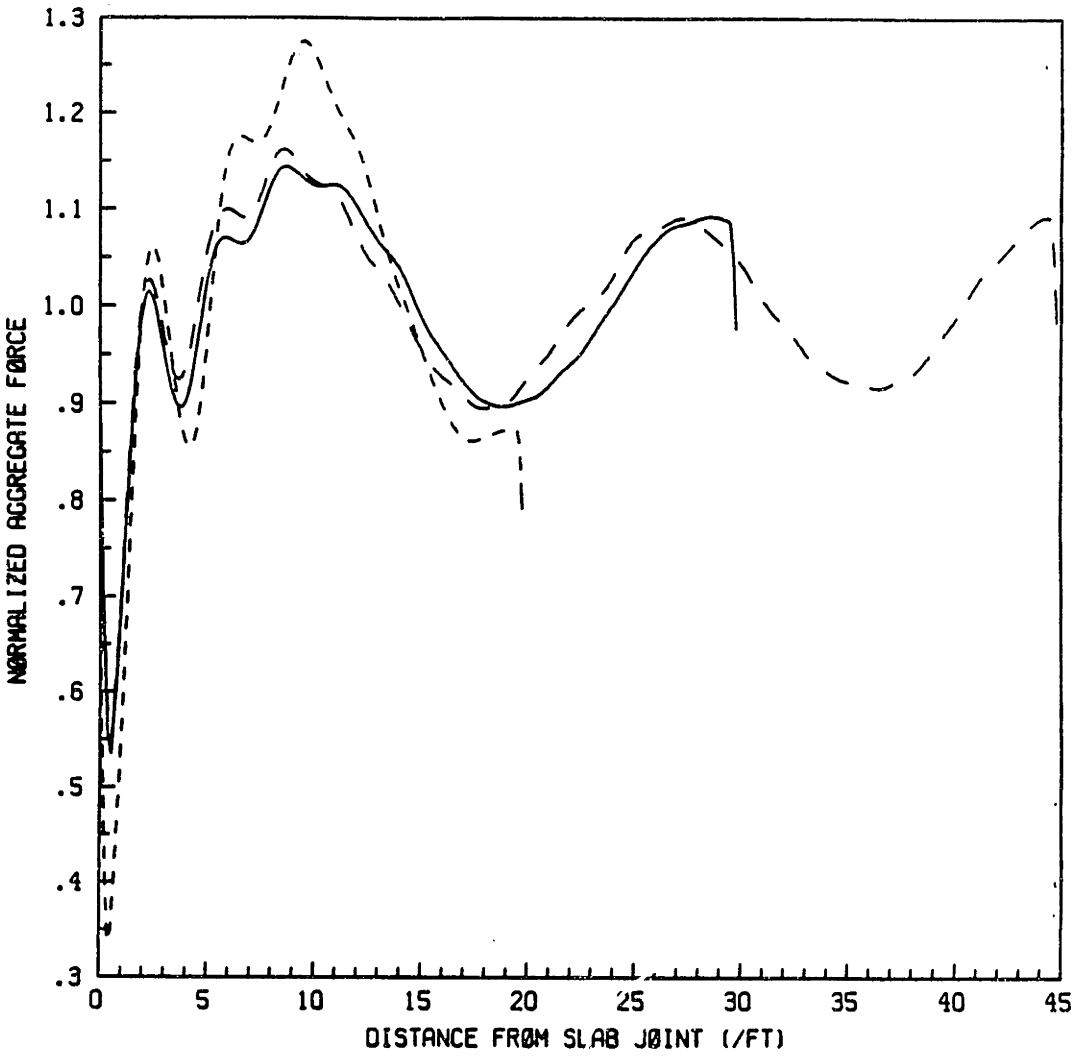

Figure 3.27 Effect of slab length on aggregate loading

$$f = \frac{v}{l} = 2.7Hz$$

where:

l = joint spacing.

As mentioned earlier for our particular slab length and vehicle wheelbase we obtain simultaneous inputs to the steer and rear axles which results in exciting the tractor/trailer out-of-phase pitch mode. This excitation will be amplified if the forcing frequency correponds to the natural mode frequency or a multiple thereof.

Figure 3.30 indicates that the effect of higher vehicle velocities is to load the middle third of the slab rather than the first third of the slab. A vehicle velocity of 55 mph is particularly damaging to the pavement since it leads to aggregate loads of 25% larger than static loading in the middle third region of the slab.

3.3.11 Effect of tire Pressure

Reducing the tire pressure increases the contact length and thus the tire acts more as a filter to road irregularities before they pass through to the suspension. We therefore, expect the vehicle response to diminish with decreasing tire pressure as illustrated in the aggregate force plot [30]. The only significant difference in aggregate loading (14%) occurs for the peak loading at 2 ft from the slab joint. At higher tire pressures the peak locations are closer to the transverse joint and have smaller variances associated with their locations.

3.3.12 Effect of Steer Axle Shock Absorber Damping

The dynamic loading coefficient (DLC) associated with the steer axle is higher than those of the drive and rear axles. This is mainly due to this vehicle having a lightly loaded (5.5 kips) steer axle resulting in wheel hop as the tire goes over the fault.

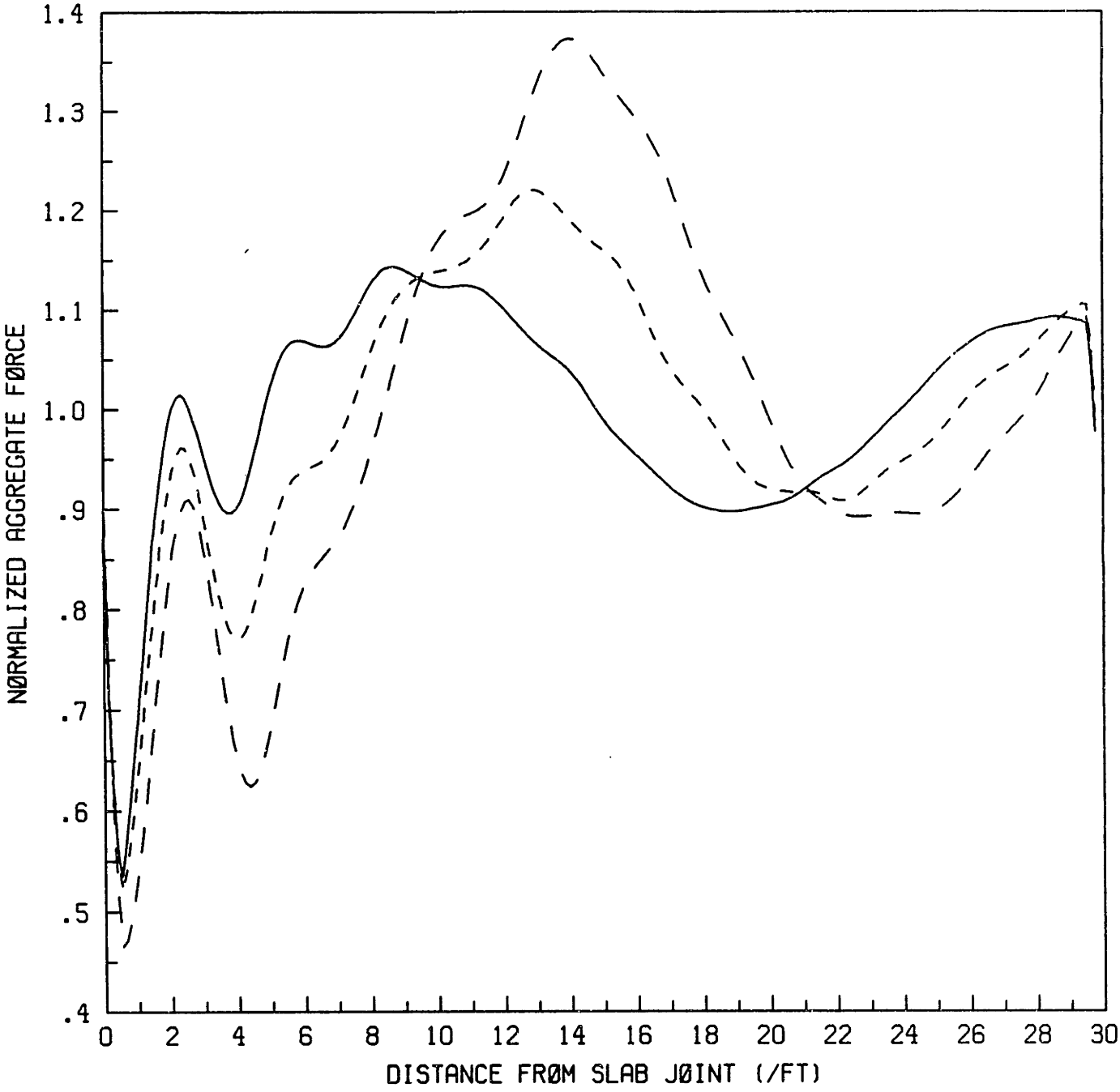

Figure 3.28 Effect of slab warping on aggregate load
——— (a) no warping
– – – – (b) mid-slab deflection $\frac{1}{2}$ inch
— — — (c) mid-slab deflection 1 inch

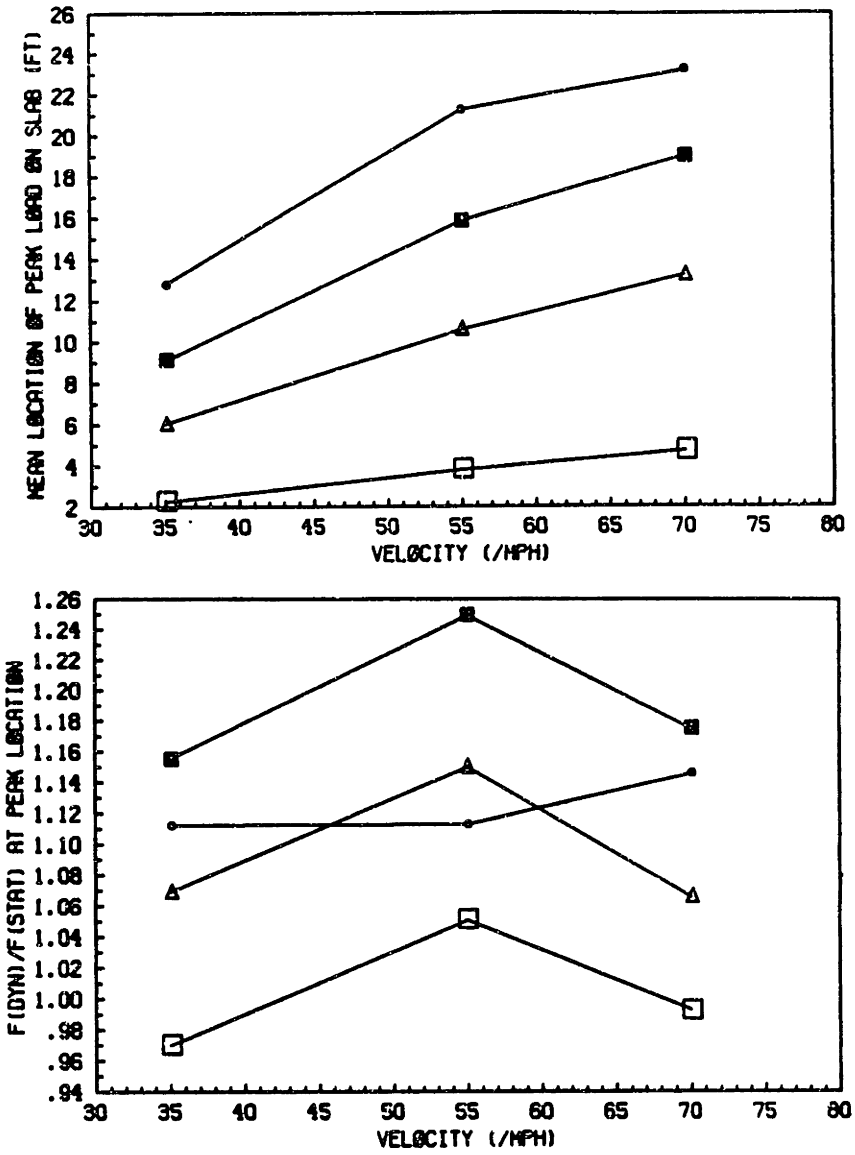

Figure 3.29 Effect of vehicle velocity on
(a) location of peak force
(b) magnitude of peak force

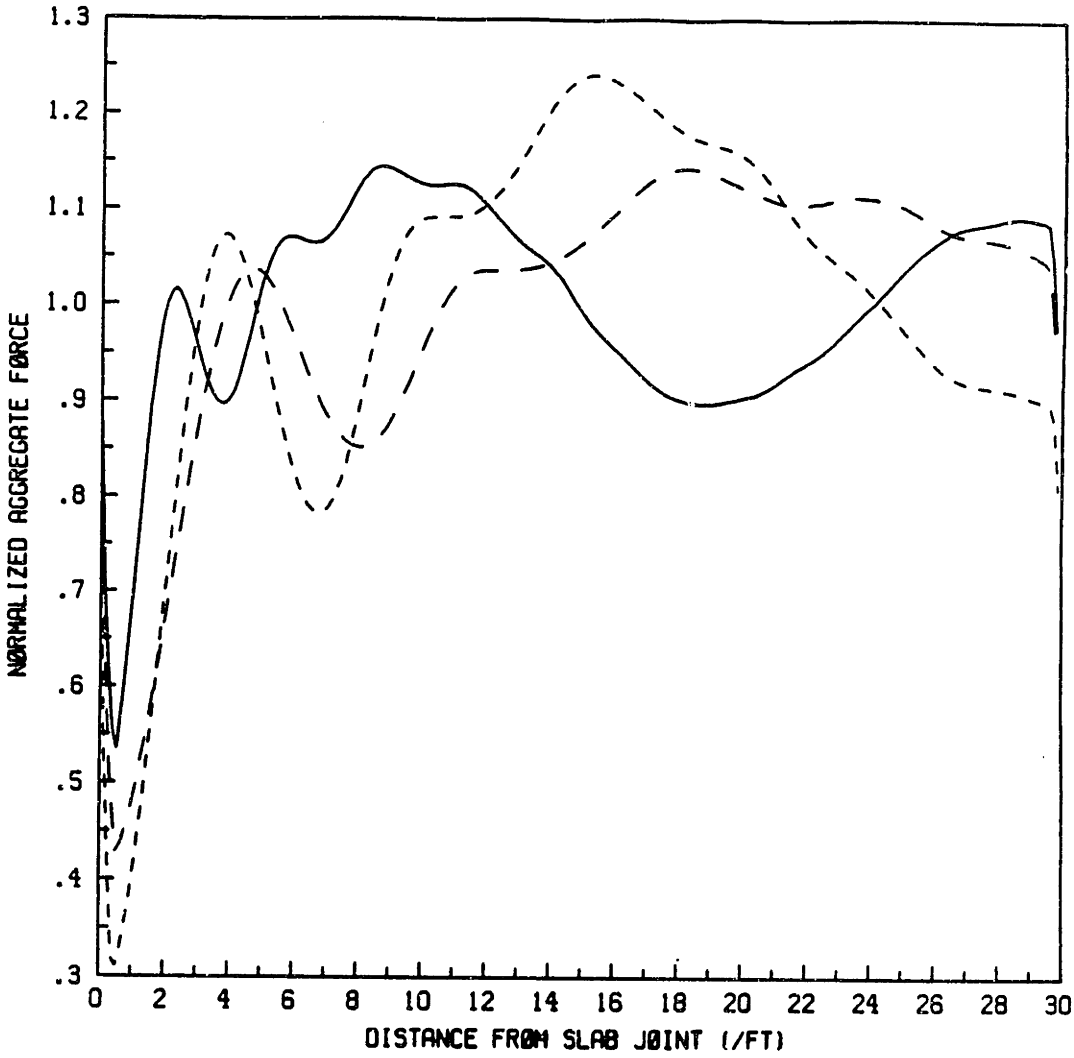

Figure 3.30 Effect of vehicle velocity on aggregate load
——— (a) 35 mph
– – – – (b) 55 mph
— — — (c) 70 mph

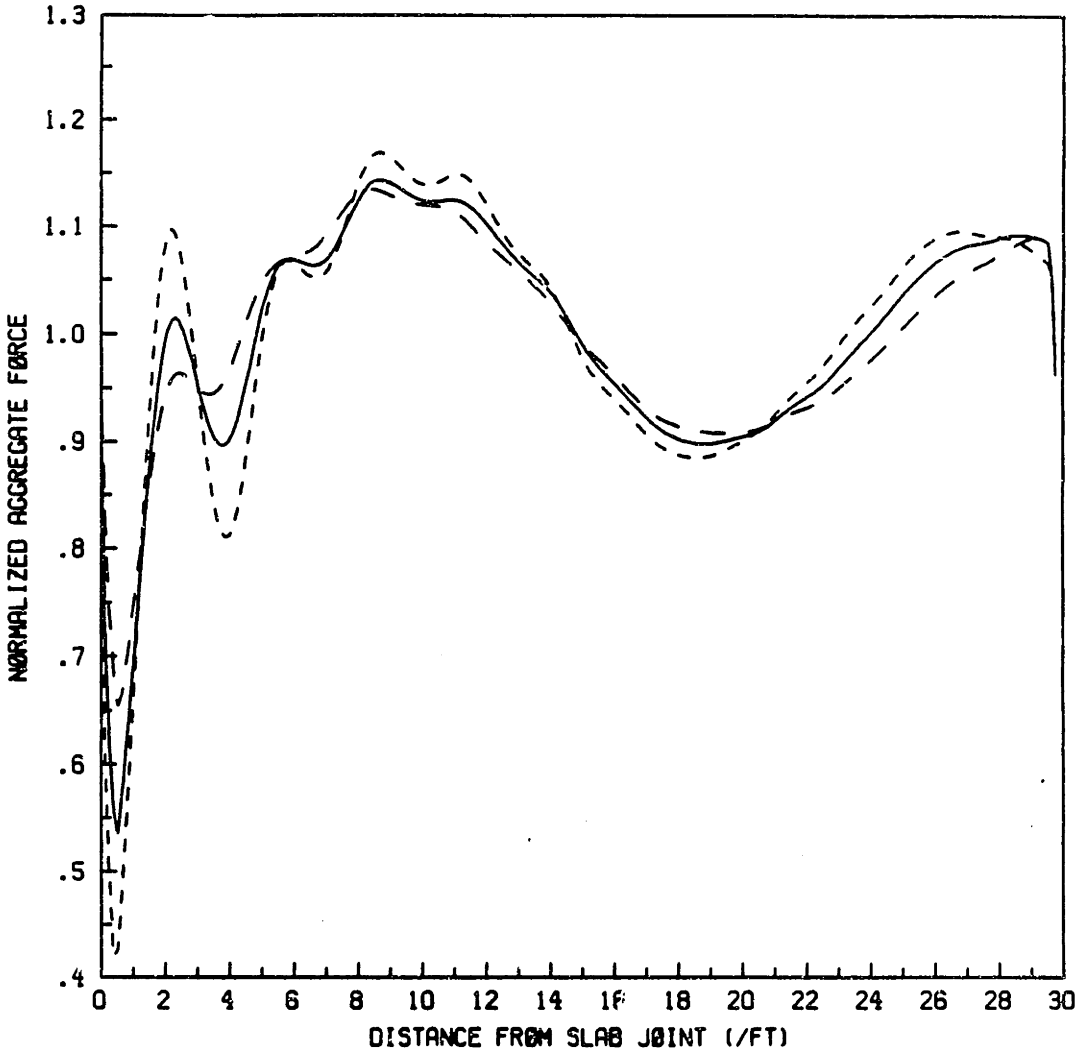

Figure 3.31 Effect of tyre pressure on aggregate load
— — (a) 75 psi
——— (b) 100 psi
- - - - - (c) 125 psi

As was mentioned earlier, the first peak loading after the slab fault is the largest loading for the steer axle and can be up to 30% larger than the mean loading if a shock absorber is not installed. Since this peak occurs close to the slab joint it contributes significantly to deterioration at the joint.

3.3.13 Conclusions on Single Axles

Of the vehicle parameters we investigated the pavement loading is most sensitive to vehicle velocity. In particular a vehicle velocity of 55 mph leads to an aggregate loading about 20% larger than the vehicle static load in the middle third section of a 30 ft slab, thereby accelerating cracking in this region. On the other hand this same velocity leads to a reduced aggregate loading at the slab transverse joint.

The loading imposed on the pavement is also sensitive to the leaf-spring β parameter and the average spring stiffness. These parameters lead to changes in aggregate loading of 10% and 5% respectively.

Pavement slab lengths of 20 ft excite vehicle dynamics leading to aggregate loading in the middle third of the slab of up to 30% higher than the vehicle static load.

The magnitude of the joint fault has a negligable effect on the aggregate pavement loading for faults under $\frac{1}{4}$ in.

Slab warping generally excites the body modes resulting in significant increases (25% for a slab with radius of curvature = 1350 ft) in the loading in the middle third of the slab. This increase in aggregate loading means that the middle third of the slab experiences a load 40% larger than the static vehicle weight.

Because the rigid pavement road input excites the body mode more than the wheel mode on single axle tractor semi-trailers the largest loads tend to be imposed in the 8 - 14 ft region of the slab rather than in the first section.

3.4 Walking Beam Suspension

3.4.1 Simple Model

If the dynamic properties of the vehicle are neglected, so that we can assume it is a single lumped mass supported by the suspension (figure 3.32a) then the equations of motion are as follows:

$$m_s z_s + f_{leaf}(z_s - z_b) = 0 \tag{3.4}$$

$$m_u z_b - f_{leaf}(z_s - z_b) + k_t \left[z_b - \frac{1}{2}(z_1 + z_2) \right] = 0 \tag{3.5}$$

$$m_u z_p + \tau + k_t \left[z_p - \frac{1}{2}(z_1 - z_2) \right] = 0 \tag{3.6}$$

where:

$$z_b = \frac{1}{2}(z_{u1} + z_{u2})$$

$$z_p = \frac{1}{2}(z_{u1} - z_{u2})$$

$\tau =$ pivot friction moment

The above equations describe bounce modes of the sprung and unsprung masses and an independent suspension pitch mode. Since our tire models do not have damping included and there is very little friction at the center pivot we included a torque at the pivot equivalent to that which would otherwise be there due to the tire damping. We may identify the natural frequency and damping ratio associated with the pitching from eqn. 3.6

$$f_n = \frac{1}{2\pi}\sqrt{\frac{k_t}{m_u}}$$

$$\varsigma = \frac{1}{2}\frac{c_s}{\sqrt{k_t m_u}}$$

Inputs of certain wavelength will excite pure pitch and bounce exclusively. When the wavelength is twice the wheelbase the two axles go up and down 180 degrees out of phase, resulting in a pure pitch input and zero bounce. If however,

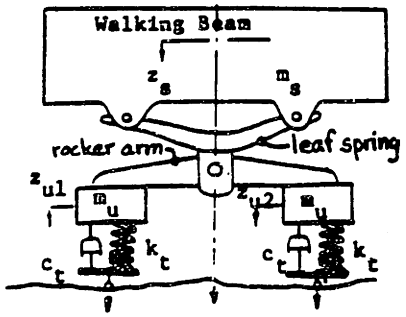

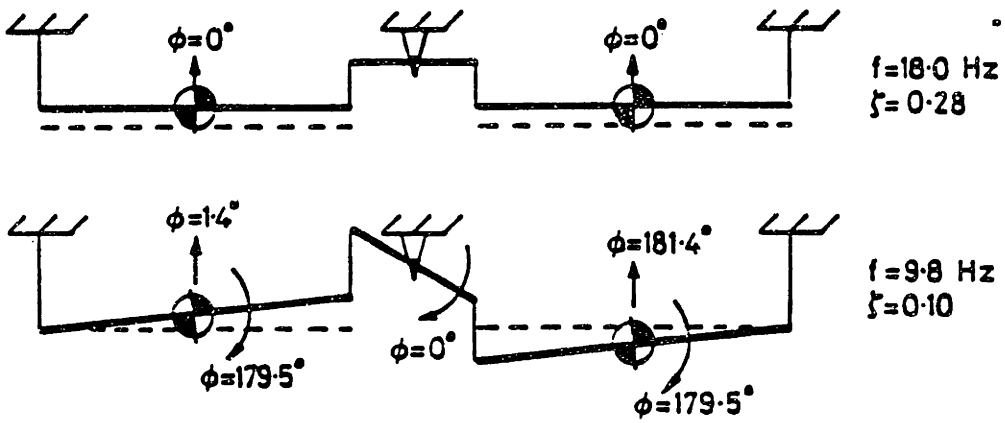

Natural modes of the "four-leaf" trailer suspension model.

Frequency (Hz)	Damping Ratio	Description of Mode
18.0	0.28	Axles bouncing in phase, sprung mass stationary.
9.8	0.10	Axles bouncing in antiphase, load leveller pitch.
2.3	0.03	Sprung mass and axles bouncing in phase.

Figure 3.32 Tandem axle characteristic
(a) Walking-beam suspension schematic [6]
(b) Four-leaf short rocker tandem modes [11]

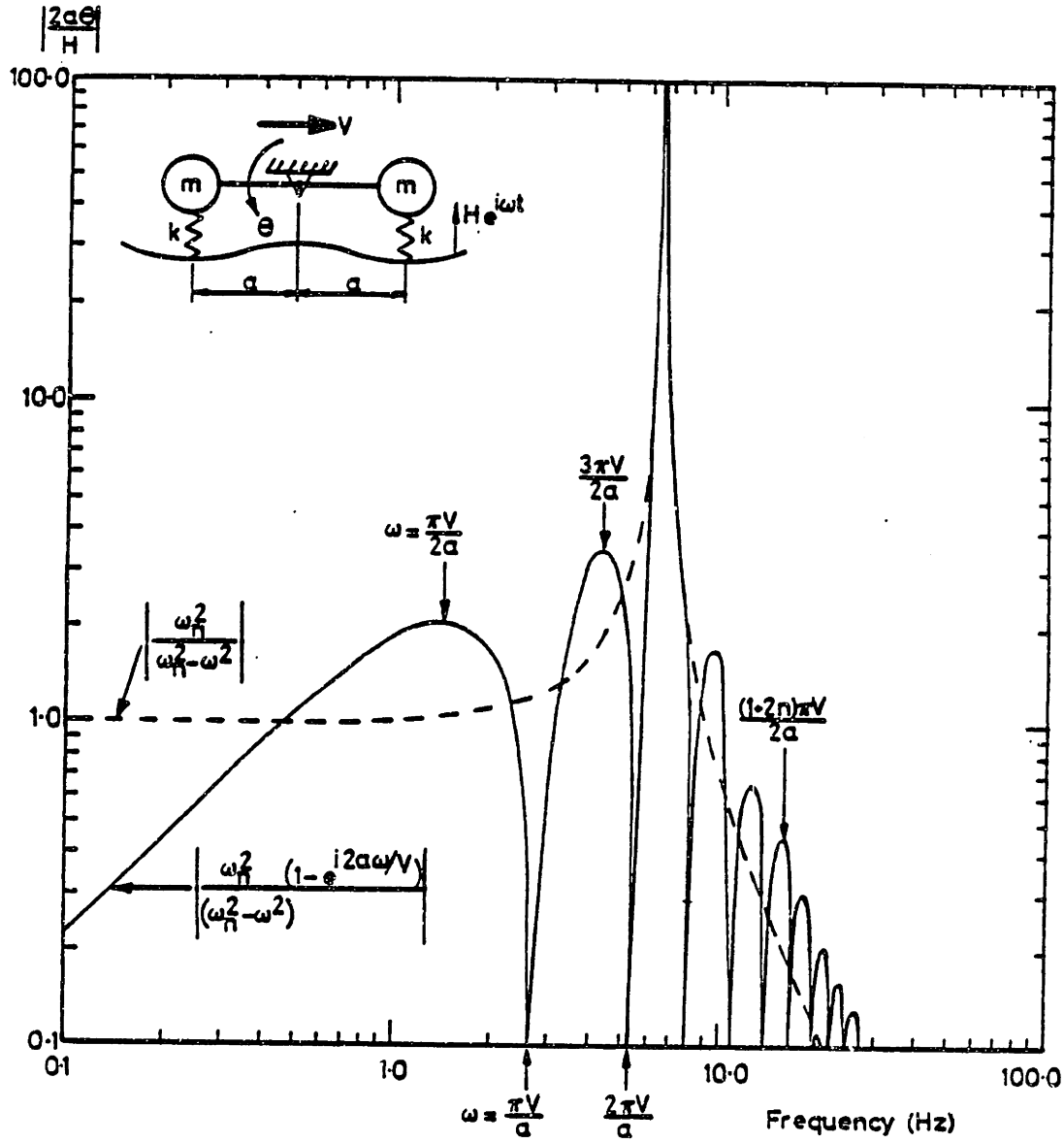

Wheelbase filtering. Pitch oscillations of the simple bogie model are magnified at frequencies of $\omega=(1+2n)\pi V/2a$, and diminish at multiples of $\omega=\pi V/a$.

Figure 3.33

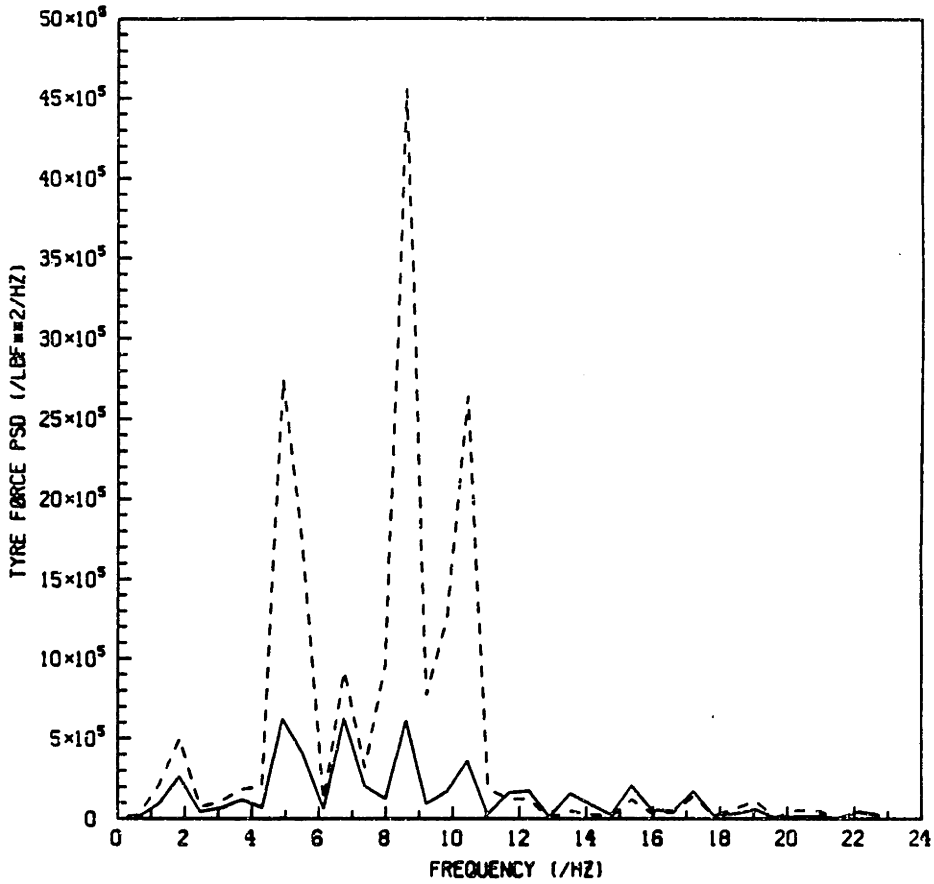

Figure 3.34 Effect of tandem axle spacing
- – – – – (a) spacing 44 inches
- ——— (b) spacing 52 inches

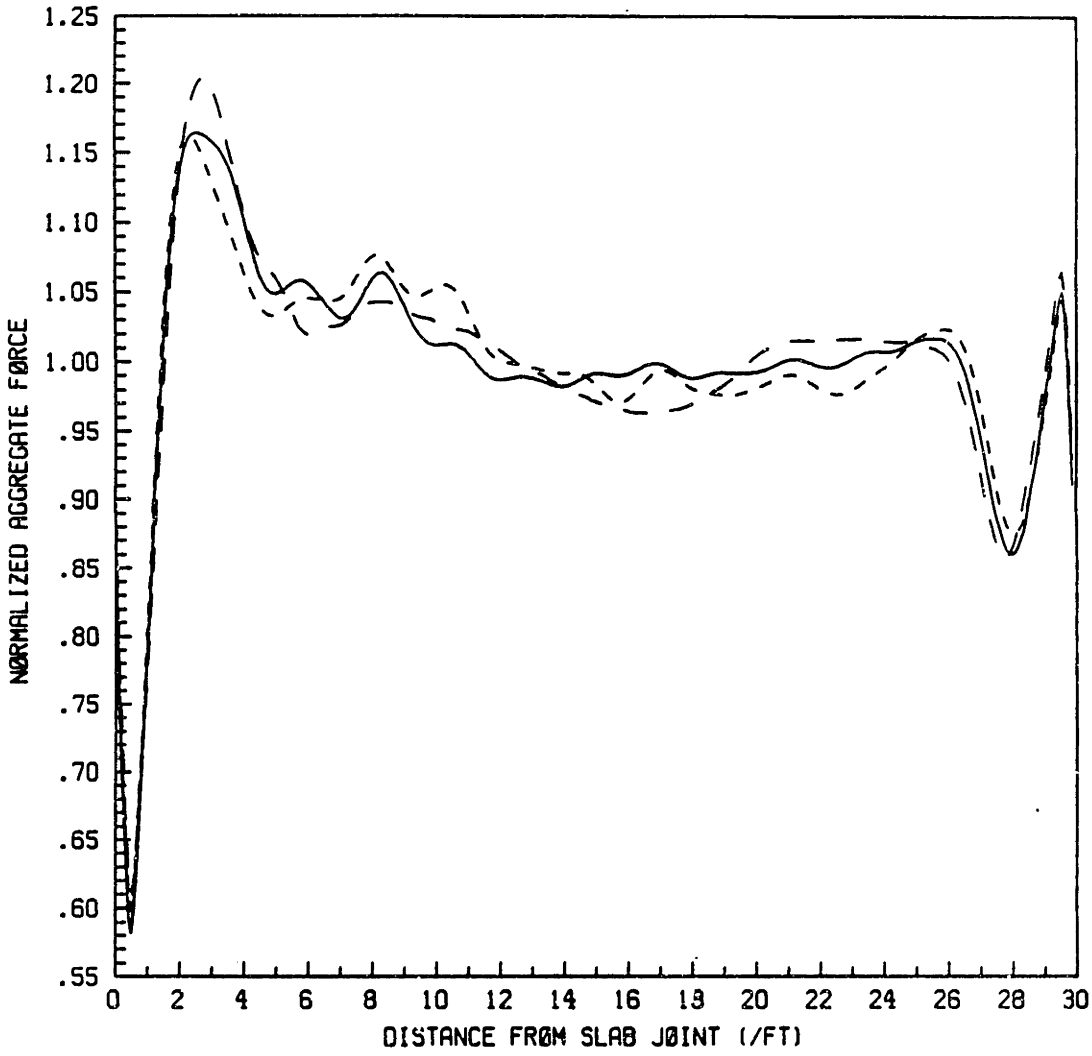

Figure 3.35 Effect of β parameter
- ---- (a) $\beta = 1 \times 10^{-3} ft$
- ——— (b) $\beta = 4 \times 10^{-3} ft$
- — — — (b) $\beta = 10 \times 10^{-3} ft$

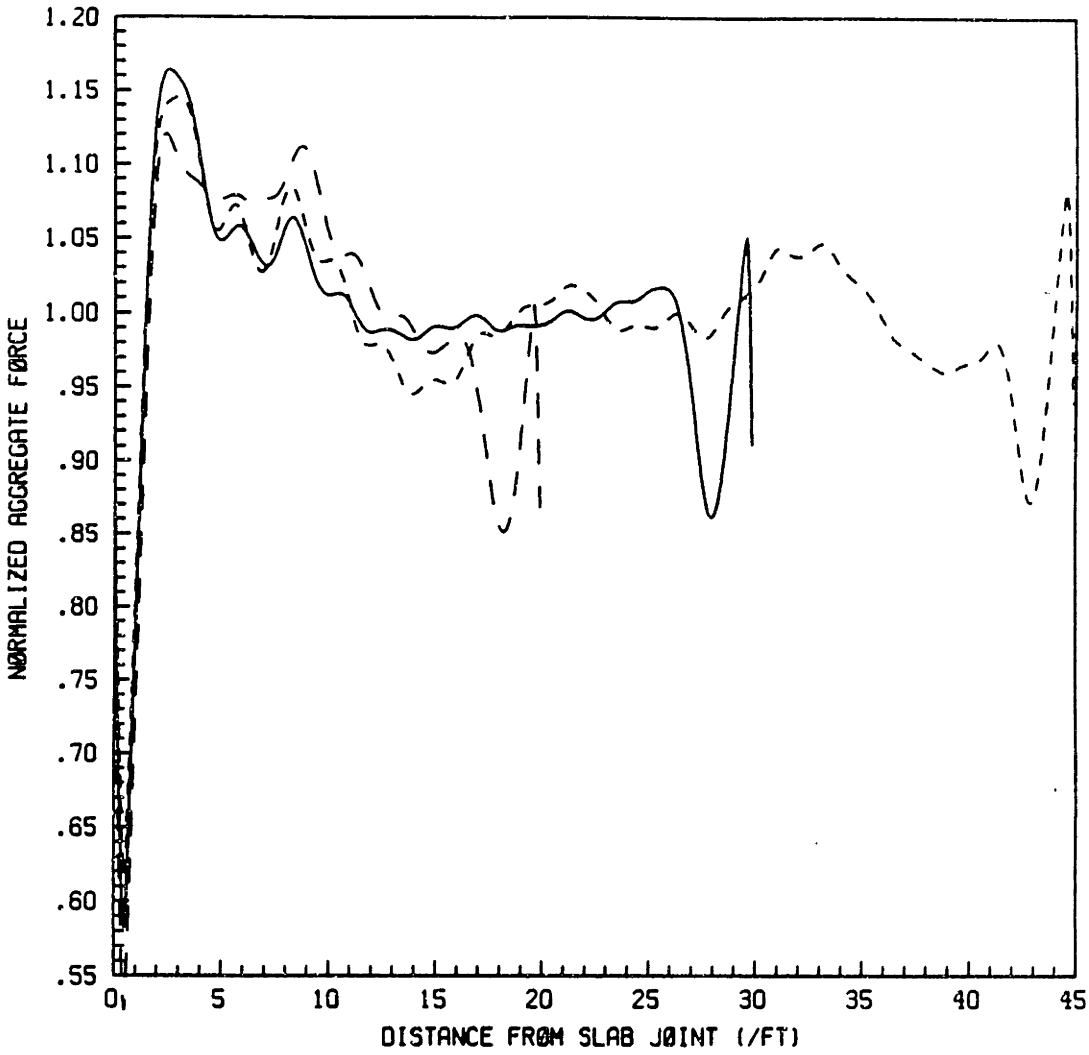

Figure 3.36 Effect of slab length

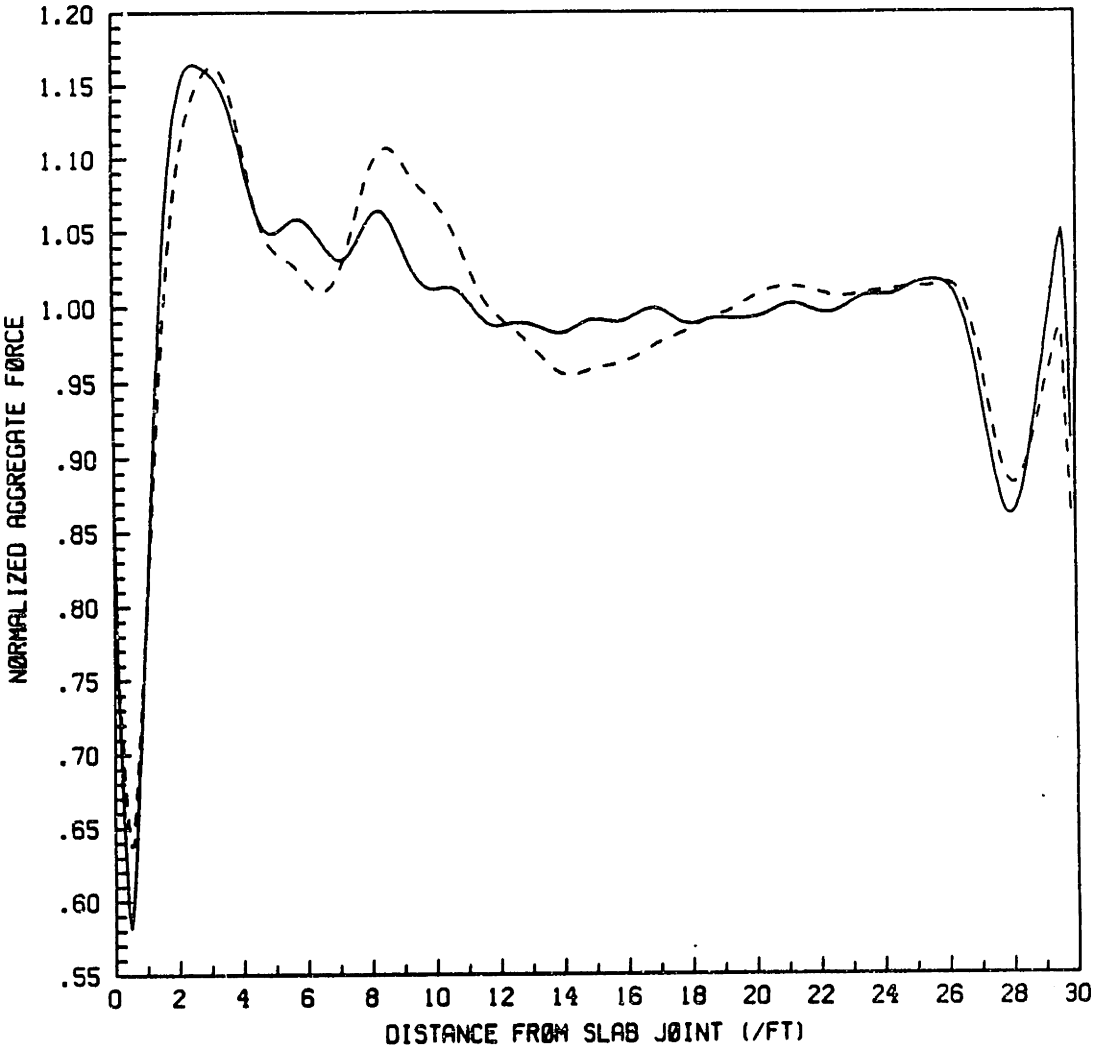

Figure 3.37 Effect of tyre pressure
- - - - (a) 75 psi
——— (b) 100 psi

the road input wavelength corresponds to the wheelbase, the axles ride up and down in phase with each other resulting in pure bouncing and no suspension pitch (figure 3.33).

Table [4] lists tandem axle spacing distances that will excite the pure suspension pitch mode (10.4 Hz) when the axle pair passes over a fault in the slab at various vehicle velocities.

Velocity (mph)	Spacing (ft)
35	2.5
55	3.9
70	4.9

Table 4 Tandem Axle Spacing Resulting in Suspension Pitching

By examining the PSDs of the dynamic tire force signal we note that the primary difference between the frequency content of profiles from the four-spring suspension and walking-beam suspension is the response at 10 Hz. The four-spring suspension has a larger body mode response, while most of the walking response occurs at the higher frequencies (figure 3.34).

3.4.2 Parametric studies

Our baseline model (Table [3]) run at 35 mph produced a dominant peak 3ft away from the slab joint and up to 17% larger than the static vehicle load. The out of phase wheel mode was not excited thus the loading was insensitive (less than 3% increases) to variations in β, joint spacing, tire pressure and road surface roughness (figures 3.35 3.36 3.37).

At the higher velocities (55, 70 mph) the contribution of the wheel modes are vastly increased. At these velocities the joint fault acts as a step input at the wheel mode frequency ($\sim$ 10 Hz) thereby resulting in pure suspension pitch that is lightly damped. Figure 3.38 indicates the change in the nature of the pavement aggregate

loading. There is a severe aggregate loading of 50% larger than the static vehicle load in the mid slab region and 20% increases in loading at the first and third peak loading regions.

We can alternatively vary the tandem axle spacing or wheelbase to tune the input forcing frequency to match the suspension pitch mode. Figure 3.33 shows the increases in wheel mode content in the tire force profile due to a change in axle spacing from 52 in (nominal) to 44 in. The resulting aggregate force on the pavement resembles the effect of higher vehicle velocity without the vast relocation of peak loading positions. Increases in the peak loading of 15% and 20% are shown in figure 3.39.

As a result of the unsubstantial contribution of the body mode to the tire force profiles of the tandem axles we note that the aggregate loading associated with the walking beam does not exhibit extended regions of peak loading which we find in the case of the four-spring suspension and is a characteristic of a large body mode content of the tire force profile.

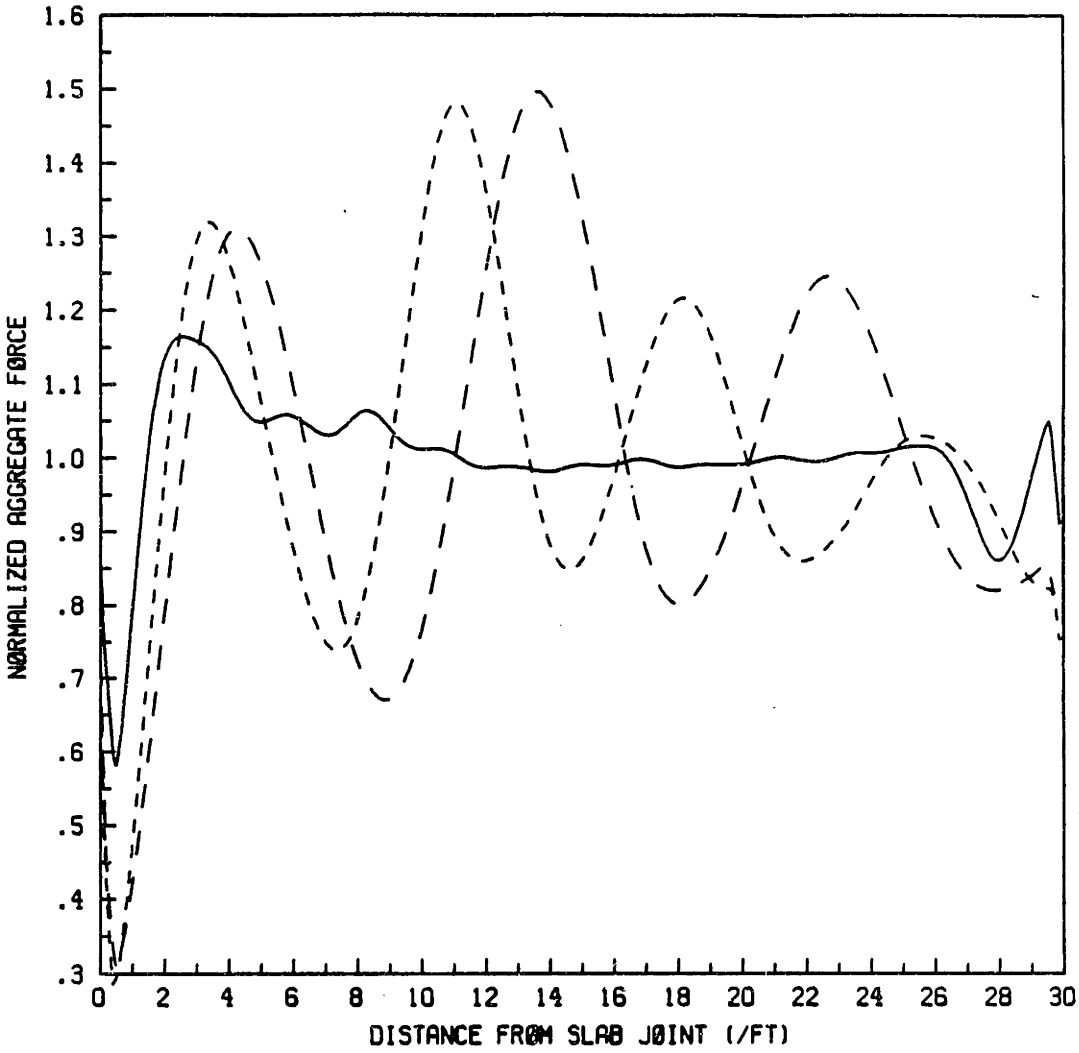

Figure 3.38 Effect of vehicle velocity
(a) 35 mph
(b) 55 mph
(c) 70 mph

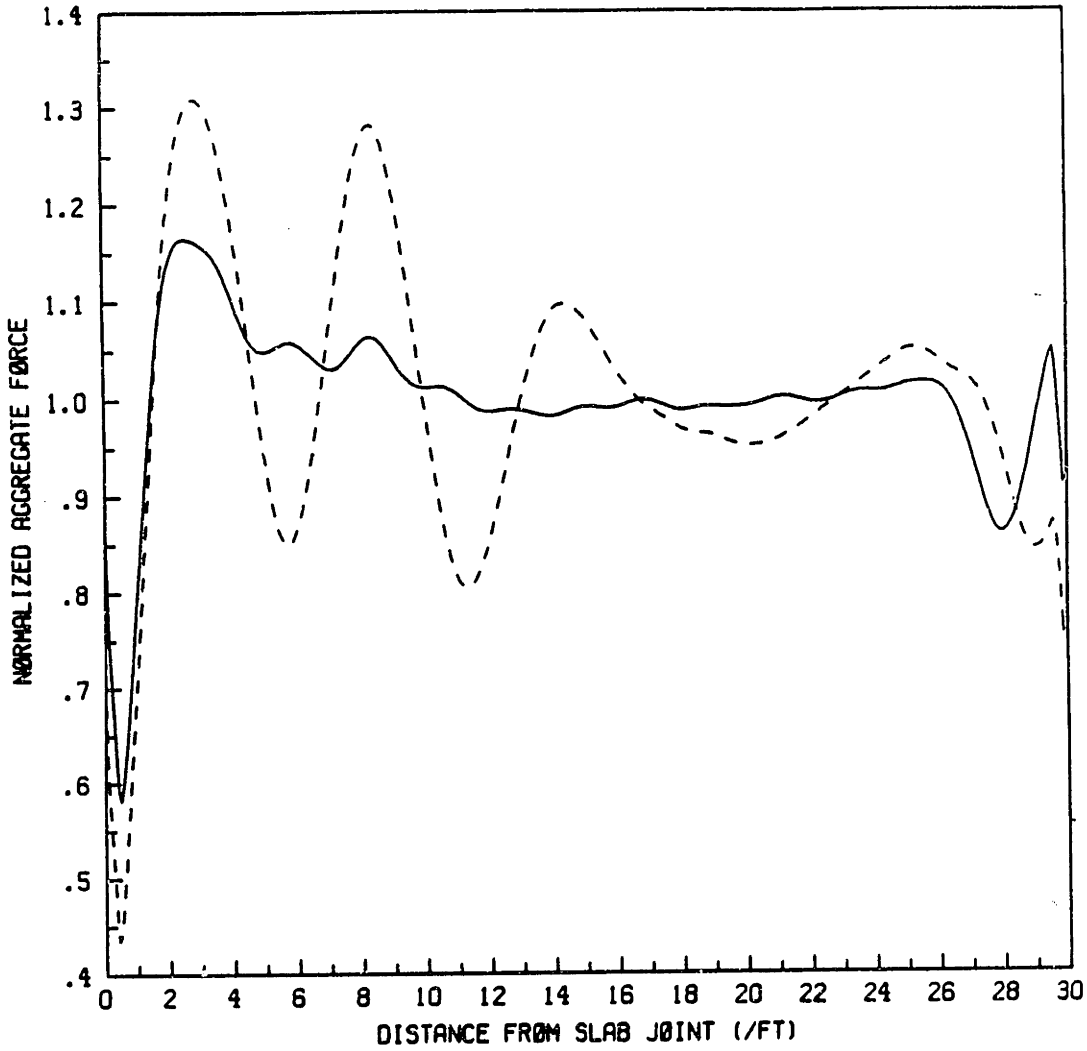

Figure 3.39 Effect of tandem axle spacing
- – – – (a) axle spacing 44 inch
- ——— (b) axle spacing 52 inch

3.5 Four-Spring Tandem

The four-spring tandem suspension has a short rocker that links the two axles together and acts as a load distributor. It is this load leveler that makes the vehicle response to a step input inherently different from that of the single axle suspension. When the net torque due acting on the rocker due to the two leaf-springs is larger than the opposing coulomb friction torque the load is equally distributed between the two axles. Otherwise the rocker arm sticks in a position that does not necessarily share the axle group loading equally.

A PSD of the leading tire force profile contains two wheel modes. The higher frequency mode ($\sim$ 14 Hz) is due to the unsprung masses bouncing in phase and the sprung mass remaining stationary. The lower ($\sim$ 10 Hz) frequency mode is due to the antiphase bouncing of the unsprung masses which involves the short rocker pitch (figure 3.32). It is important to note that the in phase bouncing mode has a larger damping ratio than the antiphase bouncing of the unsprung masses because the former mode is damped primarily by the leaf-spring whereas the second mode is damped primarily by the load leveller coulomb friction torque acting to oppose pitching of the load leveller.

The response of the steer axle (loaded to 11.5 kips with shock absorber) is dominated by a 3 Hz body mode. With a less laden axle ($\sim$ 6 kips) we expect more wheel mode response because of the tire leaving the road surface (wheel hop).

3.5.1 Location of Peaks for Baseline Model

Peak loadings incurred by the steer axle occur at 9 ft and 21 ft with magnitudes of 11.2% and 6.8% larger than the static axle load. For the 30 ft slab length the body mode frequency excited by the step generally leads to a peak loading close to the subsequent transverse joint. Also note that the body mode is lightly damped, leading to negligible decay in peak force magnitudes within two cycles (or a slab length). The peak locations for the drive and rear axle groups fall in the following regions:

Peak	Distance			AXLE			Aggregate
	(ft)	1	2	3	4	5	
1	1.8 – 2.2		1.388	1.342	1.461	1.113	1.32
2	4.7 – 6.2		1.079	1.331	1.232	1.144	1.19
3	8 – 10	1.112	1.217	1.143	1.296	1.257	1.21
4	12 – 15		1.254	1.083	1.217	1.186	1.185

Table 5 Peak Normalized Axle Loads

3.5.2 Effect of Varying β-Parameter

As was mentioned earlier, a small value of β is equivalent to increasing the coulomb damping in the leaf-spring. The result of increased damping in the leaf-springs is to reduce the in phase bounce wheel mode and thus slightly increase the body mode and antiphase bouncing wheel mode. Increasing β (or decreasing damping due to the leaf springs) increases the in phase bounce mode of wheels.

The results of varying β can be seen in terms of the aggregate force in each of the regions where the peak loading occurs (figure 3.40). An optimum value of β around 4×10^{-3} ft exists which leads to a balance of each of the modes. Also note the small effect on the location of peaks incurred by varying β. Reducing β (from 10×10^{-3} to 1×10^{-3} ft.) reduces the aggregate force at the first peak (2 ft from transverse joint) by 3% but increases the peak loading at 6 ft by 5% and the next peak by 2%.

In conclusion β has a negligible effect on location of peak loading. A small value for β will result in reducing stresses at the transverse joint and increasing stresses at the mid slab location. An optimum β exists (around 4×10^{-3} ft) which results in lowering stresses at both locations.

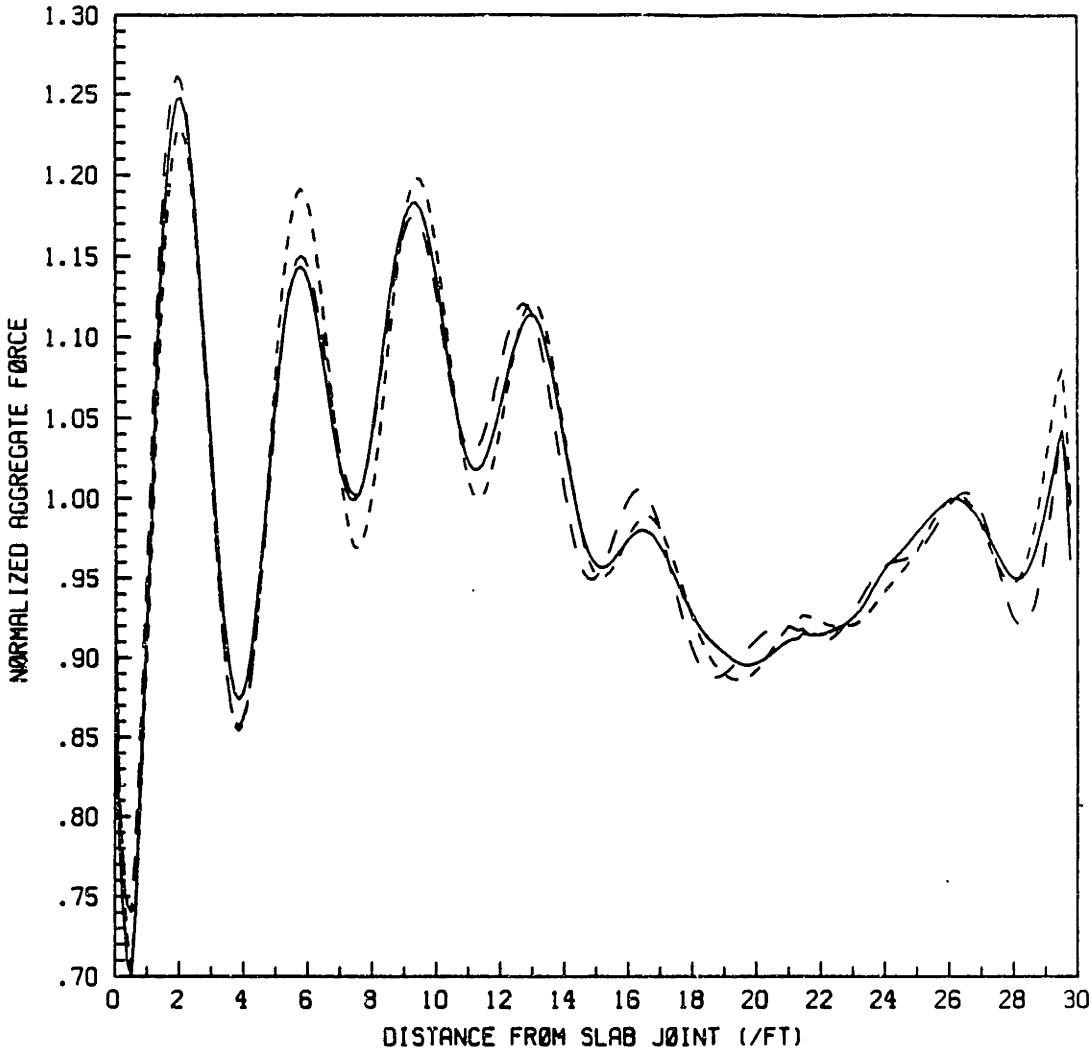

Figure 3.40 Effect of β parameter
- ----- (a) $\beta = 1 \times 10^{-3} ft$
- ——— (b) $\beta = 4 \times 10^{-3} ft$
- — — — (b) $\beta = 10 \times 10^{-3} ft$

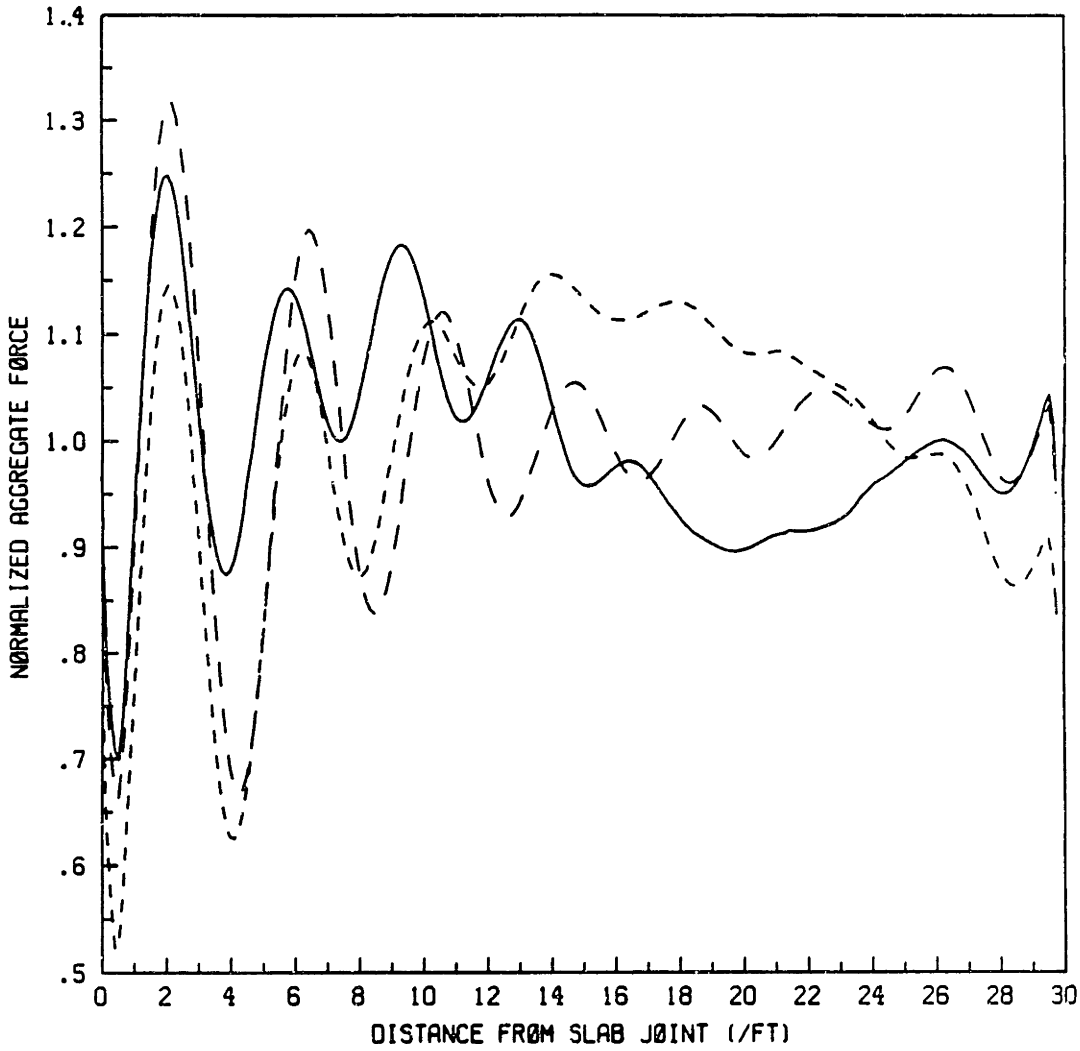

Figure 3.41 Effect of suspension stiffness on aggregate loading
——— (a) 128,000 lbf/ft (std)
– – – – – (b) 61200 lbf/ft
— — — (c) 30600 lbf/ft

3.5.3 Effect of K_s

A reduction in stiffness attenuates the contribution of the wheel modes to the tire force which results in reducing the aggregate forces in the peak regions (at 2, 6, 10 ft) by up to 12% for a 50% reduction in stiffness. Aggregate forces for a stiffness value of 30,600 lbf/ft are also plotted but are not realistic in that the nominal deflection is around 4.5 in. (average nominal deflection being 2 in.). It is clear from figure 3.41 that reducing the suspension stiffness reduces peak loading up to 10 ft from slab joint but thereafter results in a 15% increase in the middle third of the slab (for a 50% reduction in average spring stiffness). A softer suspension will produce less damage to the pavement close to the transverse joint, but more damage in the midsection. However, the vehicle designer will not have much freedom to choose the suspension stiffness since it will be determined by the static loading on the axle.

3.5.4 Effect of Tire Pressure

The effect of lowering the tire pressure on vehicle dynamic response is to filter the input to the leaf spring suspension thereby attenuating the wheel mode contribution to the tire force.

Lowering the tire pressure also leads to a larger surface contact area and therefor reduces the response (stress, deflection) of the pavement. This reduces crack initiation and propagation rates through the concrete slab.

The aggregate force plot of figure 3.42 indicates that the substantial effect of tire pressure occurs at the second peak load position where a 7% decrease in loading may be achieved by lowering the tire pressure from 125 psi to 75 psi. There is also a small change in the locations of the peaks due to changing the tire pressure.

3.5.5 Effect of Tandem Axle Spacing

Reducing the axle spacing increases contributions of both wheel and body modes with large increases to the out of phase wheel mode. The tire force response is thus dominated by this high frequency contribution leading to up to 16% increases

in the aggregate force in the region closest to the slab transverse joint and 10–12 ft region, when comparing 44 in. to 60 in. tandem axle spacing. The difference in aggregate loading is not as large ($\sim$ 4%) when comparing 52 in. to 60 in. spacing. The effect of axle spacing has been explained in terms of wheelbase filtering for the walking beam tandem suspension and will not be repeated here.

3.5.6 Effect of Slab Length

Slab lengths that correspond to vehicle wheelbases lead to excitaiton of various body modes. For the wheelbases of test vehicles (table [3]) the 45 ft and 20 ft slab lengths would increase the contribution of the out of phase tracter/trailer pitch body mode as explained in earlier sections, whereas the 30 ft slab length would increase the trailer bounce mode.

In general the contributions of all the vehicle modes increase with decreased slab length. Furthermore, the contributions of the in phase bounce and body mode increase relative to that of the out of phase bounce for the 20 ft slab. The above is reflected in the aggregate force plots of figure 3.44 by 10% increases in aggregate force for the 2nd and 4th peak loading regions for decrease in slab length from 45 ft to 20 ft.

3.5.7 Effect of Joint Fault

The fault magnitude at the slab transverse joint was varied between 1/10 in. to 3/4 in.

Small joint fault magnitudes will predominantly excite the out of phase wheel bounce mode and progressively more severe faults excite the body mode and the higher frequency wheel modes with the in phase wheel mode becoming more dominant than the out of phase mode for joint faults around 3/4 inch.

The aggregate force plot of figure 3.45 shows increases in loading around 32% for a change in fault size between 1/10 to 3/4 in. Note also the difference in mean loading in the two halves of the slab, leading to less severe loading conditions in the second half of the slab for increased joint fault magnitude.

3.5.8 Effect of Vehicle Velocity

The effect of increasing the vehicle velocity between 35 mph and 70 mph was investigated. Increasing the vehicle velocity results in an increase in excitation of the out-of-phase bounce wheel mode and vehicle body modes but not so much the in-phase bounce mode for the leading axle in the tandem pair.

The aggregate force plot of figure 3.46 shows the change in location of the peaks. The change in position of the peak is proportional to the velocity as noted in earlier sections. The increased velocity results in distributing the peak loading over the entire slab. A vehicle velocity of 55 mph is desirable if the purpose is to reduce maximum stresses in the middle third of the slab.

3.5.9 Conclusions on Four Leaf Tandems

Regions of peak aggregate loadings occur as a result of faults inherent in rigid pavements. These regions are identified and the location of the peaks was found to be proportional to vehicle velocity. Furthermore peak loading locations away from the transverse slab joint fault (3rd and 4th peak loadings) were also found to be dependent on the following vehicle parameters:

- Tandem Axle Spacing,
- Average Suspension Stiffness,
- Tire Pressure.

Note however that peak location is more sensitive to vehicle velocity and that the location of peak pavement response for a particular highway will depend on the mean and variance of vehicle velocities on the particular highway.

From the point of view of reducing the magnitude of the aggregate loading on the pavement the following parameters should be considered:

- Joint Fault Magnitude,
- Slab Length,

- Average Suspension Stiffness K_s,
- Tandem Axle Spacing.

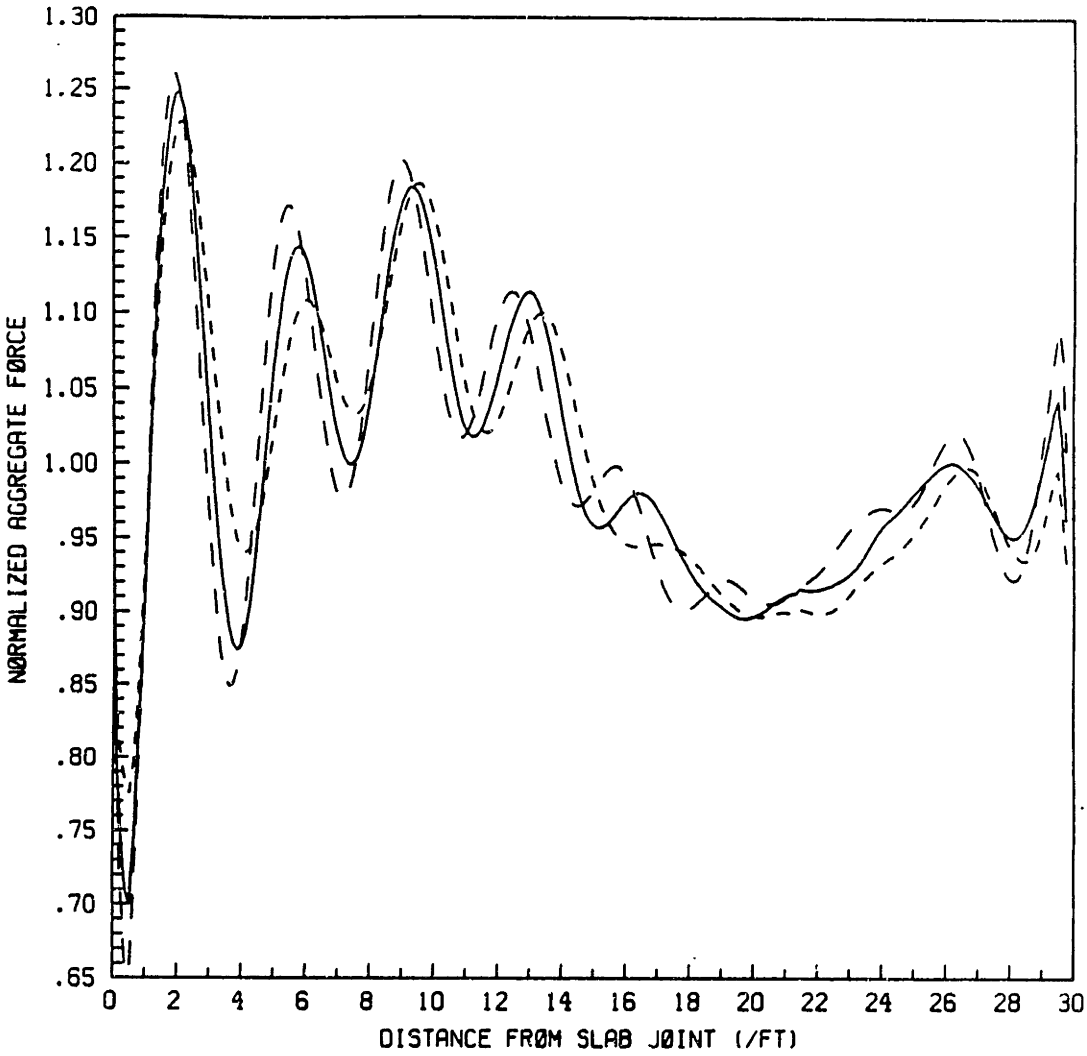

Figure 3.42 Effect of tire pressure

- – – – (a) 75 psi
- ——— (b) 100 psi
- — — — (c) 125 psi

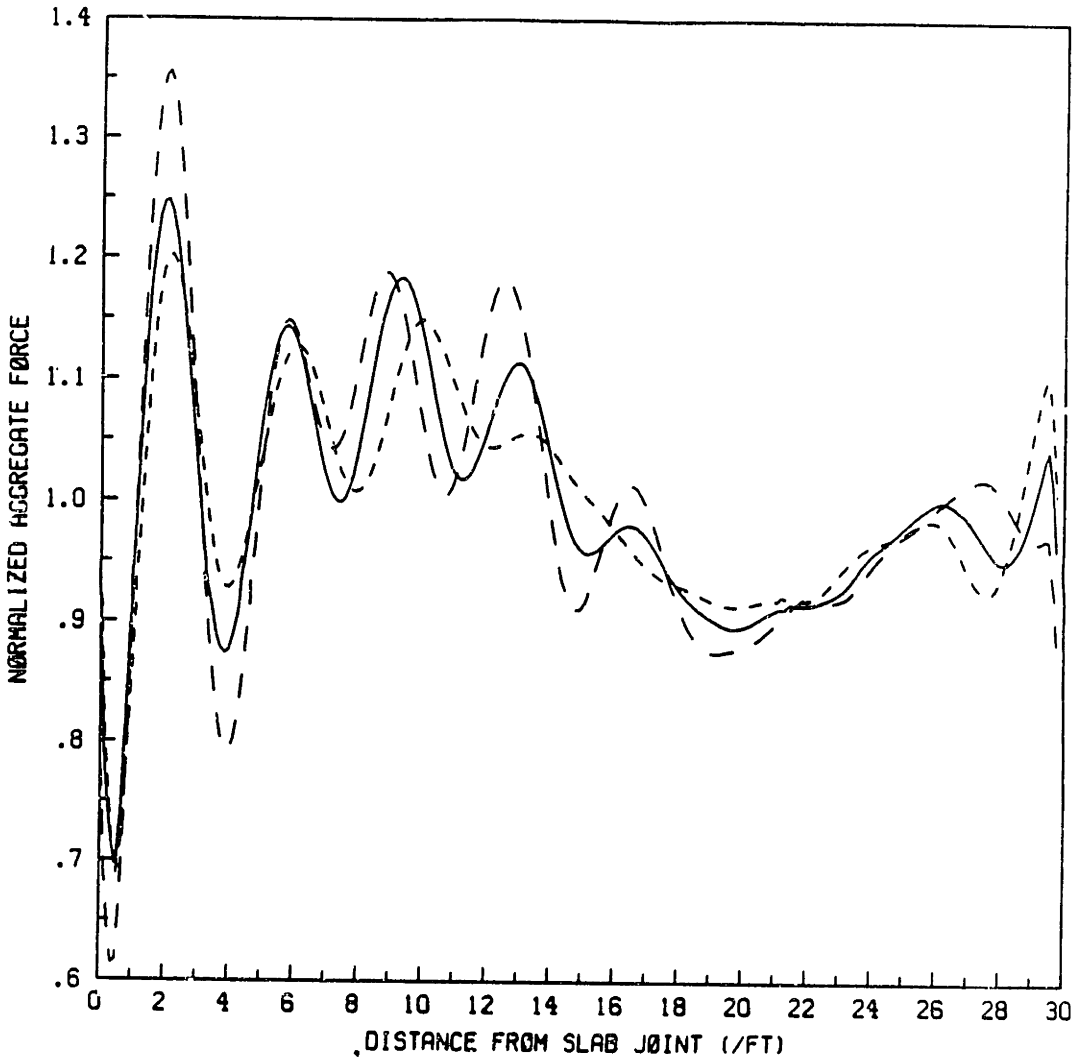

Figure 3.43 Effect of tandem axle spacing
- - - - (a) axle spacing 44 inch
——— (b) axle spacing 52 inch
- - - - - (c) axle spacing 60 inch

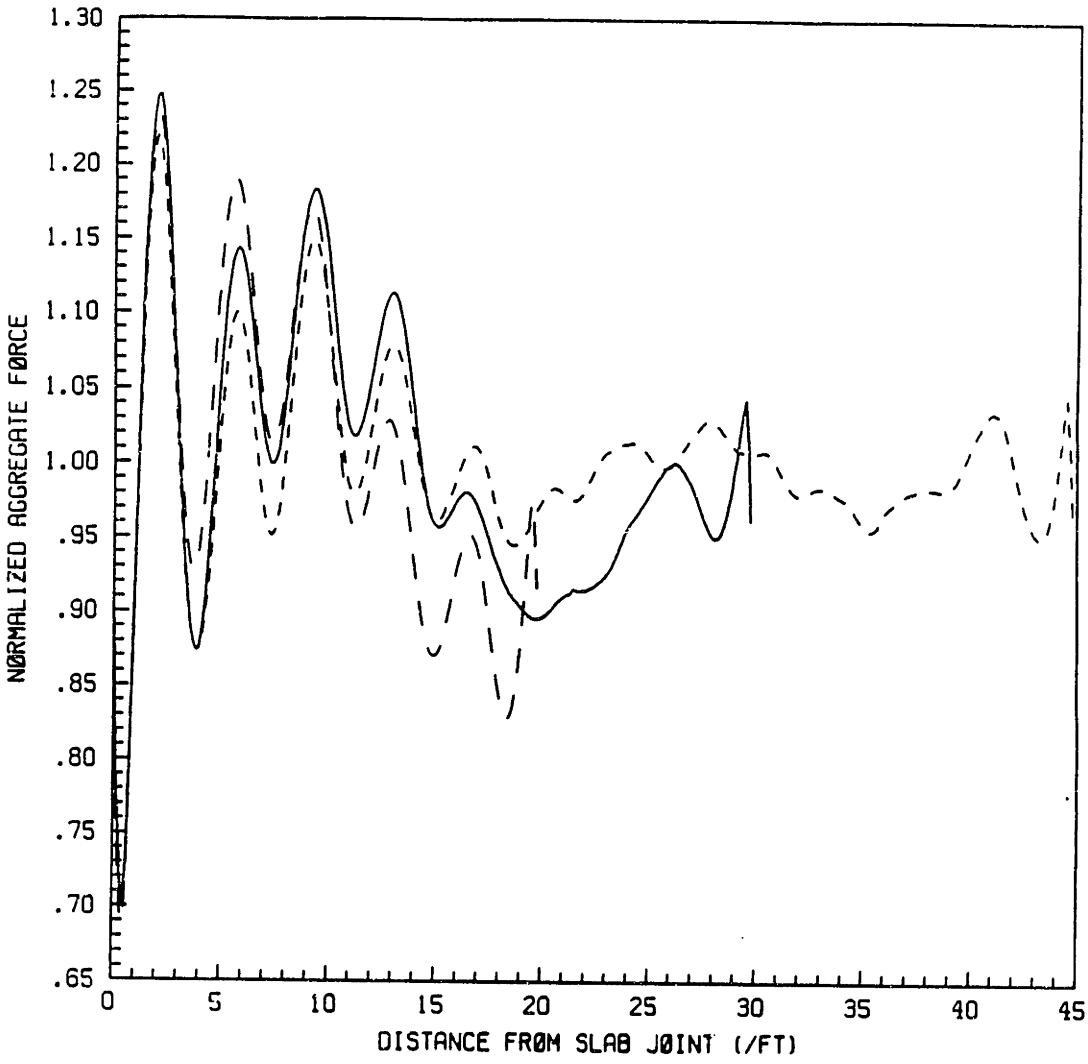

Figure 3.44 Effect of slab length
- (a) joint spacing 45 ft
- (b) joint spacing 30 ft
- (c) joint spacing 45 ft

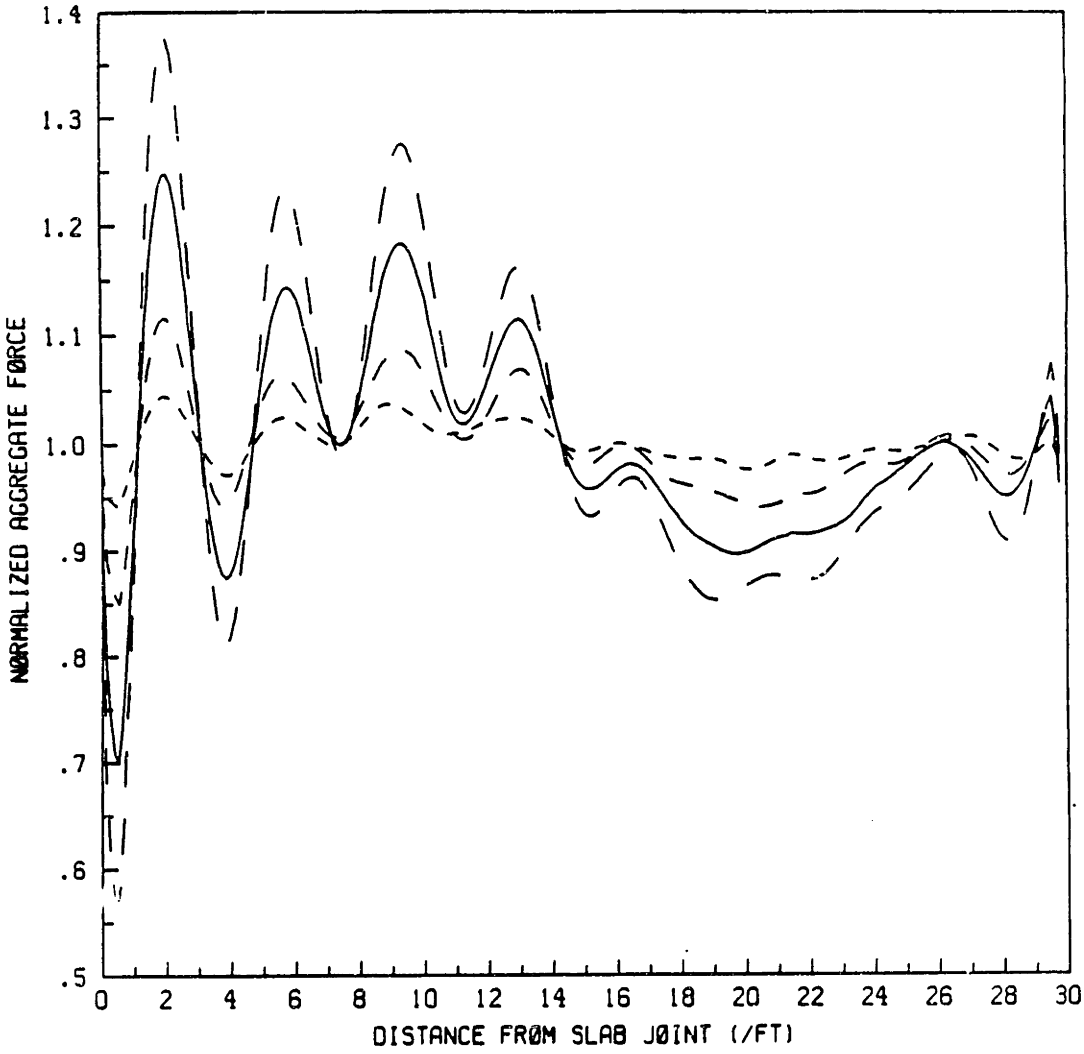

Figure 3.45 Effect of joint fault magnitude
- - - - - (a) 0.1 inch fault
— — — (b) 0.25 inch fault
——— (c) 0.5 inch fault
— — (d) 0.75 inch fault

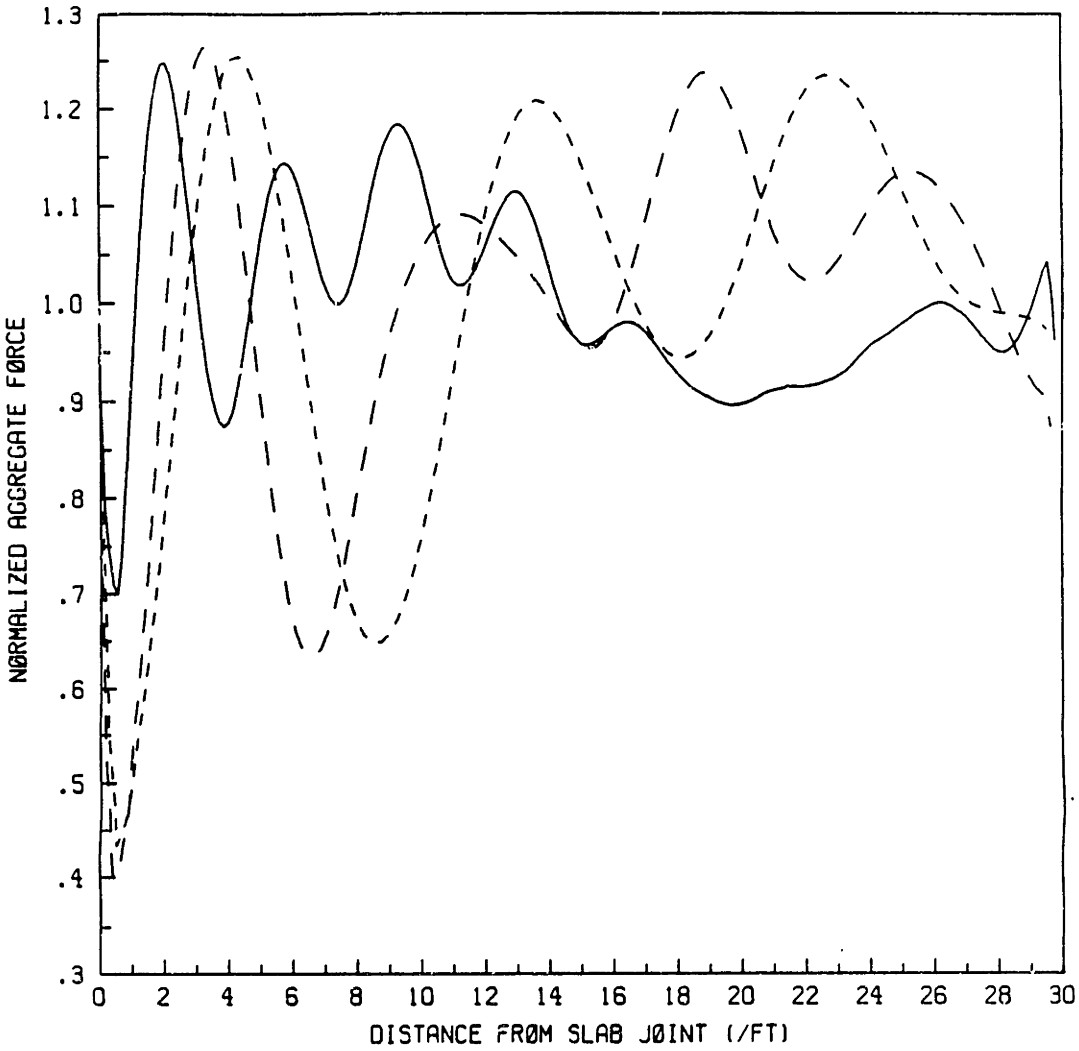

Figure 3.46 Effect of vehicle velocity
——— (a) 35 mph
— — — (b) 55 mph
— — — — (c) 70 mph

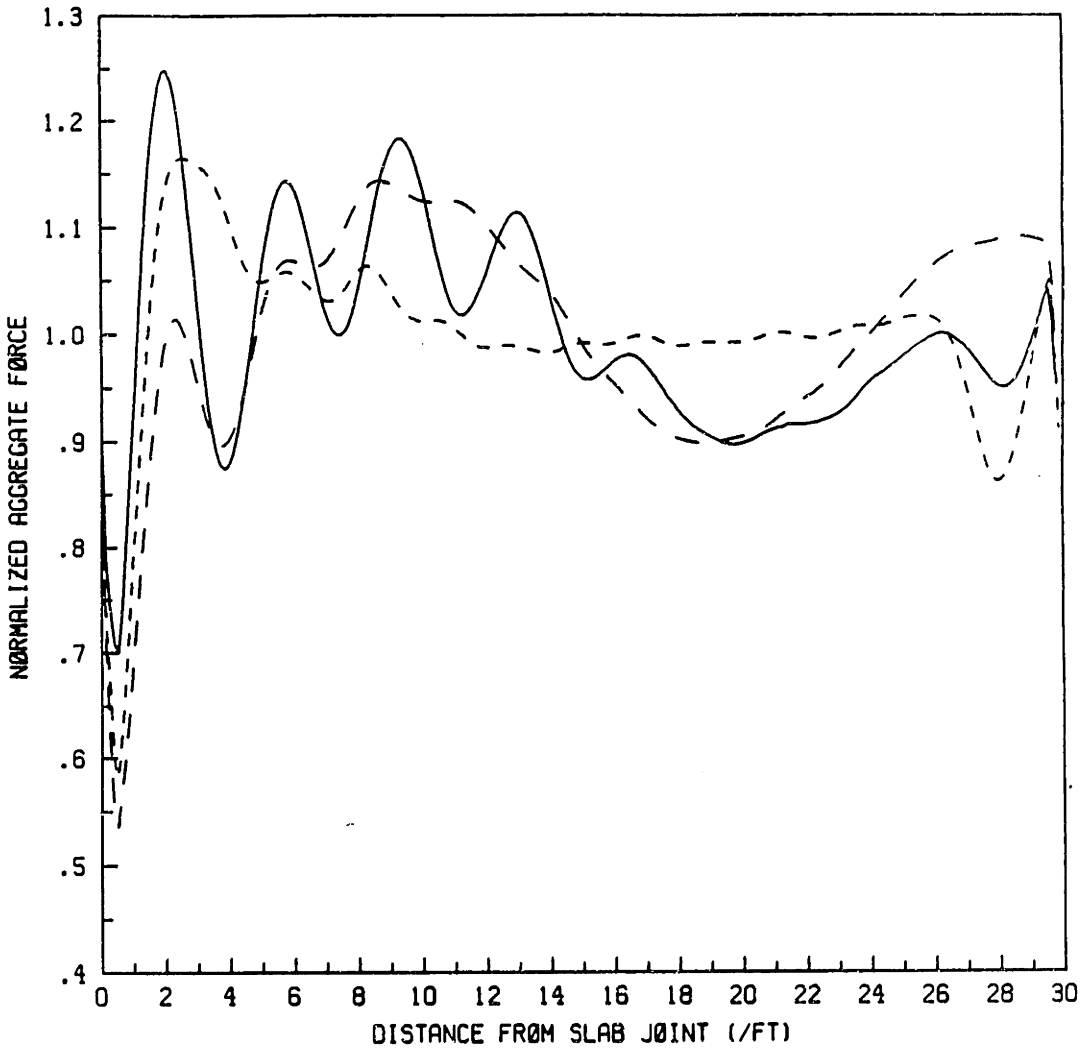

Figure 3.47 Effect of different suspension type (at 35 mph)
——— (a) Four-leaf short rocker
– – – – (b) Walking-beam
——— (c) Single-leaf spring

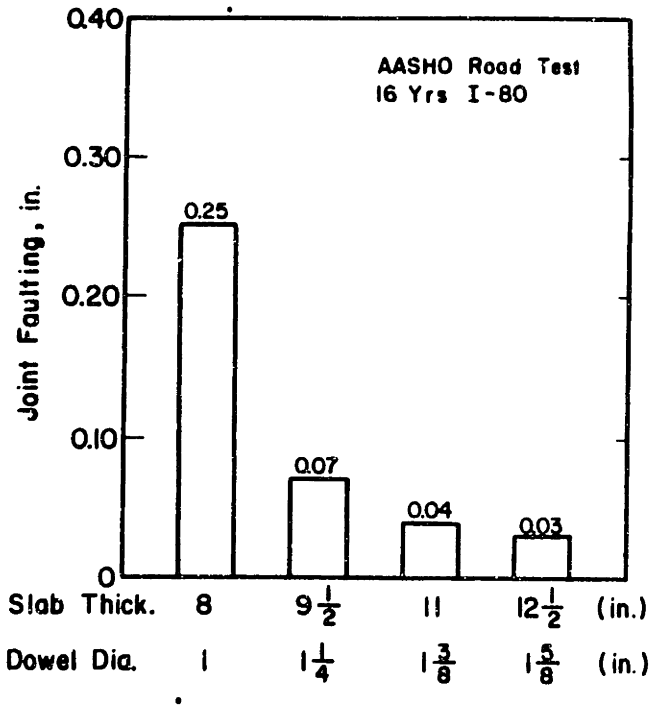

Joint Faulting on Plain Jointed Concrete AASHO Road Test Sections Left In-service on I-80.

Figure 3.48 [1]

Suspension	Single	Four-Spring	Walking Beam
Cab Mass	184.5	337.8	263.2
Cab Inertia	5619.5	5000	1909.6
Trailer Mass	921.8	1887.2	1773.9
Trailer Inertia	94,050	252,255.7	107,593
Steer Axle Mass	30	40	40
Drive Axle Mass	76	106.6	100
Rear Axle Mass	77	90	100
Gross Weight	1289.3	2461.6	2277.1
Tire Stiffness (S)	123,600	123,600	123,600
Tire Stiffness (D)	247,200	247,200	247,200
Steer Leaf-Spring			
k_1 (lbf/ft)	19,513	18,600	18,600
k_2 (lbf/ft)	15,646	12,400	12,400
Shock Damping	1000	1000	1000
Drive/Rear Leaf-Spring			
$\frac{k_1}{2}$ (lbf/ft)	76,800	70,400	146,880
$\frac{k_2}{2}$ (lbf/ft)	51,200	57,600	97,920
β (ft)	4×10^{-3}	4×10^{-3}	4×10^{-3}
Rocker Inertia		0.1	
Rocker Coulomb		1500	500
Friction Torque			
Bogi Inertia			470

Vehicle Velocity (mph)	35
Slab Length (ft)	30
Joint Fault (in)	$\frac{1}{2}$

Table 3 Baseline Vehicle Models (English Units)

3.6 CONCLUSIONS

Based on the above parametrics and the fact that the influence lines of the rigid pavements are broad (due to the rigidity of the concrete slab) we can conclude that for single-axle suspensions the body mode contribution to the tire force will produce more cracking than the wheel mode. Therefore, changes in parameters that attenuate the body mode excitation will reduce the pavement cracking damage.

It is harder though, to generalize about the tandem axle case because of the axle coupling. We can hypothesize though that the damage done by the four-leaf tandem will be closer to that of the single-axle suspension than the damage due to a walking-beam tandem. This is because of the lightly damped out-of-pitch oscillation of the walking-beam.

With the objective of minimizing pavement dynamic loading we can set general guidelines based solely on results of this investigation:

1. The joint spacing or vehicle wheelbases (distance between steer/drive/rear axles) should be adjusted such as not to excite the vehicle body modes, especially the out-of-phase tractor/trailer pitching. In particular slab length of 20 and 30 ft should be avoided since they result in simultaneous inputs to a couple of axles exciting the vehicle body modes. Guidelines should obviously depend on the wheelbases of standard vehicles. It is best though, to avoid slab lenghts shorter than 45 ft to account for most of the vehicles on the highways.

2. For tandem-axle suspensions the concept of wheelbase filtering is fundamental to minimizing dynamic pavement loading. At highway velocities and standard

axle spacings the rigid pavement faults correspond to step inputs at the wheel mode frequency. This excites the out-of-phase axle pitch mode. The four-leaf axle pitch mode is damped by the coulomb friction in the short-rocker whereas, the pitching mode in the walking-beam is only lightly damped by the bearing friction in the pivot.

3. Astute suspension choice and design for a specific set of operating conditions will help reduce dynamic pavement loading. Figure 3.47 shows aggregate loading for the three suspension types investigated in this report, for a vehicle velocity of 35 mph. Note that the at higher velocities the out-of-phase pitching mode of the tandem axle suspensions are excited. At these higher velocities the walking-beam produces the most damage.

4. A survey of joint fault magnitudes illustrated in figure 3.48 shows the majority of the fault magnitudes to be less than $\frac{1}{3}$ in. Based on our results we can conclude that the loading profile will be relatively insensitive to the joint faulting magnitude. This however, will not be the case for pavements that have aggregate interlock joints, where faults can be over $\frac{1}{2}$ in.

5. The effect of leaf-spring damping is to modify the relative contributions of the body mode and wheel mode to the tire force. For the single-axle suspension we therefore, conclude that lower leaf-spring damping produces less damage since the body mode contribution to the tyre force is attenuated.

6. The leaf-spring stiffness has a similar effect to the leaf-spring damping as it modifies the contribution of the low and high frequency modes. We therefore, propose softer suspensions to be less damaging.

7. Tire pressure has a negligable effect on vehicle dynamics and should not produce significant changes in the cracking damage since the stresses generated because of larger contact pressures will be effectively distributed over the neighbouring region of the slab. This is a result of the rigidity of the concrete slab.

8. It is important to notice the span of the peak loading region. The single-axle tends to excite the body mode more than the wheel mode. This implies that at higher velocities (55 mph) the central region of the slab will have an extended region of higher loading. The tandem suspensions however, excite the higher frequency wheel modes and result in distributing the peak loading over many more but smaller regions. The implications of the inherently different loading patterns on the different pavement distress mechanisms shall be investigated.

It is important to note however, that there is more than one distress mechanism associated with rigid pavements and thus we are concerned with obtaining guidelines for an optimal design methodology. Furthermore, we cannot make any conclusions as to which loading profile will be most damaging to each of the pavement distress mechanisms without coupling the pavement/vehicle models together (by use of influence functions).

4

Finite Element Analysis of Rigid Pavements

4.1 Introduction

Solutions to the problem of determining the primary response (deflections, stresses, etc) in concrete pavements that have joints or cracks or both have been developed over the past ten years. The difficulties that arise are due to the boundary conditions. Closed form solutions are based on an infinitely large slab that has no discontinuities and thus cannot be used in the analysis of jointed or cracked concrete slabs that have finite dimensions and load transfer systems at the joints.

The finite element procedure provides a method by which the discontinuities may be handled. It should be noted however, that the finite element method is based on a model of the physical system and the results obtained using this method reflects the understanding of the system. The complexity necessary to model crack propagation in a concrete slab and analyse stress concentrations at the concrete joints would require a three-dimensional analysis. The amount of discretization and computer costs required for the solution of these problems would be excessively high and unrealistic for our particular application. Current techniques of rigid pavement analysis employ a two-dimensional model of the slab and do not accurately predict crack propagation through the slab section. A possibility would be to perform a two dimensional analysis along with a three dimensional analysis in the areas of the slab where cracking is initiated and propagates. The difficulty would then be to maintain continuity between the two models.

An important aspect of the application of finite element methods to the solution of complex static problems is the development of a suitable model of the physical

system. The purpose of this section is to discuss the modelling assumptions and then briefly outline the finite element analysis resulting in primary response of the pavement model. The finite element method described within this section are based on [17,18].

4.1.1 Rigid Pavement Modelling

Figure 4.49 shows a cross section of a typical rigid pavement in the neighbourhood of a transverse joint. The first layer is the concrete slab which has a modulus of elasticity in the range of 3000 ksi. The slab and subbase are modelled as plate elements. Kirchoff's hypothesis (small deformations) for thin plates is used. The underlying assumptions are outlined below:

1. Transverse loading is carried by flexure (not in plane or membrane forces) and transverse shear forces are neglected which implies:

   a) Lines normal to the mid-plane in the undeformed plate will remain normal in the deformed plate.

   b) No axial or in-plane shear stress will develop due to the loading.

   c) The mid-plane renmains unstrained during bending.

2. The subgrade behaves like a Winkler foundation.

3. The dowel bars at the joints behave like a linear-elastic material and are located at the neutral axis of the slab.

Figure 4.50 shows that at each node there are three displacement components - a vertical deflection (w) in the z-direction, a rotation (θ_x) about the x-axis, and a rotation (θ_y) about the y-axis. Corresponding to these degrees of freedom, there are three force components at each node of the finite element mesh - a vertical force (f_w), a moment about the x-axis (f_x), and a moment about the y-axis (f_y). For each element we can relate the nodal displacements to the nodal point forces by the static equations:

$$\{R\}_e = [K_{slab} + K_{subgrade}]_e\{U\}_e \tag{4.1}$$

where,

$\{R\}_e$ is the element force vector,

$\{U\}_e$ is the element nodal point displacement vector, and

$$[K]_e = \iint_v [B]_e^T [C]_e [B]_e \, dx \, dy \tag{4.2}$$

where,

$[B]_e$ = strain-displacement matrix, which is obtained from appropriately differentiating $[H]$ the matrix of coordinate interpolation functions.

$[C]_e$ = elasticity matrix of element (material law).

Stresses are then computed from the strains ($\{\epsilon\} = [B]\{U\}$):

$$\sigma_x = E_x \frac{(\epsilon_x + \mu_x \epsilon_y)}{[1 - \mu_x \mu_y]} \tag{4.3}$$

$$\sigma_y = E_y \frac{(\epsilon_y + \mu_y \epsilon_x)}{[1 - \mu_x \mu_y]} \tag{4.4}$$

$$\tau_{xy} = E_x \frac{\gamma_{xy}}{12[1 + \mu_x]} \tag{4.5}$$

The subgrade is modelled as a Winkler foundation. This implies that the subgrade reaction at any point is dependent on the loading acting on that point alone and therefore the subgrade maybe repesented by a single spring element (1 degree-of-freedom element).

Figure 4.51 illustrates the beam element used to model the dowel bars at the joints. Each node has two degrees of freedom - vertical displacement in the z-direction and a rotation (θ_y) about the y-axis. There is a shear force (f_w) and a moment (f_y) about the y-axis corresponding to these displacements.

The overall structural stiffness matrix $[K]$ is formulated by superimposing the effects of the indiviual element stiffness at each node and the overall system nodal displacements obtained by solving the static equation:

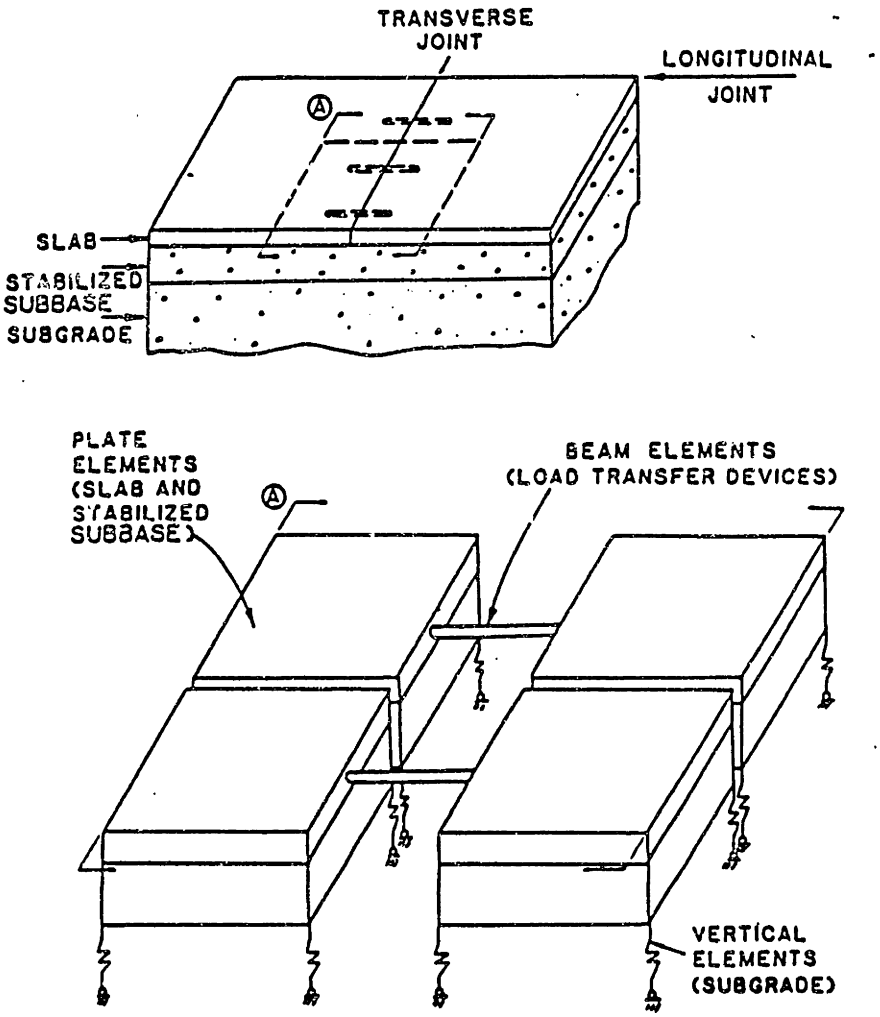

Figure 4.49 Decomposition of pavement section into finite elements [19]

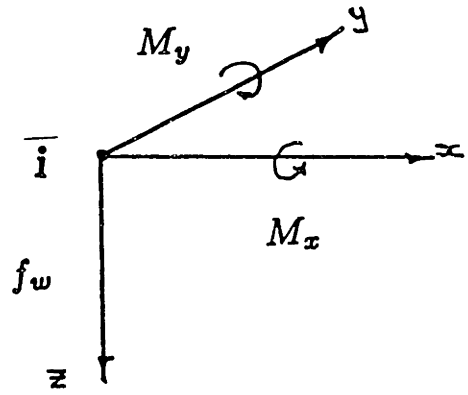

Positive force convention

Figure 4.50 Finite element nodal point convention

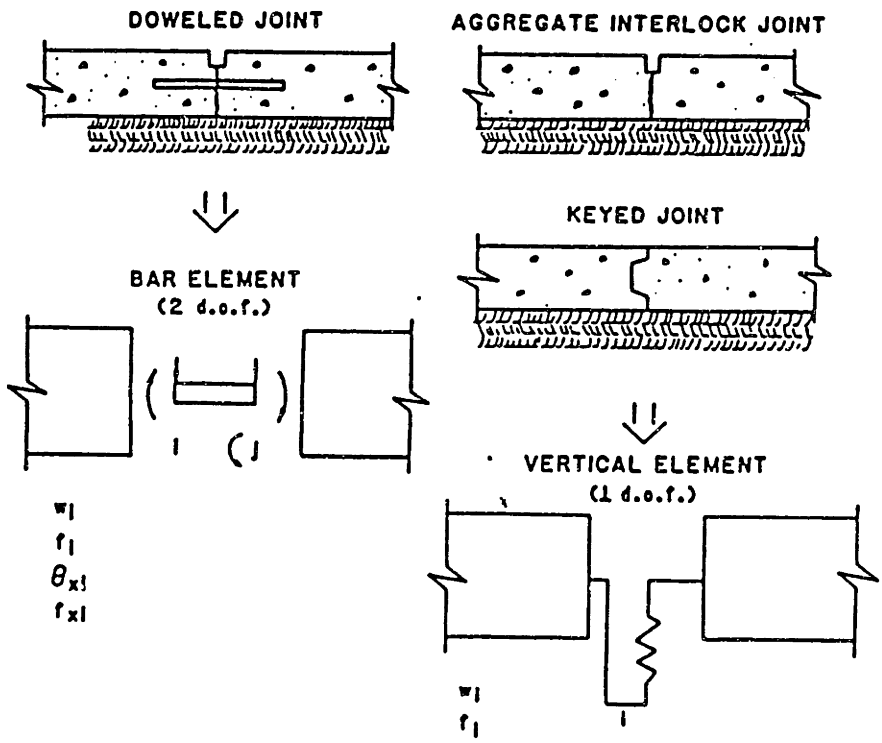

Figure 4.51 Finite element representation of pavement joint [19]

$$\{R\} = [K]\{U\} \tag{4.6}$$

where, $[K] = \sum [K]_e$

$\{R\}$: equivalent nodal forces for a uniformly distributed load over a rectangular section of the concrete slab.

$\{U\}$: Nodal displacements for whole system.

Loading Traffic and Environmental Loading

The system loading vector is composed of a component due to the traffic loading, environmental loading (thermal and moisture generated moments) and finally the slab self-weight. These effects may be linearly superposed:

$$\{R\} = \{R\}_{init} + \{R\}_{traffic} \tag{4.7a}$$

where,

$\{R\}_{init} = \{R\}_{thermal} + \{R\}_{moist} + \{R\}_{grav}$ yields the initial slab loading that exists in the absence of any traffic loading.

We may compute this initial loading vector from the integral below:

$$\{R\}_{initial} = \int_V [B]^T \{\tau\}^I \, dV \tag{4.7b}$$

where $\{\tau\}^I$ = initial stresses.

$\{R\}_{traffic}$ is the loading vector due to the traffic loading and is evaluated from the following surface integral:

$$\{R\}_{traffic} = \int_S [H]^T \{f\} \, dS \tag{4.7c}$$

where $\{f\} = [f_X^S, f_Y^S, f_Z^S]^T$ is the surface loading vector.

4.1.2 Modification of Concrete Slab Properties

The slab is modelled as an orthotropic plate. This takes into account the presence of different levels of reinforcement in the x and y-directions. An equivalent modulus of elasticity is given below [19]:

$$E = E_c + E_s \frac{I_2}{I_1} \tag{4.8}$$

where, for the X and Y-directions,

$$E_x = E_c + 0.75 p_x (\frac{d}{t})^2 E_s \tag{4.9}$$

$$E_y = E_c + 0.75 p_y (\frac{d}{t})^2 E_s \tag{4.10}$$

where,

E_x = modulus of elasticity in X-direction,

E_y = modulus of elasticity in Y-direction,

E_c = modulus of elasticity of concrete,

E_s = modulus of elasticity of reinforcement steel,

p_x = percentage reinforcement in X-direction,

p_y = percentage reinforcement in Y-direction,

I_1 = moment of inertia of the concrete section,

I_2 = moment of inertia of single reinforcing bar,

d = diameter of reinforcing bar,

t = thickness of slab.

The modulus of elasticity of the concrete is modified based on Miner's law [52]. We assume that a flexural endurance (relative stress vs. number of cycles to failure) curve (Figure 4.52 .) is known for the particular concrete section and compute the

relative stress due to the number of loadings applied for each node. The relative stress,

$$f_r = (\frac{\sigma_{mx}}{MR})_i \tag{4.11}$$

where,

σ_{mx} = maximum stress at node i,

MR = modulus of rupture of concrete.

We determine the maximum stress from the stress in the x and y-directions and the shear stress using Mohr's circle analysis :

$$\sigma_{mx} = \frac{1}{2}(\sigma_x + \sigma_y) + \sqrt{\frac{1}{4}(\sigma_x - \sigma_y)^2 + \tau_{xy}^2} \tag{4.12}$$

There are three possible cases. If $f_r \geq 1.0$ then cracking occurs in which case the thickness of the composite section is modified so that moment equilibrium in the cracked section is satisfied. If $0.5 \leq f_r \leq 1.0$ then fatigue damage occurs. In this case the value of the modulus of rupture is updated given the number of load applications. With the new modulus of rupture the new values of modulus of elasticity is computed at each of the nodes.

4.1.3 Load Transfer Efficiency

The method used for modifying the values of the load transfer efficiency is based on experimental results presented by Teller and Cashell [21].

The value of the load transfer efficiency is calculated as a function of the dowel-concrete interaction factor (DCI).

$$DCI = f(G, D, w_j) \tag{4.13}$$

where,

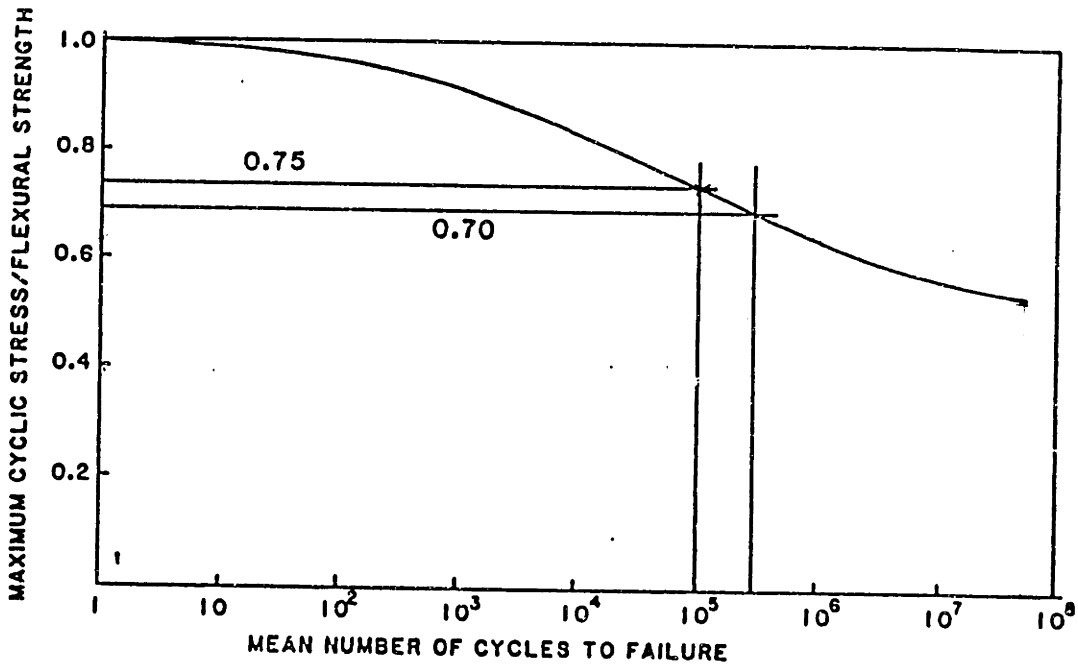

Figure 4.52 Typical flexural fatigue performance of concrete [19]

G = modulus of dowel support,

D = dowel diameter,

w_j = joint width.

The initial value of the dowel-concrete interaction factor is modified by a reduction factor which is a function of the number of load repitition and the shear force acting at the joint of the slab

4.1.4 Pumping Model

A pumping potential for the pavement is developed based on a regression analysis of the pumping indices of the AASHO Road Test [22] and the amount of energy imposed on the pavement by traffic. The amount of deformation energy imposed on a pavement section due to an application of an 18 kip axle is computed using the finite element program. This deformation energy is the total compression energy stored in the Winkler foundation,

$$E = \sum_{i=1}^{n} A_i k_i w_i^2 \tag{4.14}$$

where,

A_i = nodal area,

k_i = nodal subgrade modulus,

w_i = nodal vertical deflection.

The pumping index is normalized by the slab length. The normalized pumping is then a function of the total deformation energy. Having computed the normalized pumping index we may determine the volume of the void underneath the slab due to the ejection of the subbase, by assuming an average void depth. The nodes with zero support are then selected as being those with the largest deflections.

4.1.5 Joint Faulting Model

The joint faulting model used is the one employed in RISC [23] for undoweled pavements and is based on traffic, pavement age, joint spacing, subgrade drainage, and type of subbase:

$$JF = 0.0403 + \frac{1.53\,(DTN\ A^2)^{0.465}}{H^{3.9}} S^{0.61}\,(J - 13.5)^b \tag{4.15}$$

where:

JF = joint fault magnitude (in.);

DTN = Daily traffic number;

A = Age of pavement (yrs);

H = Slab thickness (in.);

S = Subgrade type (good = 1, poor = 2);

J = Joint spacing (ft.);

b = a factor depending upon subbase characteristics, equaling 0.241 for granular subbases and 0.037 for stabilized subbases.

The doweled pavement joint faulting model used in EAROMAR [24] is:

$$JF_{LTD} = \frac{1}{\sqrt{1 + A}}\, JF \tag{4.16}$$

4.1.6 Present Serviceability Index Model

The serviceability may be to slope variance, cracking, and patching through the following equations 22,24:

$$PSI = 5.41 - 1.801 \log(1 + SV) - 0.09\sqrt{C + P} \tag{4.17}$$

where:

PSI = Present serviceability index;

SV = Total slope variance;

C = cracking, C_l / 63.36;

P = patching, area patched / 63.36;

4.1.7 Slab Roughness Model

Roughness (measured as slope variance, SV) may be divided into two components: roughness due to slab distress and roughness due to joint distress. Slab roughness (SV_s) may be calculated using a model from EAROMAR [24] based on traffic and pavement materials properties (slab thickness, modulus of elasticity, modulus of rupture, and modulus of subgrade support). Joint roughness may be computed as shown below:

$$SV_j = \frac{7.983}{J} JF \tag{4.18}$$

or

$$SV_j = \frac{7.983}{J} JF_{LTD} \tag{4.19}$$

The total slope variance is given by the sum of the two:

$$SV = SV_s + SV_j \tag{4.20}$$

4.2 Survey of Existing Finite Element Programs

4.2.1 Introduction

We performed a survey of existing finite element programs to determine one which we could most easily use for the purpose of coupling the vehicle and pavement models. We were looking for a program with the following characteristics:

1. Finite element solution of the primary response of pavements subjected to loads at any position on the slab.

2. Include environmental effects such as slab curling and warping due to the thermal and moisture gradients across the slab cross-section.

3. Capability to relate primary response to secondary responses.

For a complete model we needed to include the secondary responses listed below:

- Fatigue cracking in the slab.
- Joint faulting model.
- Load transfer efficiency decay model.
- Pumping model.

The finite element models we considered for our project are

- PMARP [19]
- RISC [23]
- ILLISLAB [25]
- JSLAB [26]
- JCP-1 [27]

We eliminated JCP-1 on the basis that it did not solve the static equations of equilibrium for the primary response of the pavement for each loading case, but instead employed tables of results of a variety of loading cases which were obtained using

MODEL	ULTIMATE RESPONSE	LOADING	MODEL TYPE	COMMENTS
ILLI-SLAB ('79) ('85)		STATIONARY LOAD	FINITE ELEMENT	PRIMARY RESPONSE MODEL USED IN JSLAB & PMARP
JSLAB ('84)		STATIONARY LOAD TEMPERA-TURE MOISTURE SLAB - WEIGHT	FINITE ELEMENT	ALLOWS USER TO SPECIFY VOID LOCATIONS
PMARP ('86)	PUMPING CRACKING LOAD TRANS EFF.	STATIONARY LOAD	FINITE ELEMENT	VOIDS & MATERIAL PROP MODIFIED AT EACH ITERATION
RISC ('82)	JOINT FAULT CRACKING	STATIONARY LOAD TEMPERA-TURE	FINITE ELEMENT	ONLY DUAL TYRE LOADING CASE. THREE LAYER ELASTIC FOUNDATION.
JCP-1 ('77)	CRACKING PSI	STATISTICS OF LOAD TEMP	FINITE ELEMENT-REGRESSION	USES RESULTS OF FINITE ELEMENT MODEL BY HUANG & WANG ('73)

a finite element program developed by Huang & Wang in 1973 [28]. JSLAB and ILLISLAB are primary response models that do not contain any damage models. RISC and PMARP contained both primary response and damage models. PMARP was selected on the basis that it would have been difficult to add a pumping model to RISC, because it uses a homogeneous elastic half-space foundation. Also, PMARP has the ability to update the slab materials properties, which is important when considering seasonal effects. It was necessary though, to add slab thermal gradient effects to the program, a joint faulting and present serviceability index (PSI) model.

4.2.2 Slab Thermal Gradients

A difference in temperature between the top and bottom slabs causes significant stresses in the slab. These thermal stresses are superposed constructively with traffic loading stresses for the case when the top layer is warmer than the bottom layer (daytime). In fact it has been concluded [29], that warping is primarily responsible for much of the cracking in concrete pavements. The effect of slab length on curling stress is illustrated in Figure 4.53. It is interesting to note that the transverse cracking follows the same trend [27].

4.2.3 Determination of Edge Moment for Thermal Effects

Consider the simply supported slab in Figure 4.54 with a temperature difference across the bottom and top layers. The temperature distribution across the slab cross section may be written as a function of the distance from the mid-section (z)

$$\Delta T(z) = \frac{1}{2}(T_1 + T_2) + \frac{(T_1 - T_2)}{t} z \tag{4.15}$$

The moment per unit length due to the thermal effect may be obtained from,

$$M = \int_{\frac{-t}{2}}^{\frac{t}{2}} \sigma_{thermal} z dz \tag{4.16}$$

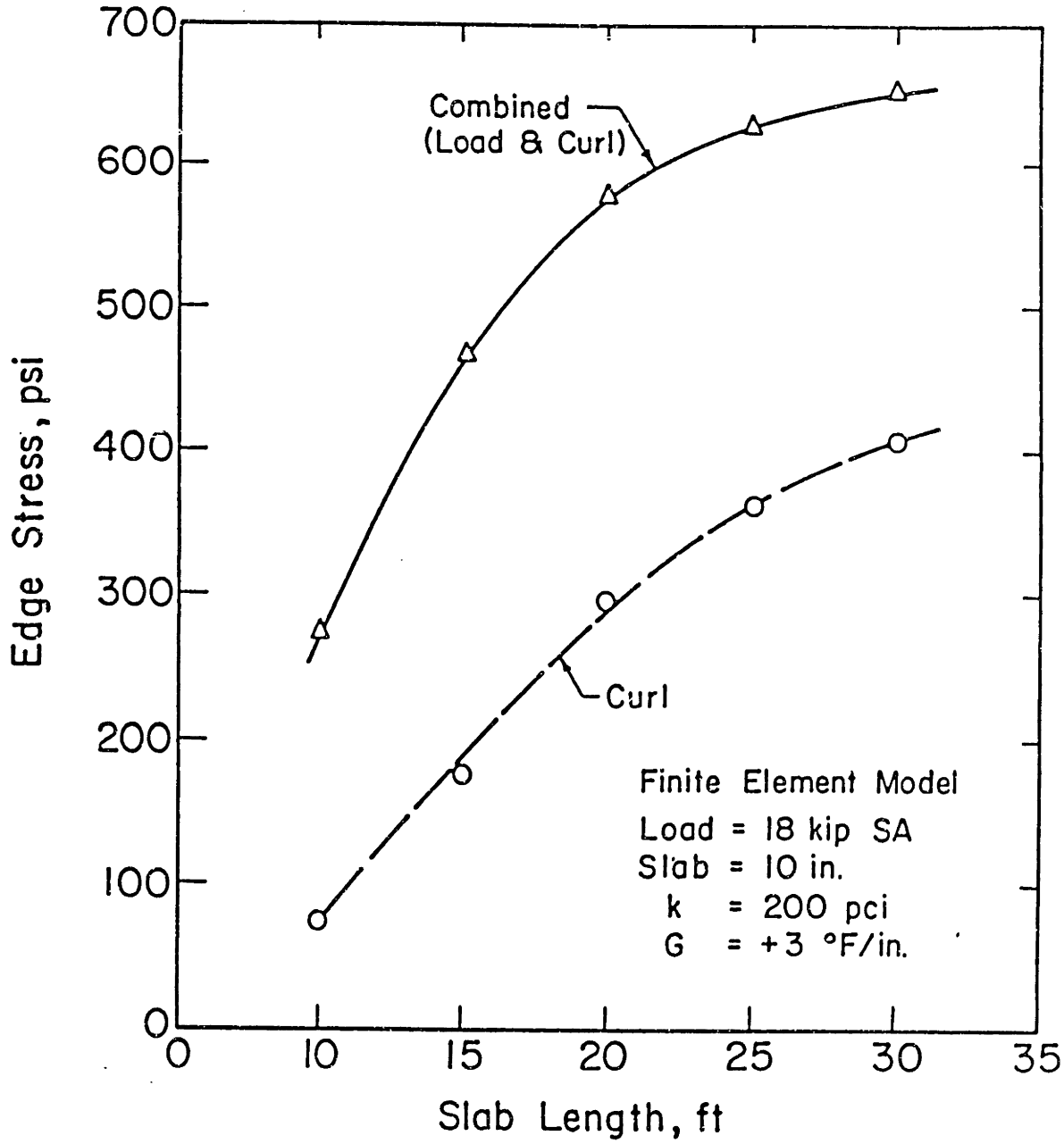

Figure 4.53 Edge stresses due to load & thermal gradients [27]

where $\sigma_{thermal} = E\epsilon$ are the thermal stresses and the strain $\epsilon = E\Delta T\alpha$ where,

E = Young's Modulus of concrete slab

α = Thermal expansion coefficient of concrete

ΔT = Temperature distribution

$$\Rightarrow M = \alpha E \int_{\frac{-t}{2}}^{\frac{t}{2}} [\frac{1}{2}(T_1 + T_2) + \frac{(T_1 - T_2)}{t}] \, z \, dz \tag{4.17}$$

Evaluating the integral we obtain,

$$\Rightarrow M = \frac{\alpha E t^2 (T_1 - T_2)}{12}$$

or

$$M = \frac{\alpha \, g \, E \, t^3}{12} \tag{4.18}$$

where g = thermal gradient = $\frac{(T_1 - T_2)}{t}$

It is important to note that the thermal gradient does not contribute to the normal nodal point force.

4.2.4 Determination of Slab Warping Effects

Variation in pavement moisture content between the top and bottom results in slab warping. Generally, the top of the slab is drier than the bottom. Since, we may treat the warping effects on the slab similarly to the curling effects, we may calculate an equivalent temperature gradient that may be linearly superposed to the thermal gradient. Thus,

$$g_e = -\frac{2 \, \epsilon_s}{\alpha \, t} \tag{4.19}$$

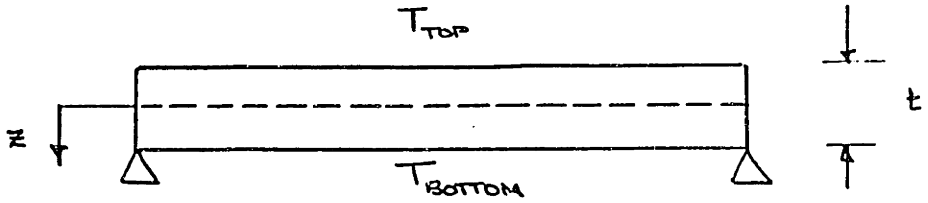

$$M = \int_{-\frac{t}{2}}^{\frac{t}{2}} \sigma_{th}(z)\, z\, dz$$

where the thermal stresses,

$$\sigma_{th}(z) = E\epsilon = \alpha E \Delta T(z)$$

$$M = \frac{\alpha g E t^3}{12}$$

M = Moment per unit length.
$g = \frac{(T_{top} - T_{btm})}{t} \geq 0 \Rightarrow$ DAYTIME
E = Young's Modulus of Concrete
α = Thermal Expansion Coefficent
t = slab thickness

Figure 4.54 Thermal gradient effects

where:

g_e = equivalent temperature gradient;

$e_s = \frac{1}{2}$ total warping shrinkage strain differential betwwen top and bottom layers;

α = thermal expansion coefficient;

t = slab thickness.

Moisture warping stresses at the slab bottom are generally of opposite sign than load stresses, and therefore tend to reduce the combined stresses occurring at the slab edge or interior.

4.2.5 Modifications to PMARP

The modifications we have made to PMARP may be divided into three categories. First, we made some changes to correct some ambiguous lines of the code itself. Secondly, we added subroutines to enable us to investigate the case of the moving dynamic loading. Finally we added the effects of thermal gradients to the system.

Alterations to PMARP code

The pressure loading and number of loading cycles specified by the user were modified in the coding. The modifications were aimed at converting the specified loading to an equivalent 40 kip axle loading. We understand the motivation behind this conversion was to take into account the effects of applying a heavy load to the pavement followed by a lighter less damaging loading. It was observed however, that by removing the equivalency factors, the relative stresses generated were below a certain threshold value ($f_r = \frac{\sigma_{max}}{MR} \leq \frac{1}{2}$). This implies that the pavement life is theoretically infinite for an 18 kip axle loading. We found however,that by removing the equivalency conversion and leaving the loading as specified by the user we obtained cracking when the stresses due to thermal gradients were added.

The second modification involved the calculation of the plane of principal stresses. The equations in the original coding were replaced by the following:

$$\tan 2\theta_1 = \frac{\tau_{xy}}{(\sigma_x - \sigma_y)/2} \tag{4.20}$$

Additional Code

Three optional analyses have been added to PMARP, in addition to the original model (Figure 4.55). These options are listed below:

1) Influence function generator: the primary response at a specified nodal point is stored as a user specified loading is stepped through selected nodal points along the slab.

2) Single moving dynamic load: in this option we store the maximum response at each node as a dynamically varying loading traverses the slab. Secondary response of the pavement is computed based on the maximum stresses generated at each of the nodes. The flow chart is illustrated in Figure 4.56.

3) Repeated moving dynamic load: this is similar to option (2) above with the distinction that now we are taking into account the seasonal effects and day and night time temperature and moisture variations in the slab, as shown in Figure 4.57.

Addition of Thermal Effects

The pavement slab experiences a warping moment due to a temperature difference between the top and bottom layers. This difference in temperature results in thermal strains which are proportional to the temperature difference and the thermal expansion coefficient of the concrete. The thermal gradient in the slab may be represented in our finite element model as an equivalent moment applied along the edge of the slab. We have shown that we may represent the stress resultant as

$$M^* = \frac{\alpha g E t^3}{12} \tag{4.21}$$

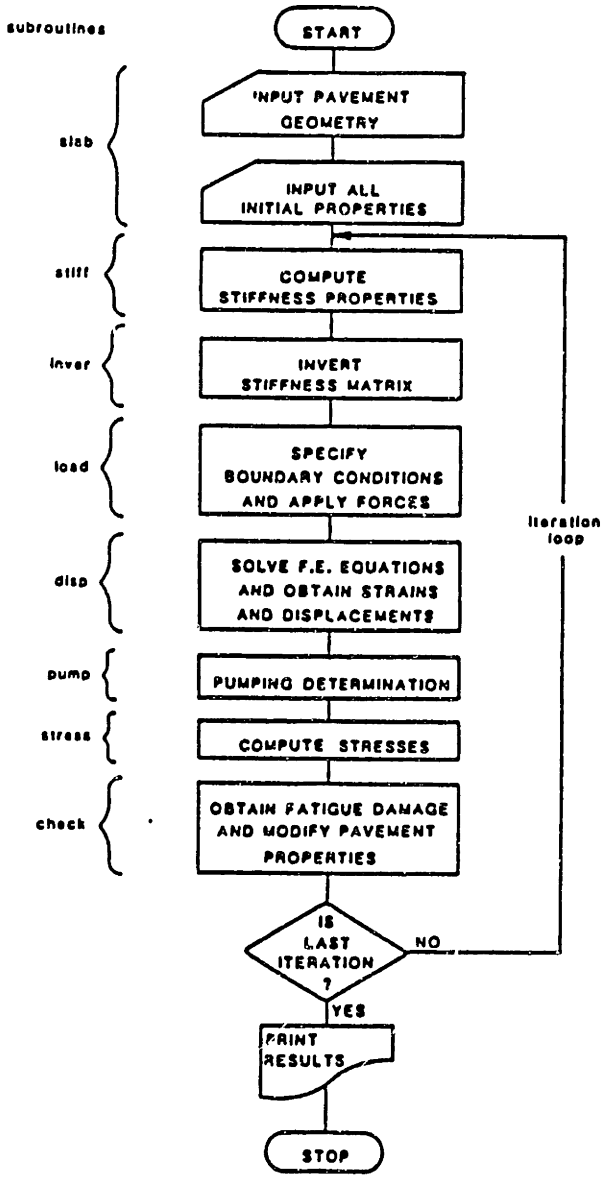

Figure 4.55 Flow chart for original version of PMARP [19]

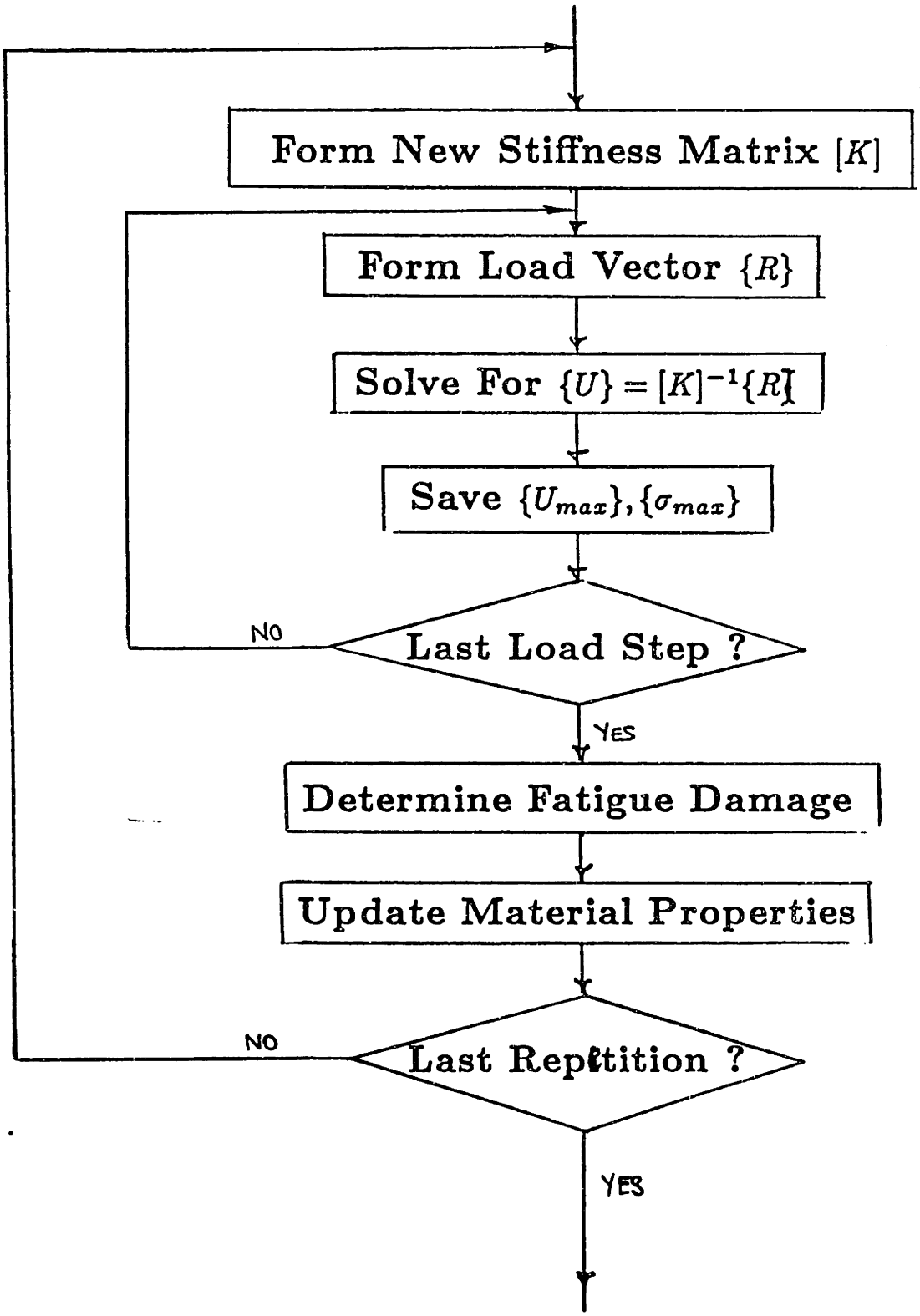

Figure 4.56 Flow chart for moving dynamic load

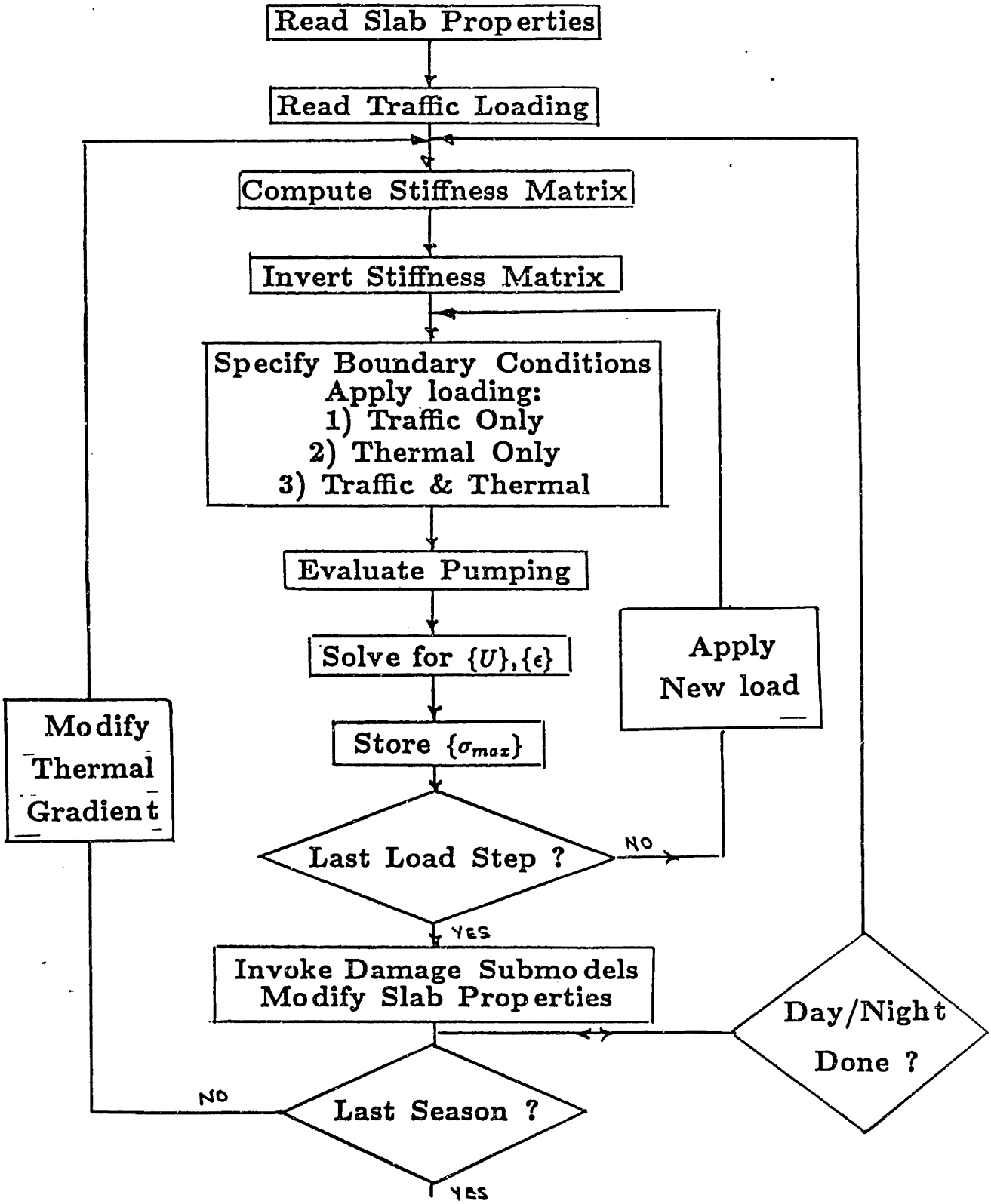

Figure 4.57 Flow chart for repeated moving dynamic load

where:

α = thermal expansion coefficient;

g = thermal gradient;

E = Young's Modulus of concrete;

t = thickness of the slab.

Consider the case for which the thermal gradient is positive ($g \geq 0$): the value of the resultant stress (M^*) is then positive and the slab would adopt a convex down shape. Given the moment and the force convention illustrated in figures 4.50 ,4.53 , the modifications made to the loading vector at each of the edge nodes of the slab is as follows:

Edge 1:

$$M_1' = M_1 - (M^* \Delta x)$$

Edge 2:

$$M_2' = M_2 + (M^* \Delta x)$$

Edge 3:

$$M_1' = M_3 + (M^* \Delta y)$$

Edge 4:

$$M_1' = M_4 - (M^* \Delta y)$$

where:

M_i' = Resulting moment applied to nodes along edge i;

M_i = Moment due to traffic loading;

M^* = Thermal stress resultant (moment per unit length).

Note, in addition when considering the thermal effects we need to include the slab self weight. This is done by distributing the weight of each element equally among the corner nodes. The loading due to gravity has no moment contribution.

PERFORMANCE MODELS

Decay in Modulus of Elasticity

Let us define ΔE as being the percentage reduction in the modulus of elasticity. That is,

$$\Delta E = \frac{E_i - E_c}{E_i} \tag{4.22}$$

where:

E_i = initial modulus of elasticity of the concrete;

E_c = current modulus of elasticity of the concrete.

We may obtain a damage index related to the decay in the modulus of elasticity by considering the decay in the modulus of elasticity at each node weighted by the effective nodal area,

$$D_E = \sum_{k=1}^{N} A_k \, \Delta E_k \tag{4.23}$$

where, N = total number of nodes.

4.3 Modelling Moving Dynamic Loading

4.3.1 Introduction

Because the vehiclular load is variable in magnitude and position we must position the load in many positions to determine the most severe effect at each different location. The method by which the structural analyst computes the loading position which will give the most severe effect is by using the concept of the influence line or function. The influence line determines the effect of the load acting in various postions on the magnitude and sign of the primary response of the structure (i.e. stresses, strains, and deflection). The influence line thus gives the variation in the response at one point due to a unit load traversing the pavement.

The concept of using the influence of a moving unit load to determine placement of actual loads to give a maximum or minimum effect was published by Winkler in 1868 [31].

4.3.2 Influence Functions

In section 4.4 we show that the pavement inertial and viscous terms are negligable and that we can treat the pavement response due to the passage of vehicular loads as a quasi-static occurrence. The response at a point of interest in the pavement x_0 due to the passage of a unit load at x is thus characterized by the static response, $\rho(x_0 - x)$. From the Influence Function $I(x_0 - x)$ we may determine the response $(R(x_0))$ at x_0 due to any load $F(x)$.

$$R(x_0) = \rho(x_0 - x)\, F(x) \tag{24}$$

Notice that the response may be the deflection, stress or strain at the point of interest. Furthermore, whereas the influence functions for flexible pavements are symmetric, this is not the case for rigid pavements. Typical influence functions

generated using PMARP are illustrated in figure 4.58. The asymmetry is due to the discontinuities in the pavement structure.

The influence functions for rutting and cracking are illustrated in figure 4.59 for comparison. These were generated using VESYS IIIA [32]. The normalized influence functions may be fitted using the following equation:

$$\rho(x) = \cos^2\left(\frac{\pi}{2}\frac{a\,x^b}{1+ax^b}\right) \tag{4.25}$$

where a and b are regression constants.

4.3.3 Maximum Response at a Point Of Interest

When considering the damage to a pavement we look at the maximum or peak response at each point along the pavement and use that maximum value to compute the damage. For flexible pavements, for example the rutting damage index Φ_R is assumed to be related to the fourth power of the peak primary response (compressive strain at the top of the subgrade). It is thus important to show that for a dynamically varying moving load the load does not necessarily have to be on the point of interest when it experiences the peak response.

If we consider a single axle load traversing a rigid pavement slab then by using the influence function we may examine the response at a critical point x_0;

$$R(x_0) = \rho(x_0 - x)\,F(x) \tag{4.26}$$

To determine the maximum response at the point of interest we need to look at the response over all values of x (i.e. apply the load at all points along the slab), thus the peak response is:

$$R_p(x_0) = max_x[\rho(x_0 - x)\,F(x)] \tag{4.27}$$

Given deterministic force profiles and influence functions we may differentiate equation (4.26) to determine the location of the peak response, therefore:

$$\frac{\partial R}{\partial} = \rho(x_0 - x)\frac{\partial F(x)}{\partial x} + \frac{\partial \rho(x_0 - x)}{\partial x}F(x) \tag{4.28}$$

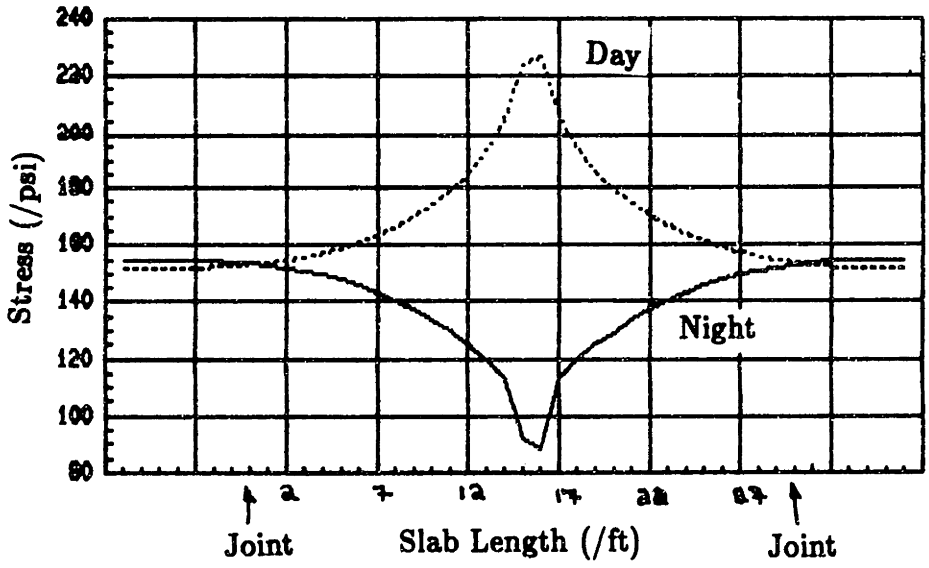

Figure 4.58 Typical influence functions for rigid pavements

max stress influence

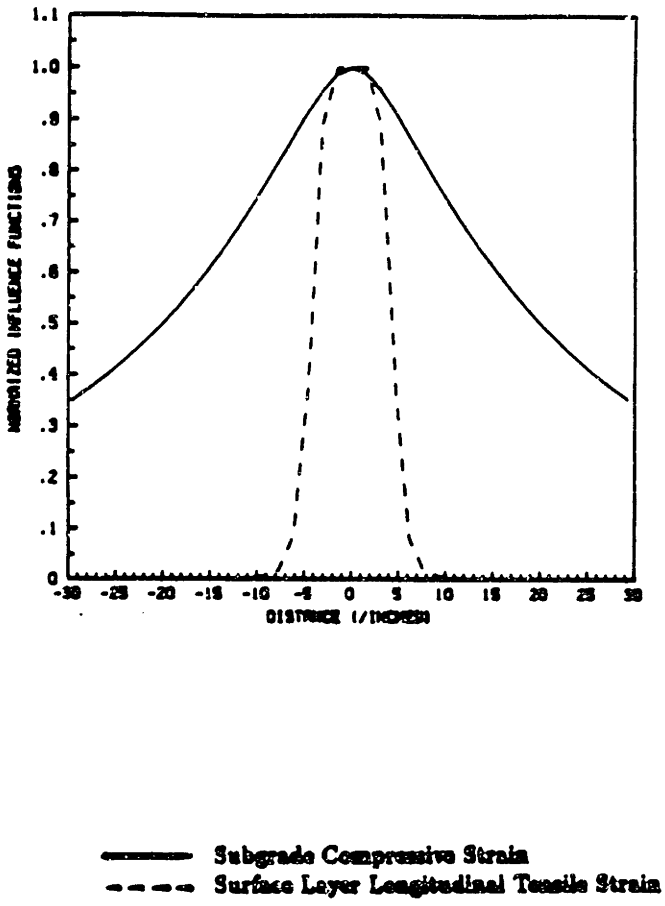

Figure 4.59 Typical influence function for flexible pavement

For the maximum response we need to set $\frac{\partial R(x_0)}{\partial x} = 0$, which does not neccessarily occur over the point of interest unless:

(1) $F(x) = const$, i.e a static moving load assumption and

(2) The influence function has $\frac{\partial \rho(x_0 - x)}{\partial x} = 0$ evaluated at $x = x_0$.

We therefore expect that the critical or maximum response at any point along the pavement may occur when the load is not directly over the point itself. Models that use a static loading case applied at what is believed to be the critical point (i.e. midslab loading) are therefore using an inadequate representation of the vehicle loading. Two observations about the nature of rigid pavements make an influence function approach especially important when dealing with rigid pavements:

- Higher levels of dynamics (larger dynamic load coefficient (DLC)) are excited when the vehicle encounters faults along the rigid pavement.
- Because the elastic modulus of concrete is considerably larger than that of asphalt, the ifluence functions associated with rigid pavements is broader. Therefore, the effects of larger dynamic load coefficients are more significant at the critical points along the slab.

4.3.4 Multiple Axles Traversing Slab

When the joint spacing of the rigid pavement is larger than the vehicle axle spacing or when considering tandem axles where the axle spacing is generally about 52 inches, we need to compute the peak response at a point of interest due to more than a single load. If $F(x_1)$ and $F(x_2)$ are the point loads where $x_1 - x_2 = d$, the spacing, then the response at x_0 due to each load is given by:

$$R_1(x_0) = \rho(x_0 - x_1)\, F_1(x_1) \tag{4.29}$$

$$R_2(x_0) = \rho(x_0 - x_2)\, F_2(x_2) \tag{4.30}$$

Since we are modelling the system as linear elastic we may therefore, express the total response at x_0 due to the combined loading as

$$R_{T_2}(x_0) = R_1(x_0) + R_2(x_0)$$

$$= \rho(x_0 - x_1)\, F_1(x_1) + \rho(x_0 - x_1)\, F_2(x_2) \tag{4.31}$$

The extension to the case of N-loads follows directly:

$$R_{T_N}(x_0) = \sum_{i=1}^{N} R_i(x_0)$$

$$= \sum_{i=1}^{N} \rho(x_0 - x_i)\, F_i(x_i) \tag{4.32}$$

The influence function concept is applied when solving a statics problem using the finite element formulation. The static equation :

$$K\,U = R \tag{4.33}$$

where

K = system stiffness matrix;

U = system nodal degrees of freedom;

R = system loading vector.

For N-axles

$$R = \sum_{i=1}^{N} R_i$$

Note that for a finite element mesh with p-nodes each with q-degrees of freedom, the K matrix has dimensions $(p \times q)$ by $(p \times q)$ and the dimensions of the U and R vectors are $(p \times q)$ by 1.

Figure 4.58 illustrate graphically the occurence of the peak response when the load is not directly over the point of interest.

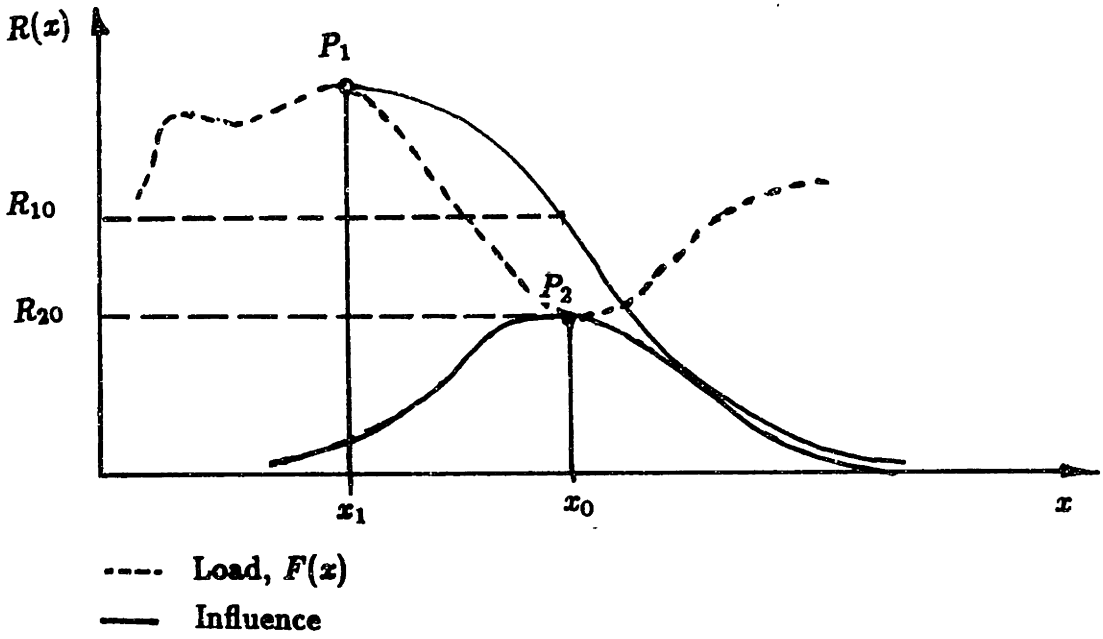

R_{10}, Response due to P_1 at x_0
R_{20}, Response due to P_2 at x_0
$P_1 = F(x_1)$
$P_2 = F(x_0)$

Figure 4.60 Graphical illustration of load position for peak response

4.4 Justification of Quasi-static Loading Model

The finite element analysis programs available are based on a static analysis. In our modification of these programs to consider a moving dynamic loading we are essentially treating the problem as a quasi-static problem and solving the static equations at each progression step of the loading, neglecting inertial and damping effects. These would otherwise be taken into account by forming the mass and damping matrices:

$$M = \int_V \rho\{H^T\}_e \{H\}_e \, dV \tag{4.34}$$

$$C = \int_V \kappa\{H^T\}_e \{H\}_e \, dV \tag{4.35}$$

where:

ρ is the mass density of the element;

κ is the damping property of the element;

$\{H\}_e$ is the element nodal point interpolation function.

The equations of equilibrium governing the linear dynamic response of a system of finite elements

$$M\ddot{U} + C\dot{U} + KU = R \tag{4.36}$$

where K is the stiffness matrix and M and C are defined above; R is the external load vector, and $\ddot{U}, \dot{U}, U$ are the displacement, velcity and acceleration vectors of the finite element assemlage. The choice for a static or dynamic analysis (i.e. for including or neglecting velocity and acceleration dependent forces in the analysis) is usually decided by engineering judgement, the objective thereby being to reduce analysis effort required. However, it should be realized that the assumptions of a static analysis should be justified, since otherwise the results would be meaningless.

The dynamics of the pavement system become important as the velocity fo the moving load appraoches a critical velocity (V_{cr}). This velocity has been defined as the propagation velocity of a transverse displacement wave through the pavement.

If we model the rigid pavement structure as an elastic plate on an elastic foundation the governing differential equation of motion may be written as [33]:

$$D\frac{\partial^4 w}{\partial x^4} + \rho V^2 h\frac{\partial^2 w}{\partial t^2} - cV\frac{\partial w}{\partial t} + Kw = P(x,t) \tag{4.37}$$

where:

D = flexural rigidity of slab, $\frac{E h^3}{12(1-\mu^2)}$;

w = vertical displacement of point on slab;

ρ = density of slab;

h = thickness of slab;

c = subgrade damping coefficient;

K = subgrade spring constant per unit area;

E = modulus of elasticity of slab;

μ = Poisson's ratio of concrete.

The solution of the eigenvalue problem gives the critical velocity:

$$V_{cr} = 4\sqrt{\frac{4KD}{(\rho h)^2}} \tag{4.38}$$

For typical values of the parameters:

ρ = 150 pcf;

h = 14 inch;

K = 2000 psi per inch;

$E = 4 \times 10^6$ psi;

μ = 0.15;

We obtain $V_{cr} \approx 952$ mph. The vehicle velocities we are concerned with are less than 10 % of the critical velocity which means that the dynamic response of the pavement structure is negligable in our application.

5

Parametric Study

5.1 Introduction

The method outlined in the previous section whereby we apply a moving dynamic loading to the pavement by day and night each season is very expensive. Typically it required about 5 minutes per season simulation time on a VAX 11/750 series. This is equivalent to approximately 10 hours simulation for a pavement life of 30 years. Given the expense and time involved in performing parametric studies with the model described we decided to make the approximations described below.

Primarily we realized that the main effect of pavement age on the vehicle dynamics was due to the increased joint faulting magnitude. We computed vehicle loading profiles for a series of joint fault heights ($\frac{1}{10}, \frac{1}{4}, \frac{1}{2}, \frac{3}{4}$ inch). We determined that it was valid to interpolate force profiles for intermediate joint fault magnitudes. Furthermore, we assumed that the reduction in the elastic modulus of the slab was within 5 % of its original value for the majority of the pavement life and thus assumed it was constant. We also assumed an average value for the modulus of rupture of 80 % of its initial value.

Given the above assumptions we determined the pavement response at the selected fault heights and determined the damage that would be incurred due to the dynamic loading at each fault height. Based on the joint fault model we simulated the pavement life seasonally by interpolating for the response at intermediate joint fault magnitudes. This method of simulation would thus cut down computer simulation time to 80 minutes representing an 86 % reduction in cost.

In summary the assumptions made are listed below:

- The vehicle loading profile may be interpolated for joint fault heights not simulated using the vehicle model.

- The elastic modulus of concrete and the modulus of rupture are assumed to remain constant over the life of the pavement and are taken as average values.

- The pavement damage at each node may be interpolated for intermediate values of the joint fault magnitude.

- Currently the subgrade weakening due to pumping is neglected, since we have no model to relate the amount of pumping to joint fault magnitude. Given this information we can present the damage at each node as a function of joint fault height and subgrade condition.

Some results of interpolating load profiles between joint fault magnitudes are illustrated in figure 5.61. We define the percentage error due to the interpolation as

$$e = 100 \frac{\Delta X_i}{P} \tag{5.1}$$

where :

ΔX_i is the difference between the actual force profile and the interpolated profile at station i along the slab;

P is the mean tire force.

Using this definition we obtained peak errors within 5 % - 10 % of the actual loading profile.

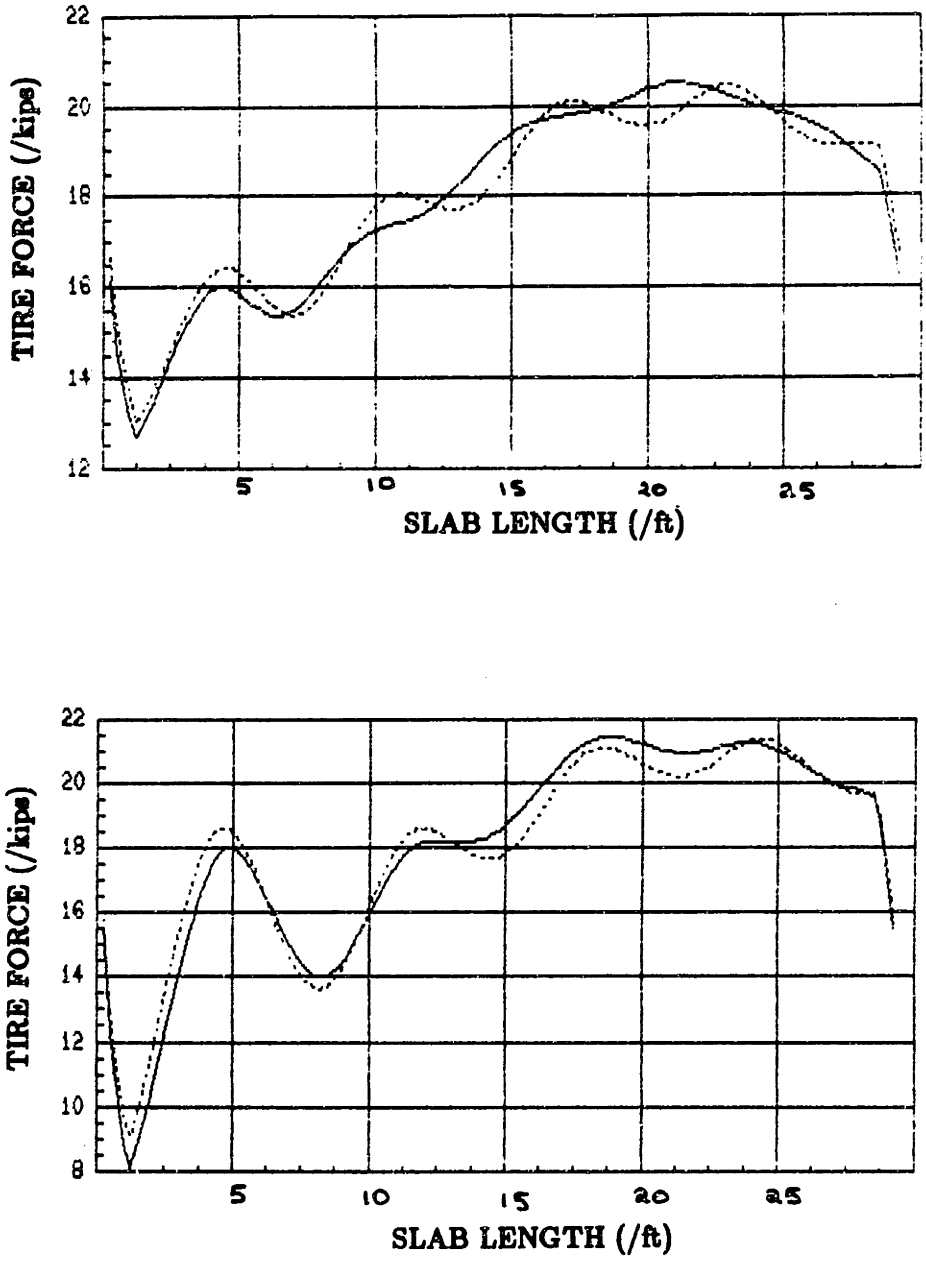

Figure 5.61 Interpolation of loading profile between joint fault values
(a) 0.3 inch
(b) 0.6 inch
—— ESTIMATE
----- ACTUAL

5.2 Static versus Dynamic Moving Load

We compared the cracking damage obtained by considering the vehicle load as a static moving load to the case of a dynamic moving load and obtained the results illustrated in figure 5.62.

The case of the dynamically moving load produces approximately 38 % larger cracking damage than the static moving case after fifteen years of pavement service. This indicates the importance of considering the vehicle dynamic loading when assesing pavement performance. It is also interesting to note that the cumulative damage over time is linear. We expected the additional dynamics excited to produce an incraese in the rate of pavement cracking. A possible reason for not obtaining this result may be due to the assumptions made at the beginning of this chapter, in particular the constant values of the concrete elastic modulus.

If we analyze the cracking as it is distributed over a single slab which is divided into five regions (the vehicle travels from region 1 across to region 5), figure 5.62b illustrates the result for the static and dynamic moving load cases. We obtain a symmetrical distribution of cracking over the slab with the most severe cracking occuring in the regions close to the edge of the slab. By comparing this to the dynamically moving load we note that there is a 15 % decrease in the cracking that occurs in the regions close to the joints. Furthermore, there is a large increase in the cracking in the mid-slab regions, which may be directly attributable to the body mode contribution to the tire force (figure 3.30). There is therefore good correlation between the aggregate force plot of figure 3.30 and the distribution of cracking damage over the slab.

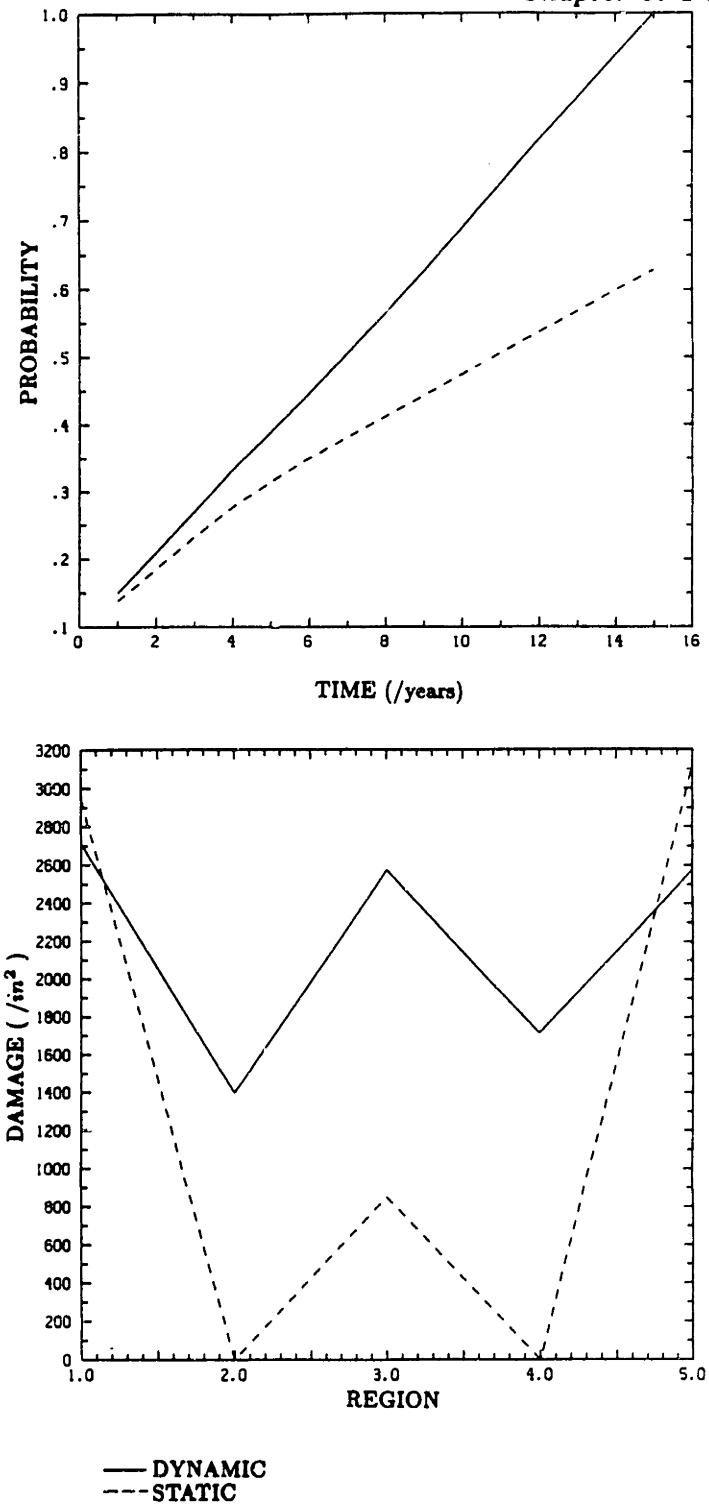

Figure 5.62 Dynamic moving versus static cracking damage
(a) Probability of cracking versus time
(b) Cracking by region

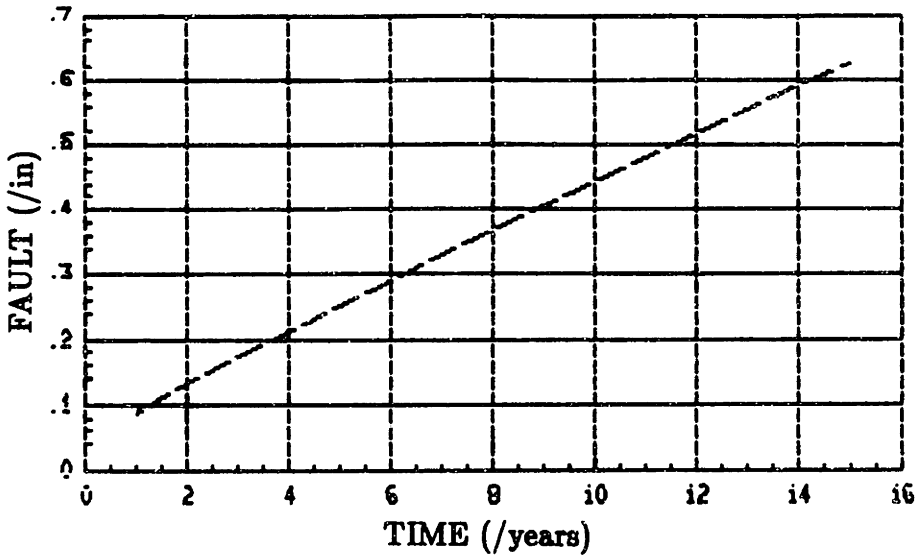

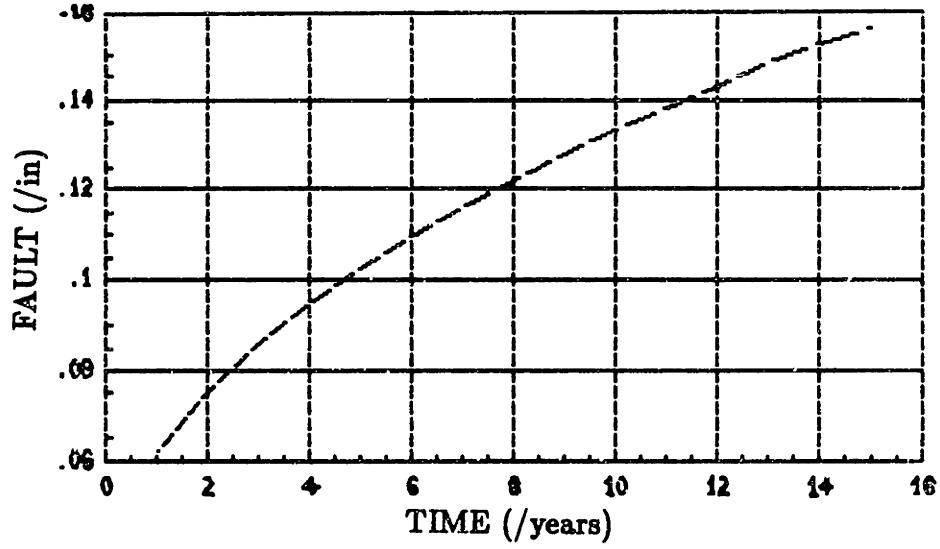

Figure 5.63 Joint fault magnitude vs time
(a) Aggregate Interlock
(b) Doweled

5.3 Single-Axle Suspension

The effect of varying selected vehicle parameters is investigated for the three axle tractor semi-trailer in an attempt to correlate the effects of the resulting change in dynamics to pavement damage. The following parametric studies were performed on rigid pavements with aggregate interlock joints. Doweled pavement joints generally maintain faulting within $\frac{2}{10}$ inch over the pavement service life. For small fault heights (under $\frac{1}{4}$ inch) we do not see the variation in the vehicle dynamics as a result of changing vehicle parameters. This can be illustrated by observing that there is little effect of varying vehicle parameters on cumulative damage for pavement age under six years or fault heights under $\frac{3}{10}$ inch.

5.3.1 Effect of Suspension Stiffness

In section 3.34 we concluded that increasing the leaf-spring stiffness leads to reduction in the wheel mode and an increase in the body mode. Figure 5.64 illustrates the above result. Over the whole slab we obtain a 10 % reduction in the cracking damage by halving the leaf-spring stiffness.

When we analyze the effect of the spring stiffness on the distribution of cracking we note that there occurs a considerable decline in the cracking in regions 3 and 4 due to a reduction in the leaf-spring stiffness. The increase in cracking in the region close to the joint is due to an increase in the wheel mode contribution to the tyre force that is a result of reducing the leaf-spring stiffness. Note however, that the effect of changing the stiffness has a bigger effect in the mid-slab region.

To reduce pavement damage therefore, we recommend softer suspensions. However, we realize that the main factor determining the choice of suspension stiffness is the axle load.

5.3.2 Effect of Leaf-spring Damping

The effect of decreasing the leaf-spring damping (increasing β) is to increase the wheel mode contribution and reduce the body mode contribution as illustrated

in figure 3.19 and 3.20. The reduction in the cracking occurs in the mid-slab region (figure 5.65). There is also an increase in the cracking that occurs in region 5 that is directly due to an increased loading in that region, with a reduction in leaf-spring damping. Figure 5.65a indicates that a larger value of β or reduction in leaf-spring damping produces a reduction in cracking (approximaltely 12 %) over the entire slab, due to the reduction in the body mode contribution.

A reduction of the body mode contribution to the tyre mode can therefore be achieved by reducing the amount of damping in the leaf-spring. We therefore recommend leaf-spring suspensions with high values of β.

5.3.3 Effect of Velocity

We determined that at a vehicle velocity of 55 mph the vehicle is in tune with the road inputs. This results in larger tire forces being generated. At velocities other than this critical velocity the dynamic forces excited are reduced. For vehicle velocities of about 35 mph the effect of dynamics become less important and the damage distribution resembles that of a static moving loading. Figure 5.66b also illustrates this shift in the largest damage regions to the latter part of the slab with the increase in velocity from 55 to 70 mph.

Due to the dimensions of the vehicle wheelbases and slab length the vehicle experiences simultaneous inputs to the steer and rear axles. The frequency at which the vehicle experiences these inputs should be adjusted such that it is not in the range of the body mode frequency. The adjustment is made through the vehicle velocity, or by changing the slab length.

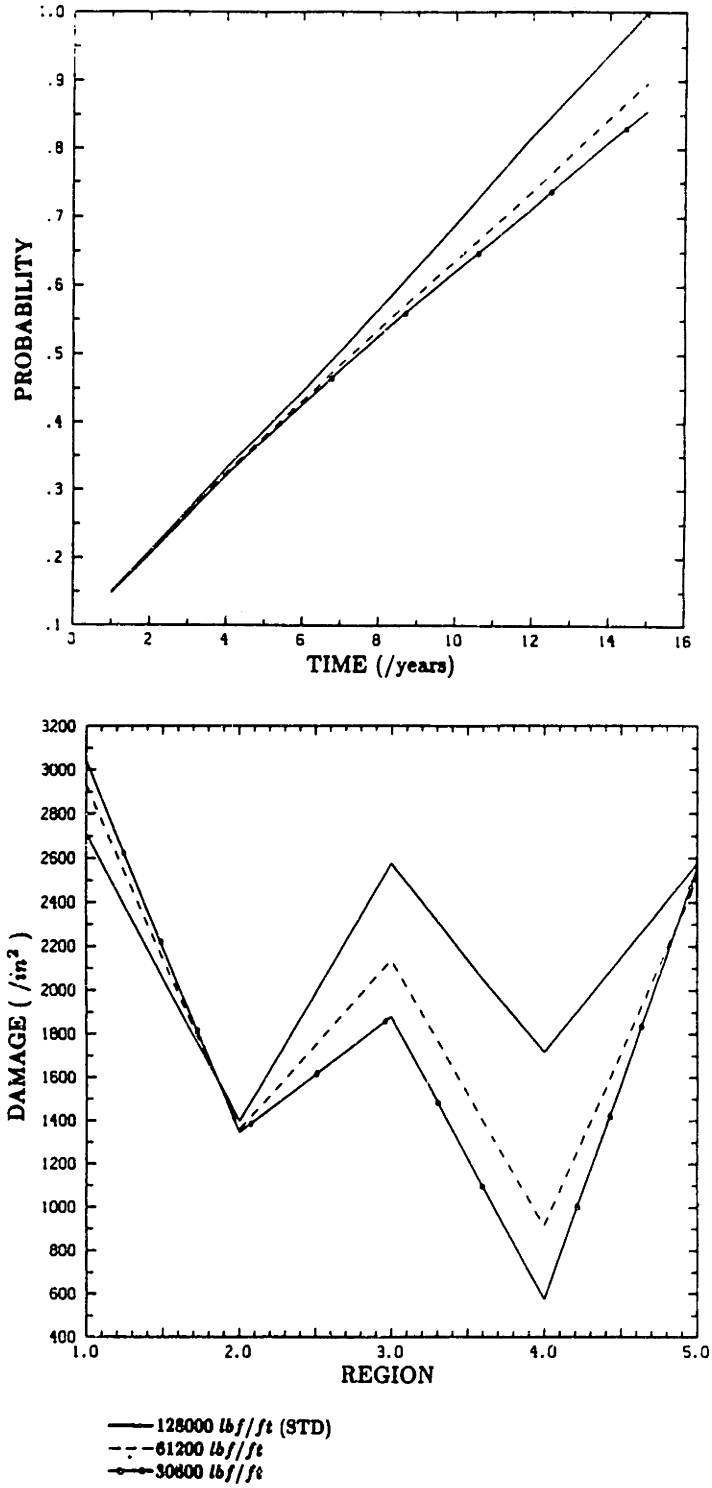

Figure 5.64 Effect of average spring suspension stiffness (Single)
(a) Probability of cracking versus time
(b) Cracking by region

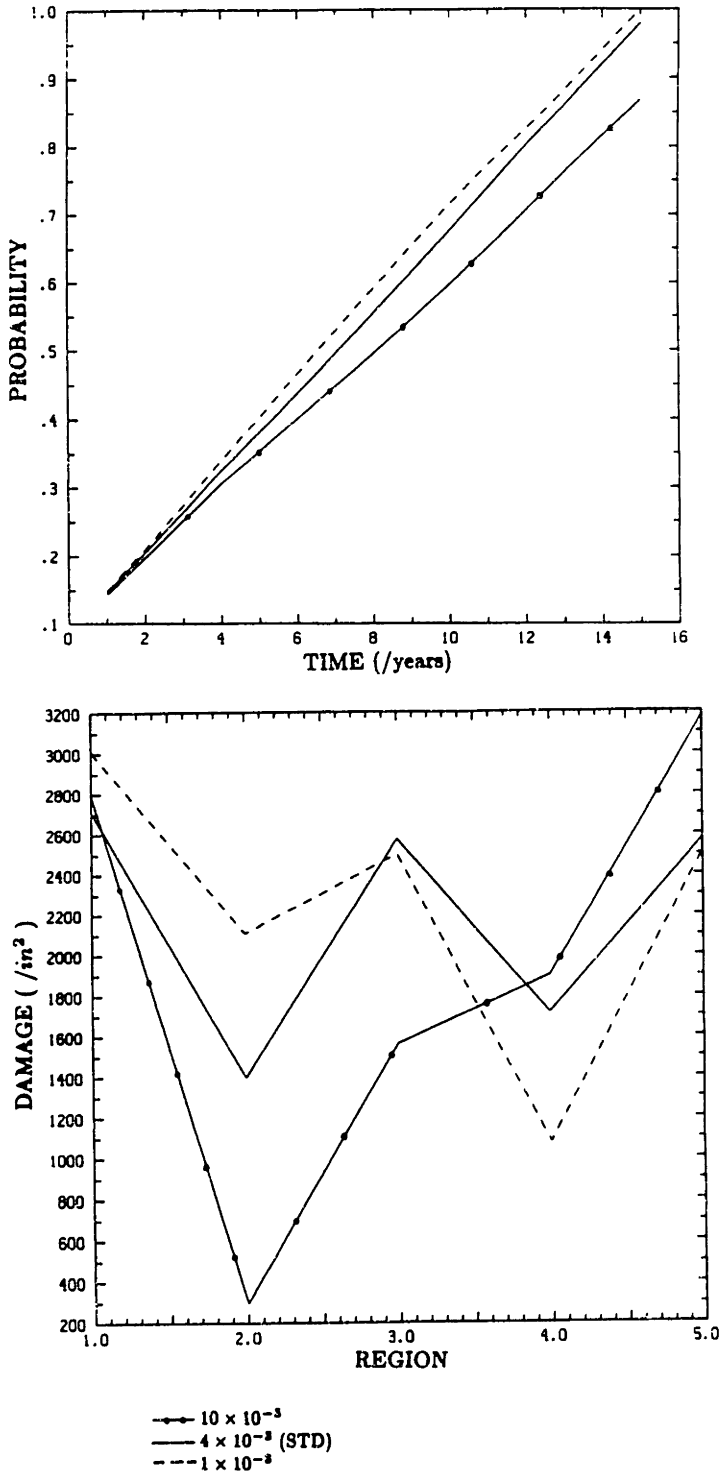

Figure 5.65 Effect of leaf-spring β parameter (Single)
(a) Probability of cracking versus time
(b) Cracking by region

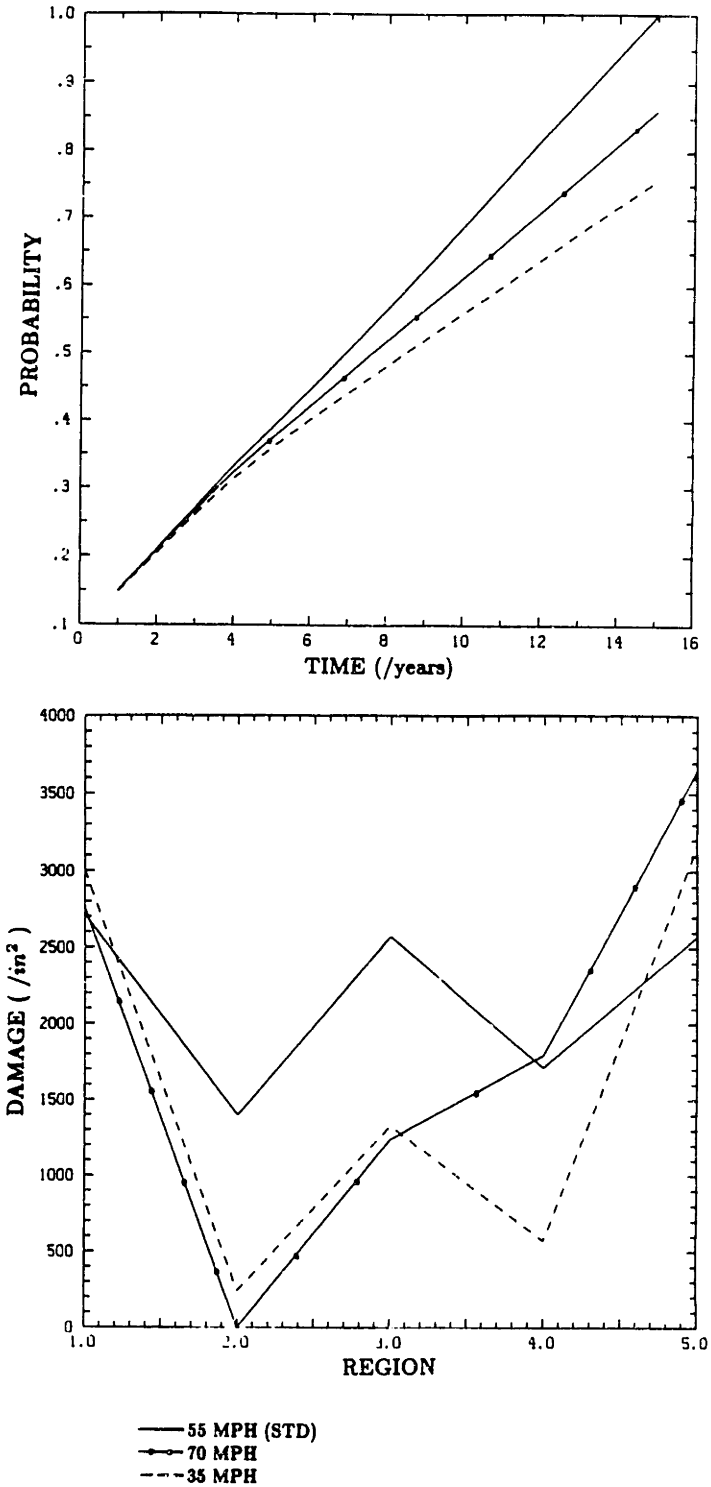

Figure 5.66 Effect of velocity (Single)
(a) Probability of cracking versus time
(b) Cracking by region

5.4 Walking-Beam Tandem Suspension

We investigated the cases of varying the vehicle velocity and axle spacing. We determined from chapter 3 that these were the vehicle parameters to which the dynamics were most sensitive. We also determined earlier that the effect of increasing the velocity and reducing the axle spacing were equivalent, since they altered the extent of the out-of-phase pitching of the axles. The results of varying these two parameters are illustrated in figures 5.67 and 5.68. A vehicle velocity of 35 and 70 mph represent 45 % and 30 % reductions in cracking damage as compared with 55 mph. To minimize the damage at 55 mph the axle spacing should be reduced to 40 inch from the standard of 52 inch (figure 5.68).

5.5 Comparison of Tandem to Single Axle Suspension

The results of figure 5.69 indicate the damage that the two suspensions would produce at a vehicle velocity of 55 mph. This velocity is the worst case for both axle types but is particularly bad in the case of the walking-beam because of the lightly damped out-of-phase axle pitch mode being excited.

The walking-beam suspension thus performs better than the single axle suspension at low velocities, since it has the ability to filter out the faults in the pavement. This filtering occurs without excessively exciting the axle pitching mode at low velocities.

At 55 mph the walking-beam tandem produces up to 40 % more cracking damage after 15 years of pavement service life. There would not be such a dramatic difference at other velocities.

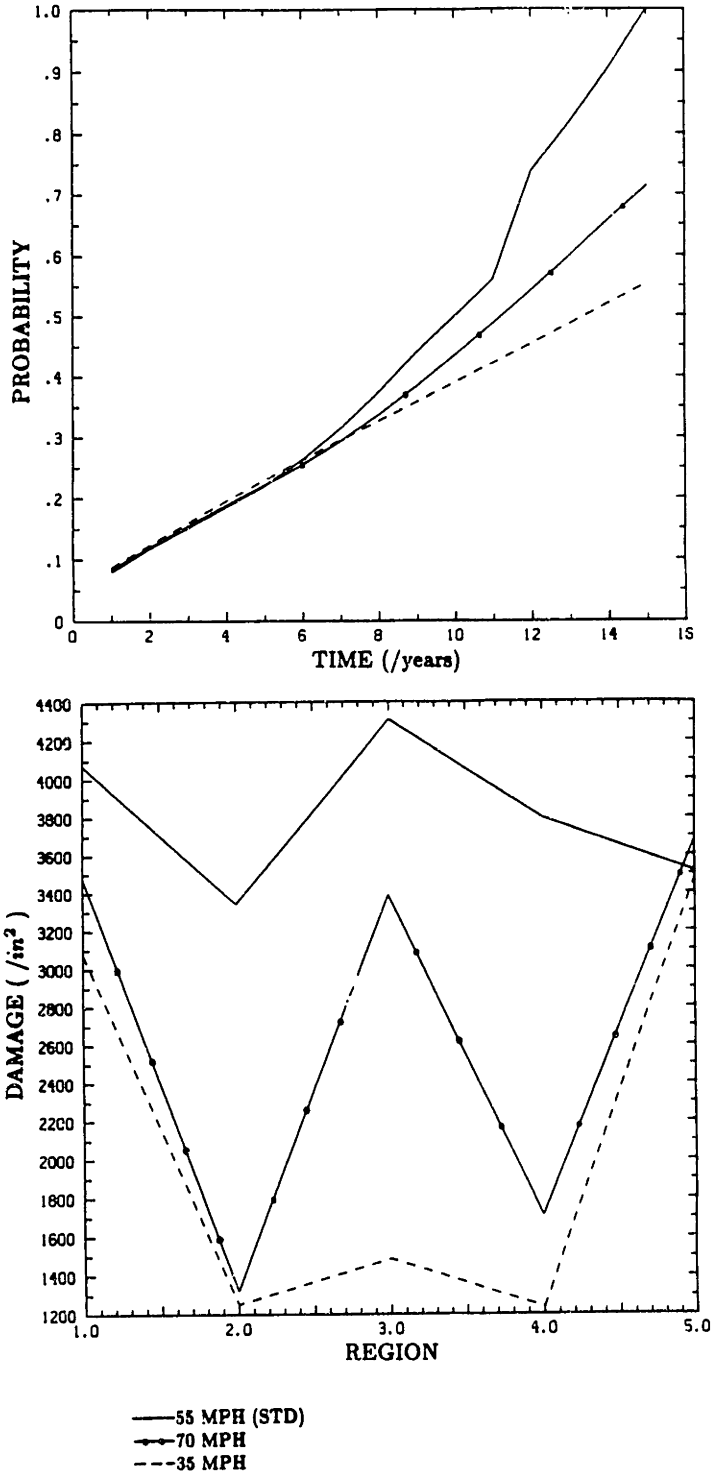

Figure 5.67 Effect of velocity (Walking-beam)
(a) Probability of cracking versus time
(b) Cracking by region

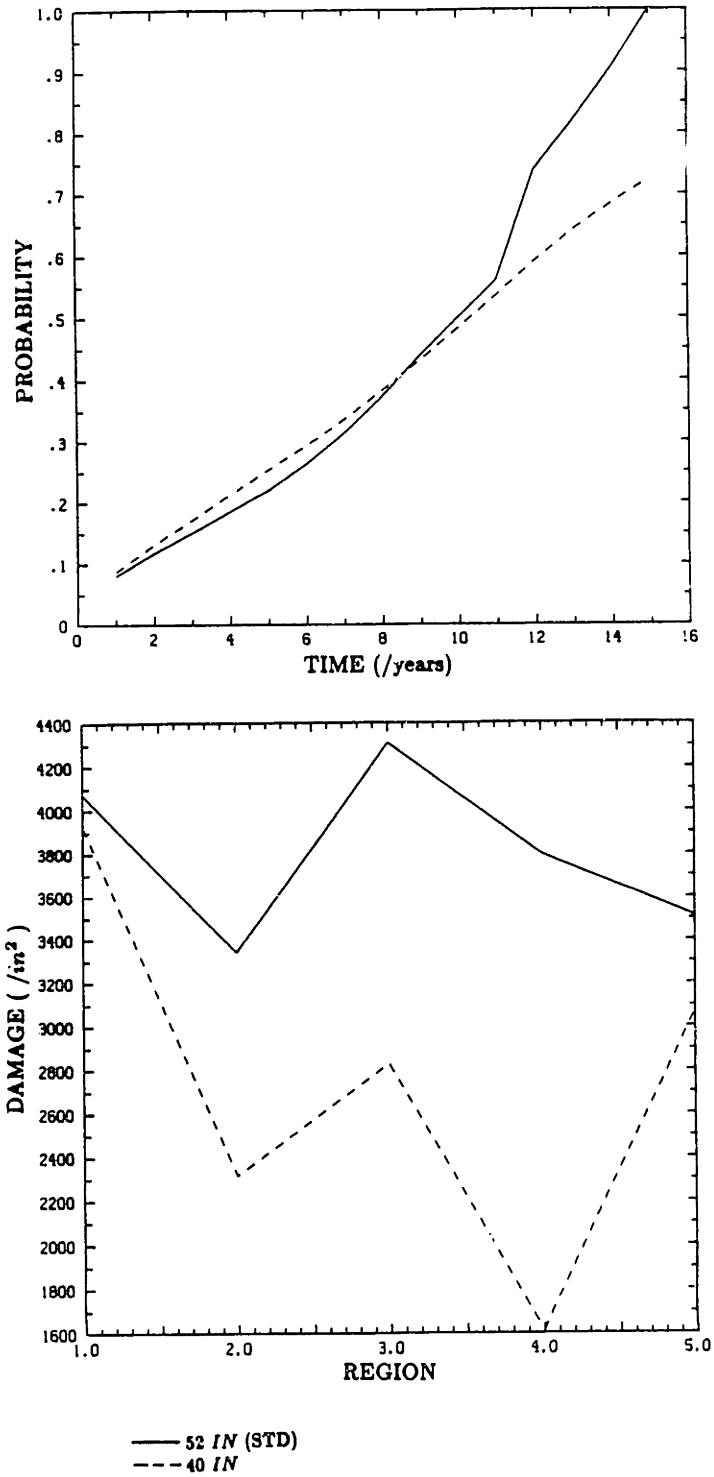

Figure 5.68 Effect of axle spacing (Walking-beam)
(a) Probability of cracking versus time
(b) Cracking by region

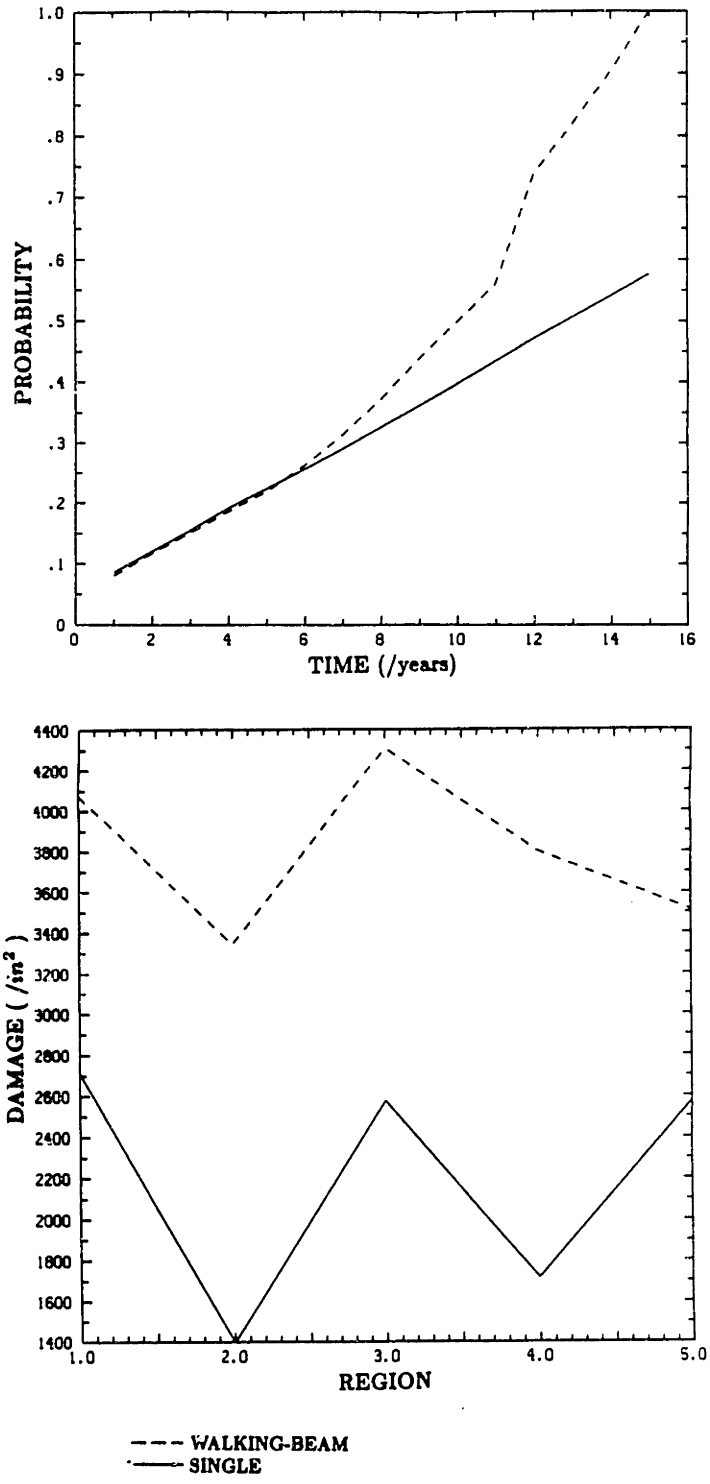

Figure 5.69 Walking-beam tandem versus Single axle
(a) Probability of cracking versus time
(b) Cracking by region

5.6 Four-Leaf Tandem

In comparison to other axle groups the four-leaf does damage equivalent to the walking-beam at the slab joints and as much damage as the single-axle suspension in the mid-slab regions. The reason for the four-leaf doing less damage than the walking-beam is because the out-of-phase pitching mode is more restricted by the inherent coulomb friction.

We investigated the effect of varying β, leaf-spring stiffness, tandem axle spacing and the load sharing coefficient for the four-leaf tandem suspension.

The amount of cracking that occured was relatively sensitive to the β parameter. We determined that there is an optimum value of leaf-spring damping around $\beta = 4 \times 10^{-3} ft$. Note that for single-axle suspensions we concluded that higher values of β were preferable.

The difference in response to β, between the axle groups is due to the coupling of the tandem axles through the short-rocker. A lower value of β in the single-axle suspension translates to a larger contribution of the body mode, resulting in larger damage. In the tandem-axle case the lower β (higher coulomb friction) results in increasing the contribution of the body mode to the tyre force thereby, increasing the damage. An increase in β will excite the axle out-of-phase pitching mode and results in an increase in damage. Therefore, there exists an optimum value of β for the four-leaf tandem.

Increasing the leaf-spring stiffness by 50 % produced a 6 % reduction in the overall damage produced. This trend is reversed for the case of the single-axle leaf-spring where we predict that softer suspensions are more favourable. We expect that the stiffer the leaf-spring the less is the wheel mode excited thereby, transmitting the wheel input to pitching of the rocker. Note that the pavement damage is not very sensitive to the leaf-spring stiffness in the case of the four-leaf tandem suspension.

The pavement damage is increased by 9 % by reducing the axle spacing from 52 to 40 inch. This is opposite to the effect it produces in the walking-beam suspension where we determined that the higher stresses produced by bringing the

axles together is far out-weighed by the reduced dynamics. In the four-leaf tandem, increased stresses produced by reducing the axle spacing is more significant than the change in the dynamics. There is less of a change in dynamics because the axle pitching mode has more inherent damping in the four-leaf tandem than the walking-beam.

Changing the load sharing coefficient (LSC) from perfect load sharing (LSC = 1.0) to LSC = 0.9 does not result in a significant change in the damage over the slab but results in a redistribution of damage over the slab. The significant increase occurs at the beginning of the slab close to the joint, due to the additional redistribution of the load on to the lead-axle as the tandem passes over the joint.

5.7 Rigid and Flexible Pavement Cracking Damage

O'Connell [4] performed an extensive study on the effect of vehicle dynamics on flexible pavement damage and shed light on the relationship between the dynamic load coefficient and the rutting and cracking damage modes. Furthermore, O'Connell determined that the damage caused by single-axle suspensions is not sensitive to vehicle dynamic effects and studied the four-leaf short-rocker tandem suspension. Based on the results of that study we perform a comparison of the effects of dynamics on cracking damage for both rigid and flexible pavements.

It is apparent from table 6 that the effect of dynamics on the cracking damage is more significant for flexible pavements than rigid pavements. This is due to the narrowness of the influence functions for cracking in flexible pavements as compared to rigid pavements.

Trends in the parametric studies are consistent but are generally larger for flexible pavements. It is important to note that varying vehicle parameters has an effect on the distribution of cracking over a slab and that this is an important consideration from the point of view of reducing pumping, edge cracking, mid-slab cracking and joint faulting.

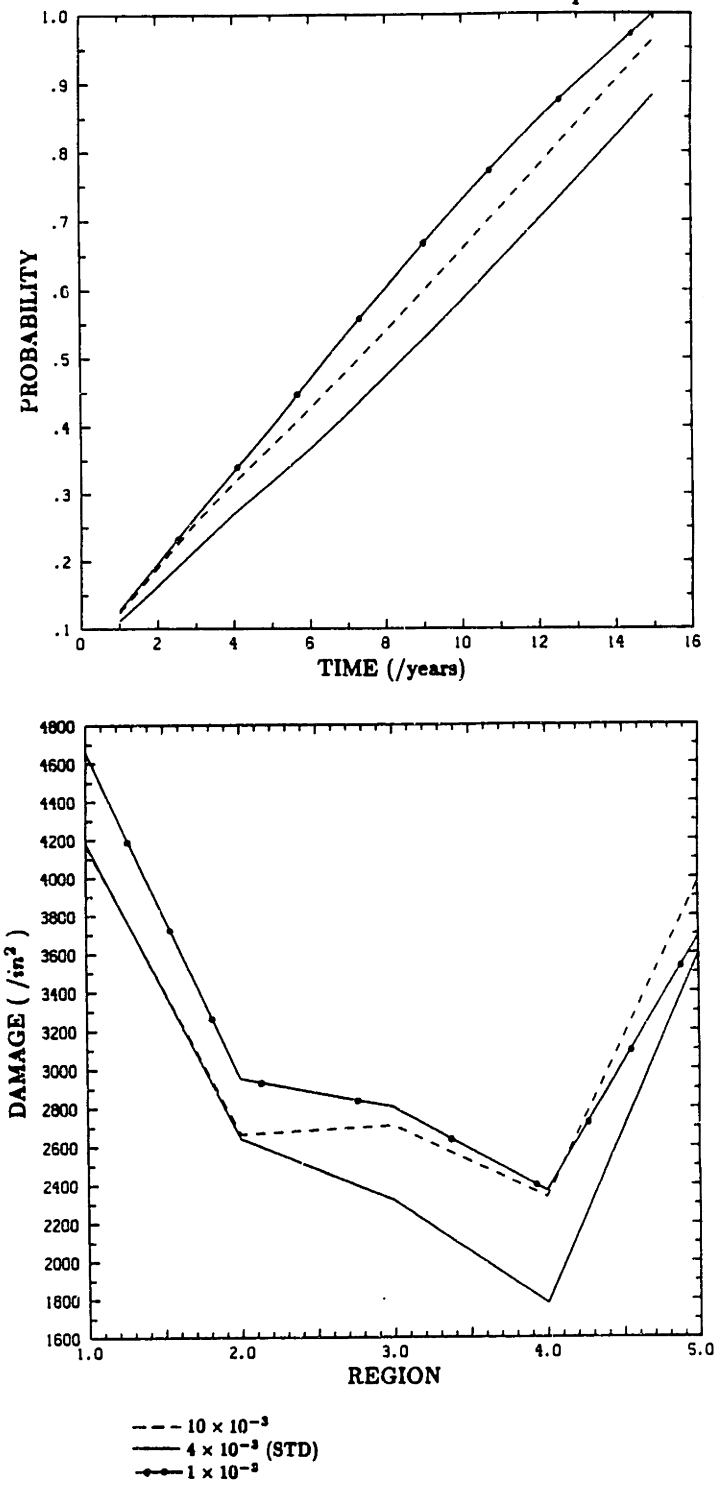

Figure 5.70 Effect of leaf-spring β parameter (Four-leaf)
(a) Probability of cracking versus time
(b) Cracking by region

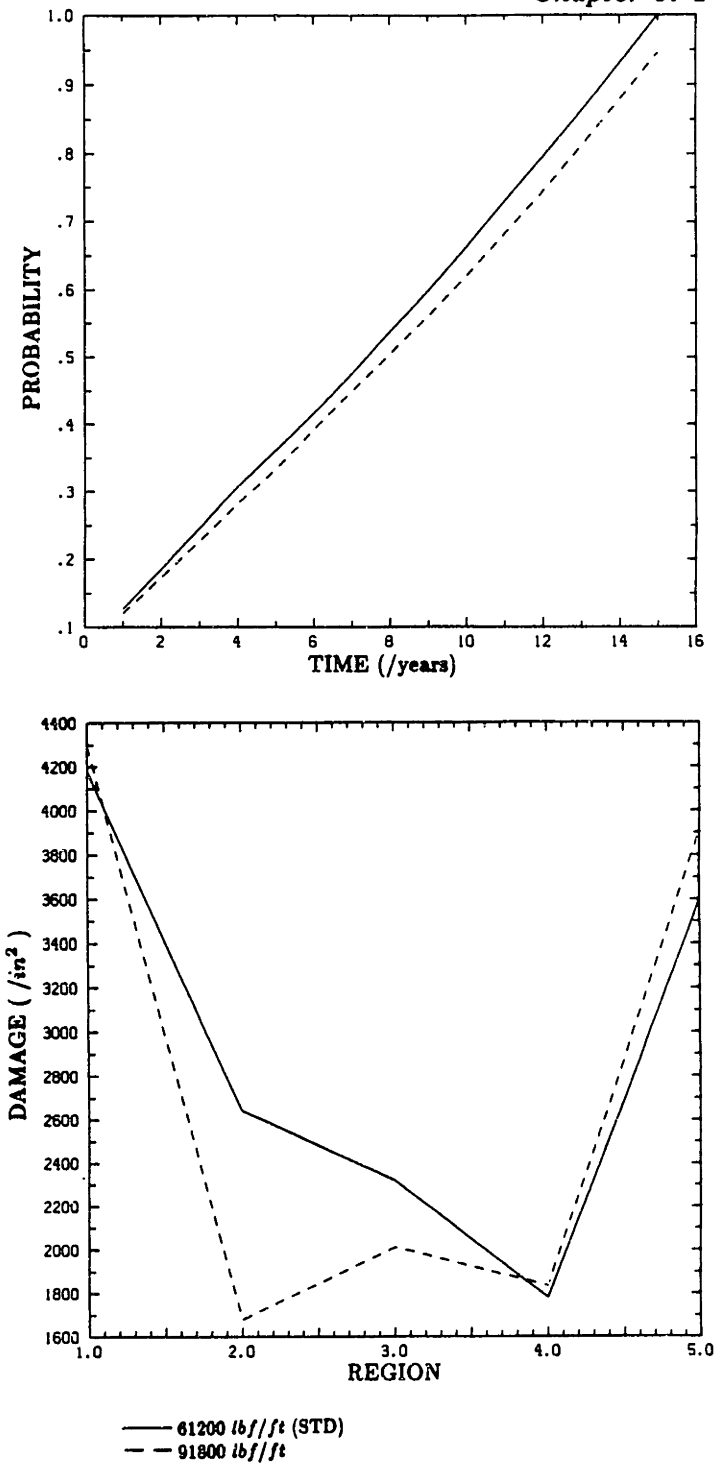

Figure 5.71 Effect of average spring suspension stiffness (Four-Leaf)
(a) Probability of cracking versus time
(b) Cracking by region

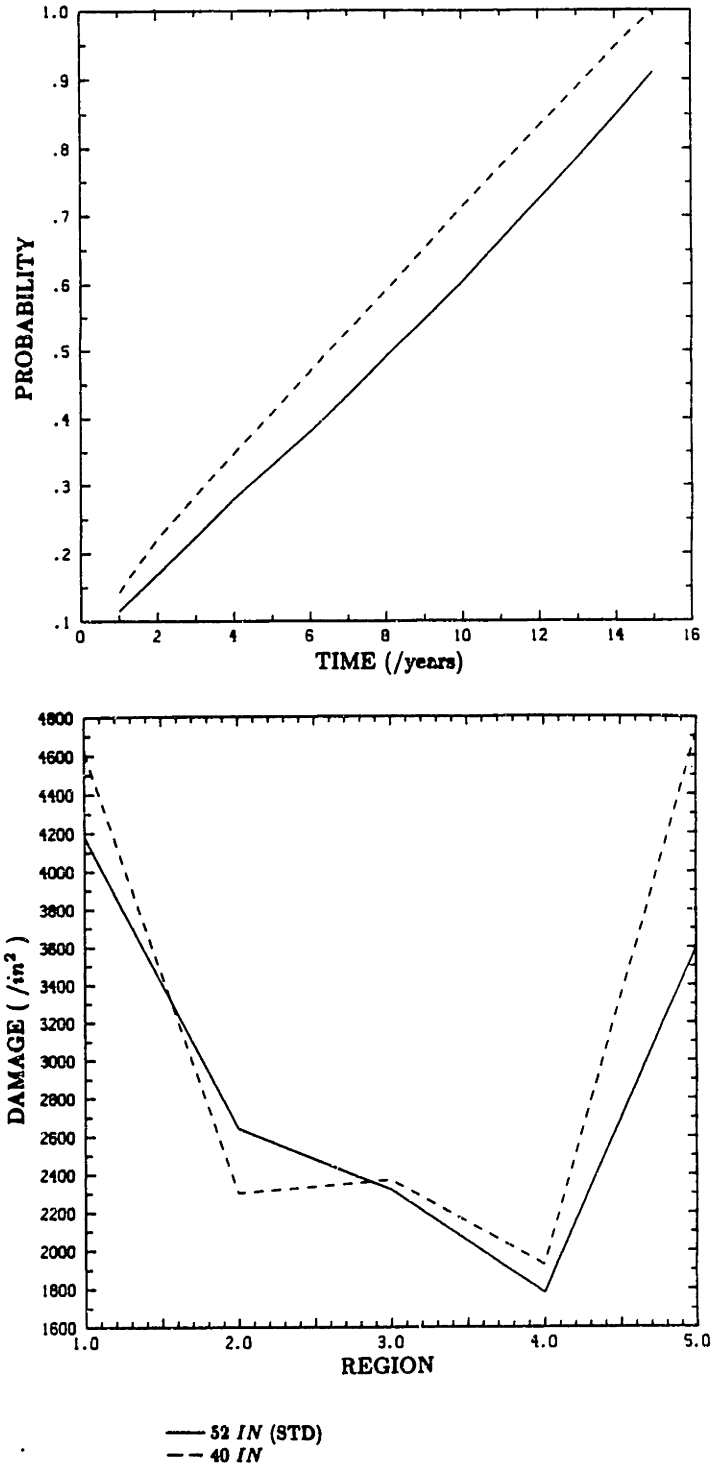

Figure 5.72 Effect of tandem-axle spacing (Four-Leaf)
(a) Probability of cracking versus time
(b) Cracking by region

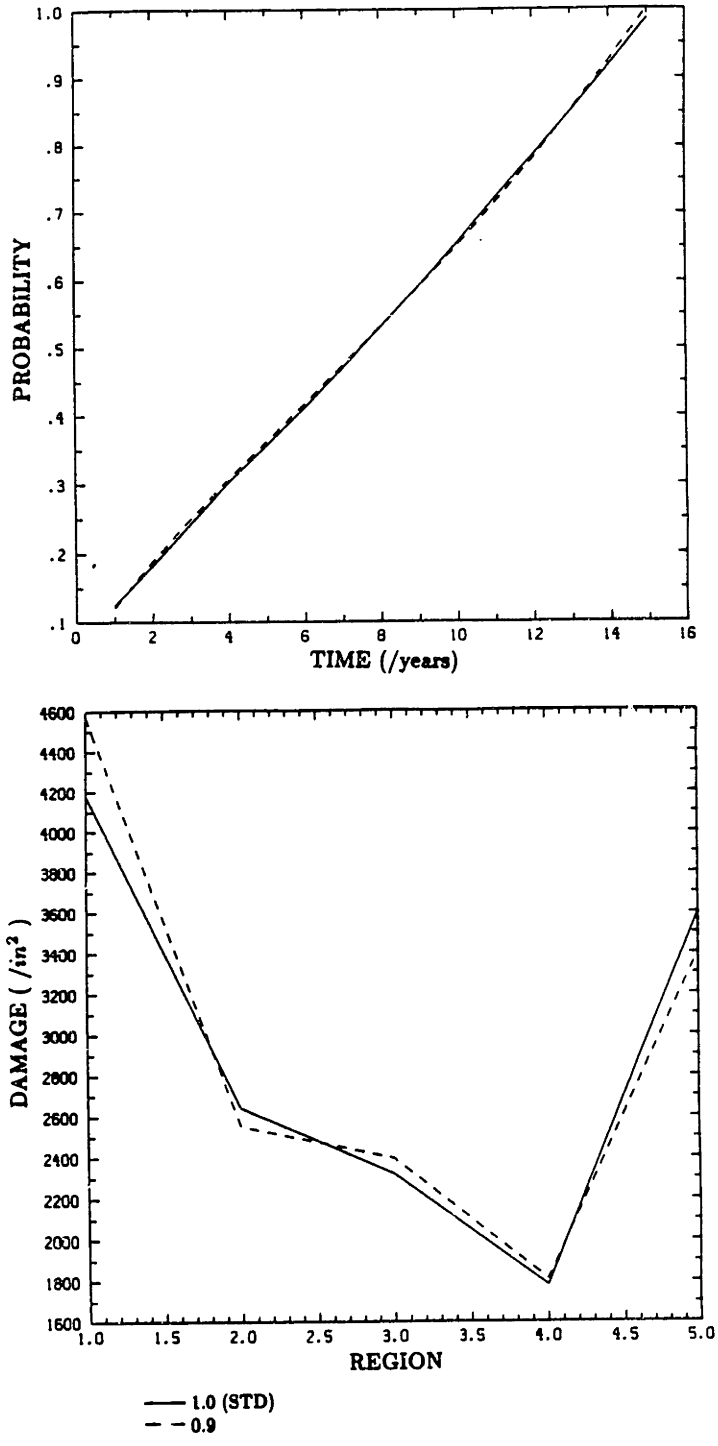

Figure 5.73 Effect of Load Sharing Coefficient (LSC = 0.9; Four-leaf)
(a) Probability of cracking versus time
(b) Cracking by region

Since the influence function for cracking in flexible pavements is narrower than that in rigid pavements we expect that the stresses due to traffic loading will not be distributed over a large region in flexible pavements.

Whereas, increasing the tyre pressure may not alter the vehicle dynamics significantly, it will increase the contact pressure and stress the pavement experiences. The elevated stresses will produce a marked increase in cracking in flexible pavements but not as much in rigid pavements.

This means that the rigid pavements will not be as sensitive to changes in vehicle parameters unless there is a considerable change in the vehicle dynamics. Examples of such parameters include axle spacing vehicle velocity, joint spacing and faulting.

COMPARISON OF FLEXIBLE AND RIGID PAVEMENT DAMAGE

FOUR-LEAF TANDEM SUSPENSION

SUSPENSION PARAMETER	RIGID	FLEXIBLE	EFFECT
BETA	Optimum at 0.004 ft. 10 - 13.5 % increase at 0.01 - 0.001 ft.	Optimum at 0.004 ft. 25 - 55 % increase at 0.01 - 0.001 ft.	leaf-spring damping
TYRE PRESSURE	Small change in dynamics and cracking.	Small change in dynamics but twice as much cracking due to narrow influence function	changes contact pressure & stress
SPRING STIFFNESS	6 % increase in overall cracking for an change from 60000 - 90000 lbf/ft	25 % increase in cracking	alters body mode contrib-ution to tyre mode
AXLE SPACING	Significant change in dynamics and 10 % increase in cracking	Small change in dynamics with 4 % increase in cracking	Out-of-phase pitch mode & road stress
LOAD SHARING COEF.	Insignificant effect	9 % increase in cracking	Uneven load distrib-ution

TABLE 6

6

Conclusions

6.1 Introduction

This paper has reported on research results from an on-going USDOT/FHWA research project. Detailed heavy truck dynamic simulation programs have been developed, and significant modifications have been made to an existing rigid pavement program (PMARP) to account for dynamic tire loads due to single and tandem axles. General conclusions concerning modelling of vehicle loads as dynamic moving loads are:

- The static load case indicates that the mid-slab region has a lower fatigue damage than the transverse joint regions.
- For the dynamic loading case the mid-slab and transverse joint regions have similar fatigue damage values.
- The dynamic moving load fatigue damage case is up to 40 % larger than that of the static load case.
- The mid-slab regions are more sensitive to dynamics then are the transverse joint regions.
- Cracking in flexible pavements is generally more sensitive to changes in suspension parameters than cracking in rigid pavements.
- Slabs that use dowels as pavement joints do not excite significant dynamics since the joint-faulting magnitude is generally under $\frac{2}{10}$ inch over the pavement life. Aggregate interlock rigid pavement joints however, tend

to have joint fault magnitudes above $\frac{3}{10}$ after only 6 years of pavement service.

We have clearly demonstrated that the effect of dynamic vehicle loading cannot be neglected when assesing the damage done due to traffic loading on rigid pavements. Not only are the influence lines of response broader than those for flexible pavements, due to the rigidity of the concrete slabs, but also the faults which occur between the concrete slabs excite vehicle dynamics.

The results of extensive vehicle simulations indicate that vehicle parameters that are important to take into consideration when analyzing vehicle dynamic response to rigid pavements include:

a) Vehicle Velocity;

b) Suspension Stiffness;

c) Leaf-Spring Damping;

d) Tandem Axle Spacing;

e) Suspension Type.

An astute choice of suspension type for a particular set of operating conditions will produce significant reductions in the degree of pavement damage. In addition, it was determined that the joint fault height and the slab joint spacing were critical pavement parameters which effected the level of vehicle dynamics excited.

Cracking in the slab is more sensitive to changes in the dynamics in the mid-slab regions than in the regions close to the joints. Therefore, vehicle and pavement parameters that alter the contribution of the body mode to the tire force alter significantly the amount of cracking that occurs over the slab. Below we propose suspension design guidelines aimed to minimize cracking damage to rigid pavements.

6.2 Single-Axle Suspension

Based on the analyses of chapters 3 and 5 we determined that the vehicle parameters of importance include:

- Vehicle Velocity;
- Suspension Stiffness;
- Leaf-Spring Damping.

The tire pressure did not produce significant effect on the dynamics of the vehicle. The effect of the tire pressure would be to change the contact area and pressure exerted on the pavement. The effect of altering the contact pressure in the case of rigid pavements is not as significant as the case of flexible pavements. An explanation of this being that the influence functions of rigid pavements are broader than those for the flexible pavement cracking mode and therefore distribute the higher stresses due to the elevated contact pressure more effectively over the entire slab.

For our particular vehicle dimensions and slab length we determined that the vehicle excitation frequency was in the region of the body mode for a vehicle velocity of 55 mph. We therefore, suggest velocities off this value will reduce damage significantly.

We also suggest that a choice of a soft suspension is better than a stiffer suspension, since this would reduce the contribution of the body mode to the tire force and therefore reduce the mid-slab cracking.

In terms of leaf-spring damping we propose that the smaller the damping the lower the overall damage. The result of this again is to excite the wheel mode while reducing the excitation to the body mode.

It is important to bear in mind at this point that we are suggesting guidelines for minimizing pavement damage and that these guidelines do not take into account equally significant factors such as vehicle stability or ride quality.

6.3 Walking-Beam Tandem Suspension

Once again the important parameters here are listed below:

- Vehicle Velocity;
- Suspension Stiffness;
- Leaf-Spring Damping;
- Tandem-Axle Spacing;

The same ideas that were presented for single-axle suspensions apply for the case of tandem-axle suspensions. We also have to take into consideration the coupling of the tandem axles.

Because the influence functions for rigid pavements are broad, stresses are more effectively distributed over the pavement. The implications of this in terms of axle spacing is that increases in the stresses produced by reducing the spacing is not as significant as the resulting change in dynamics of the vehicle. A significant change in the damage occurs by altering the tandem axle spacing such that the joints faults do not excite the axle pitching mode. The desired spacing is thus also a function of vehicle velocity. The vehicle velocity should therefore be selected with consideration of the vehicle axle and joint spacing as well as tandem axle spacing when minimizing pavement damage.

The four-leaf short-rocker and walking-beam suspensions produce about the same damage for small fault heights (under $\frac{2}{10}$). Over more significant faults however, the walking-beam suspensions produces a significantly larger amount of damage, because of the excitation of the lightly damped pitching mode of the tandem axles. The four-leaf suspension has considerably more damping than the walking-beam because of the coulomb friction damping that exists in the short-rocker.

6.4 Four-Leaf Tandem Suspension

A summary of the conclusions presented in chapter 5 are listed below:

- An optimum value of β around 4×10^{-3} exists. A similar value was found for flexible pavements.
- The cracking damage is not very sensitive to variations in leaf-spring stiffness.
- The load sharing coefficient does not have an effect on the overall cracking but produces up to a 10 % increase in cracking close to the joint.

REFERENCES

1. "Infrastructure", Constructor, May 1983.

2. Westergaard, H.M., "Stresses In Concrete Pavements Computed by Theoretical Analysis", Public Roads, Vol 7, No 2, April 1926.

3. Sweatman, P.F., "A Study of Dynamic Wheel Forces in Axle Group Suspensions of Heavy Vehicles", Australian Road Research Board, Special Report No. 27.

4. O'Connell, S., "The Influence of Heavy Vehicle Dynamics on Pavement Response",S.M. Thesis, Massachusetts Institute of Technology, May 1986.

5. Gibson, A., "Modeling of Heavy Truck Dynamics for Computing Pavement Loads", S.M. Thesis, Massachusetts Institute of Technology, May 1985.

6. Sayers, M., and Gillespie, T.D.,"Dynamic Pavement/Wheel Loading for Trucks with Tandem Suspensions", 8th IAVSD Symposium on the Dynamics of Vehicles, Cambridge, MA, USA, August, 1983.

7. Robson, J.D., Dodds, C.J., "Stochastic Road Inputs & Vehicle Response", Vehicle System Dynamics 5, 1975/76, p1-13.

8. Captain, K.M., Boghani, A.B., & Wormley, D.N., "Analytical Tire Models for Dynamic Vehicle Simulation", Vehicle System Dynamics, 8, 1979, pp 1-32.

9. Bernard, J., Vanderploeg, M., & Jane, R., "Tire Models for the Determination of Vehicle Structural Loads", 7^{th} IAVSD Symposium September 7-11, 1981.

10. Fancher, P.S., Ervin, R.D., Mac Adam, C.C., & Winkler, C.B. ,"Measurement & Representation of the Mechanical Properties of Truck Leaf Springs", SAE Trans. 800905, 1980.

11. Cebon, D., "An Investigation of the Dynamic Interaction between Wheeled Vehicles and Road Surfaces", PhD dissertation, Cambridge University, England, June 1985.

12. Tretter, "Discrete Time Signal Processing", John Wiley and Sons, N.Y., 1976.

13. Stearns, "Discrete Signal Processing", Hayden Book Company, Inc., Rochelle Park, N.J., 1975.

14. Bendat, J.S, and Piersol, A.G., "Random Data: Analysis and Measurement Procedures". John Wiley and Sons, New York, 1971.

15. Hedrick, J.K. et al, "The Influence of Fifth Wheel Location and Braking Characteristics on Articulated Vehicle Motion", Final Report for USDOT, Nov 1977

16. Darter, M., "Design of Zero Maintenance Plain Jointed Concrete Pavement", Final Report prepared for FHWA, June 1977.

17. Zienkiewicz, O.C., "The Finite Element Method", Third Edition, Mc Graw Hill Book Co., New York, 1977.

18. Bathe, K. J., "Finite Element Procedures in Engineering Analyisis", Prentice Hall, 1982.

19. Larralde, J., "Design to Prevent Pumping in Concrete Pavements", Final Report for FHWA, December 1984.

20. Miner, M., "Cumulative Damage in Fatigue", ASCE Transactions, Vol. 67, 1945.

21. Teller, W., Cashell, H.D., "Performance of Dowelled Joints under Repetitive Loading", Public Roads, 1955.

22. AASHTO, "Interim Guide for Design of Pavement Structures", American Association of State Highway & Transportation Officials, 1981.

23. Majidzadeh, K., Ilves, G., Sklyut, H., "Mechanistic Design of Rigid Pavements".

24. Markow, M.J., Brademeyer, B.D., "Modification to the System EAROMAR", Final Technical Report, FHWA, June 1981.

25. Barenberg, E.J., et al., "Finite Element Analysis of Jointed or Cracked Pavements", Transportation Research Board, (676), 1978.

26. Tayabji, S.D., "Analysis of Jointed Concrete Pavements", FHWA, Feb. 1984.

27. Darter, M., "Design of Zero Maintenance Plain Jointed Concrete Pavement", Final Report prepared for FHWA, June 1977.

28. Huang, Y.H., Wang, S.T., "Finite Element Analysis of Concrete Slabs & its Implications for Rigid Pavement Design", Highway Research Record (466), 1973.

29. Teller, L.W., Sutherland, E.C., "The Structural Design of Concrete Pavements", Public Roads, Vol 16, No 9, 1935.

30. Weiss, R.A., "Pavement Evaluation & Overlay Design Using Vibratory Nondestructive Testing and Layered Elastic Theory, Vol 1 - Development of Procedure", FAA Report, December 1978.